1979

Physics of the solar pond

John Ralph Hull
Iowa State University

PLEASE NOTE:

In all cases this material has been filmed in the best possible way from the available copy. Problems encountered with this document have been identified here with a check mark ✓.

1. Glossy photographs _____
2. Colored illustrations _____
3. Photographs with dark background ✓
4. Illustrations are poor copy _____
5. Print shows through as there is text on both sides of page _____
6. Indistinct, broken or small print on several pages _____ throughout _____
7. Tightly bound copy with print lost in spine _____
8. Computer printout pages with indistinct print _____
9. Page(s) _____ lacking when material received, and not available from school or author _____
10. Page(s) _____ seem to be missing in numbering only as text follows _____
11. Poor carbon copy _____
12. Not original copy, several pages with blurred type _____
13. Appendix pages are poor copy _____
14. Original copy with light type _____
15. Curling and wrinkled pages _____
16. Other _____

University Microfilms International

300 N. ZEEB RD., ANN ARBOR, MI 48106 (313) 761-4700

Physics of the solar pond

by

John Ralph Hull

A Dissertation Submitted to the

Graduate Faculty in Partial Fulfillment of

The Requirements for the Degree of

DOCTOR OF PHILOSOPHY

Major: Physics

Approved:

Signature was redacted for privacy.

In Charge of Major Work

Signature was redacted for privacy.

For the Major Department

Signature was redacted for privacy.

For the Graduate College

Iowa State University
Ames, Iowa

1979

TABLE OF CONTENTS

LIST OF FIGURES

LIST OF TABLES

PARTIAL LIST OF SYMBOLS

C_V	heat capacity at constant volume
C°	Centigrade degree
cm	centimeter
D	declination of the sun
d	depth of fluid slab
dT_R	radiative temperature correction term
dm	decimeter
e_{ij}	strain tensor
g	acceleration of gravity
gm	gram
$H(\lambda)$	surface radiation flux that is not reflected
hr	hour
I	radiation intensity
i	angle of incidence
J	Joule
K_S	coefficient of solute diffusivity
K_T	coefficient of thermal diffusivity
K°	Kelvin degrees
k	thermal conductivity, also wavenumber
kg	kilogram
km	kilometer
L	latitude
m	meter
n	index of refraction

nm	nanometer
P	isotropic pressure
P_{ij}	stress tensor
p	density
p_m	mean density
R_S	salinity Rayleigh number
R_T	thermal Rayleigh number
R_{TR}	radiation thermal Rayleigh number
r	angle of refraction
S	solute concentration
T	temperature
T_o	temperature at top of slab
t	time
u_i	velocity
W	Watt
X_i	force
x_i	spatial distance
α	temperature density expansion coefficient
β	solute density expansion coefficient
ΔS	salinity difference across fluid slab
ΔT	temperature difference across fluid slab
δ	characteristic attenuation length
δ_{ij}	Kronecker delta function
λ	wavelength

μ	effective attenuation coefficient
ν	absolute viscosity, also kinematic viscosity
σ	ν/K_T
τ	K_S/K_T

I. INTRODUCTION TO SOLAR PONDS

Today, in 1978, the industrialized nations of the earth are struggling with the recently recognized problem of the finite planetary supply of energy resources. In industrialized nations the standard of living of the populace, as measured by the Gross National Product (GNP) per capita, is roughly proportional to energy consumption per capita (1). This relationship suggests that a decline in the standard of living might accompany the exhaustion of energy resources. While it may be possible to have a long, healthy, and fulfilling life without prodigious energy consumption, the exhaustion of energy resources would mean an end to many of the lifestyle options currently available to us. One of the motivations responsible for the work reported in this manuscript has been the assumption that the existence of energy dependent lifestyle options is desirable.

Solar energy, radiant energy generated by fusion reactions in the sun, is an energy resource that will be available for hundreds of millions of years. Before the industrial revolution, solar energy supplied almost all of mankind's energy through use in windmills, water turbines, wind powered ships, and in biological cycles. An average of about 10^{15} W of solar radiation is received at the surface of the 48 coterminous states. If this is compared with the current United States power consumption of about 3×10^{12} W, one realizes that solar energy still has the potential to provide a large portion of our current energy needs. To realize this potential one must overcome several problems associated with solar energy. First, solar energy is diffuse. To collect large

amounts of solar energy, large amounts of surface area need to be used. One needs to collect solar energy relatively efficiently to reduce the required surface area. Second, solar energy is variable, both diurnally and seasonally. One needs to store sufficient energy for use when radiation input is low. It is currently technologically and economically feasible to store adequate amounts of energy for several days. Longer term storage is desirable.

The production of low temperature heat, i.e. heat at temperatures less than 100° C, is a significant sector of current energy consumption. 18% of the total primary energy consumption in the U.S. is devoted to commercial and residential space heating (2). In addition, many industrial processes such as wood and grain drying use low temperature heat. One device for generating low temperature heat from solar energy, the solar pond, will be explored in the rest of this manuscript.

Before describing a solar pond, let us review briefly what happens in an ordinary pond, such as a farm pond. Part of the sunlight incident on the pond is absorbed in the water, and part is absorbed on the bottom of the pond. The latter absorption leads to heating of the water in the lower part of the pond. Being warmer, and hence less dense than the cooler water above it, the heated water begins to rise, setting up convection currents that eventually lead to dissipation of the absorbed heat at the surface of the pond. A solar pond is designed to suppress this convection and retain the heat at the bottom of the pond.

The solar pond is a solar collector and seasonal heat storage device whose structure is shown schematically in Fig. I.1. The solar

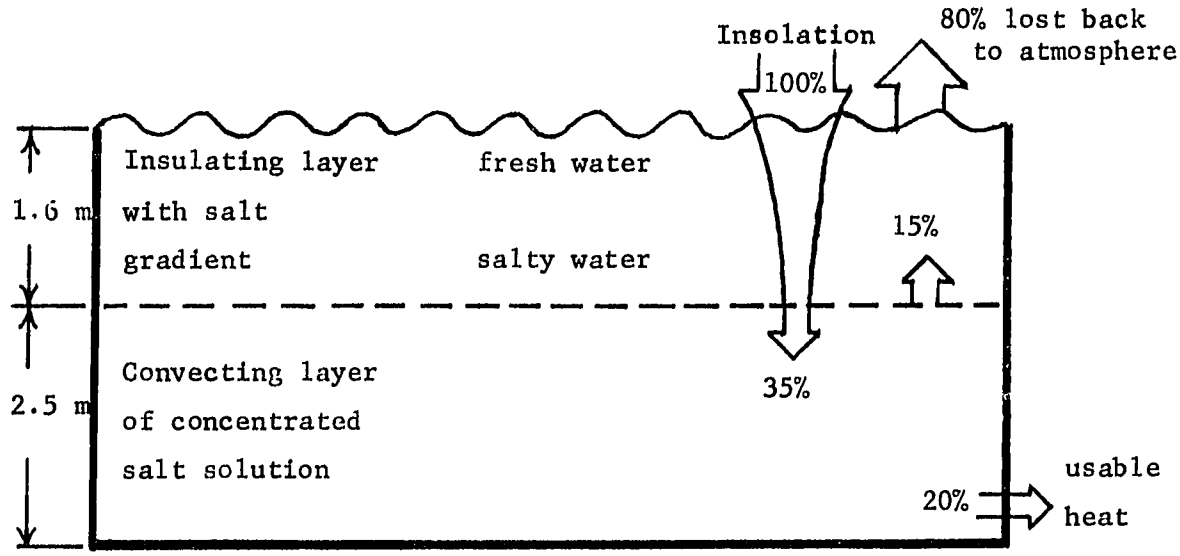

Fig. I.1. Schematic of typical solar pond structure and heat flow.

pond is a body of water consisting of a convective layer and an insulating layer. The bottom convecting layer is a concentrated salt solution. It is covered by an insulating layer which contains a salt gradient such that water closer to the surface is always less salty than the water below it. If the salt gradient is large enough, there will be no convection in the insulating layer when heat is absorbed on the bottom, since the hotter saltier water at the bottom of the gradient will be denser than the colder less salty water above it. Since water is transparent to visible light but opaque to infrared radiation, heat in the form of sunlight reaches the darkened bottom, is absorbed there, and can escape only via conduction. Since the thermal conductivity of water is moderately low, and since the insulating layer is more than a meter thick, heat escapes upward from the convecting layer very slowly. This makes the solar pond not only a thermal collector but also a seasonal

heat storage device. Due to the large heat capacity of water, heat collected in the summer can be stored in the bottom of the pond and used throughout the winter, and the maximum temperature at the bottom of the pond, near the boiling point, is reached in early fall. As seen in Fig. I.1 the pond is about 20% efficient in converting solar energy to usable low temperature heat.

Heat extraction from the solar pond is usually accomplished by placing a heat exchanger at the top of the convecting layer where pond temperatures are highest. A separate fluid circulates through the heat exchanger, picking up heat from the solar pond and delivering the heat to a load. The hot salt water could be circulated but would present a corrosion and possible contamination problem.

If the flow of ground water underneath the pond is slow enough, i.e., if the distance the water moves in a year is less than the pond diameter, then the ground underneath the pond can be used as additional thermal mass. However, if the ground water flow is too fast, then all heat flowing to the ground is lost, and the pond must be insulated from the ground.

The amount of salt necessary to maintain the salt gradient in the insulating layer will depend on the depth of the layer, type of salt used, and the temperature gradient across the layer. To maintain a temperature of over 90° C in the convective layer, a NaCl solution of 15-20% by weight would be necessary. For the pond depicted in Fig. I.1 this would require about 500 kg of salt per square meter of solar pond area. Salt will slowly diffuse upward through the insulating layer degrading the

salt gradient. To maintain the salt gradient, salt must be added to the bottom of the pond, and the surface flushed with fresh water periodically. If convection in the insulating layer is effectively suppressed, then for each square meter of pond surface about 10 kg of salt per year is required to maintain the salt gradient. The salt from the flushed surface water could be recovered and reused by pumping the water into an evaporation tank.

The solar pond has several advantages as a solar energy device. It combines both heat collection and heat storage in one device. It is able to store heat for long periods of time - up to six months. It utilizes low technology components, is simple in design, and is fairly easy to maintain. The most sophisticated part of a solar pond is probably the plastic pond liner. Hopefully, an appropriate clay or other material substitute will be found to replace plastic for use as a liner. The biggest disadvantage of solar ponds is that they do require considerable surface area and large quantities of salt. Other types of solar collectors can be incorporated onto roofs or into other building structural elements. It does not appear feasible to do this with solar ponds, which might limit their use to rural areas or to cluster family dwellings. Environmental contamination from the salt required by solar ponds could also be a problem. Solar ponds must be built so that salt does not leak from them, and salt runoff from the surface must be contained.

The rest of this manuscript will be devoted to discussing the physics of the solar pond and the results to date from an experimental solar pond located at Living History Farms near Des Moines, Iowa.

Chapter II will discuss the major past research on solar ponds. Chapter III will present a mathematical model of the solar pond. Chapter IV will present a computerized version of the mathematical model and compare it with data. Chapter V will discuss the theory of convective stability in the solar pond salt gradient. Chapter VI will discuss the results to date of the solar pond project at Living History Farms. Appendix A contains a compendium of physical data of those salt solutions that are useful in solar ponds. Appendix B contains a listing of the computer program discussed in Chapter IV.

II. HISTORY OF SOLAR POND RESEARCH

A. Natural Solar Ponds

The concept of the solar pond first appeared in the scientific literature at the beginning of the twentieth century as an explanation for the temperature phenomena observed in several naturally occurring lakes in a salt region of Hungary. These lakes, the largest of which has a surface area of 42,000 m^2 and a depth of 15 m, are in the foothills of the Carpathian Mountains (46° 35' N, 25° 6' E), in the north-central section of what is now Romania. The lakes exhibit typical solar pond behavior, obtaining a temperature in late September of 65° C about a meter below the surface while maintaining near ambient temperature at the surface. Kalecsinsky (3) first measured the salt concentration as a function of depth in these lakes and was the first to suggest that the suppression of convection by the salt gradient and absorption of solar radiation below the gradient were responsible for the high temperatures a meter below the surface. A graph of Kalecsinsky's temperature and salt profiles of Lake Medve, the largest of the lakes, is given in Fig. II.1. Rozsa (4) later confirmed the salinity measurements and extended the explanation of the temperature phenomena to include the seasonal temperature variations. A graph of Rozsa's temperature data as a function of time for Lake Bären is given in Fig. II.2. Since the surface salt concentration of Lake Bären is 7.5%, it cannot support as large a temperature gradient as Lake Medve.

More recently (5-10) solar pond behavior has been found in Lake Bonney and Lake Vanda in the area of McMurdo Sound, Antarctica. Lake

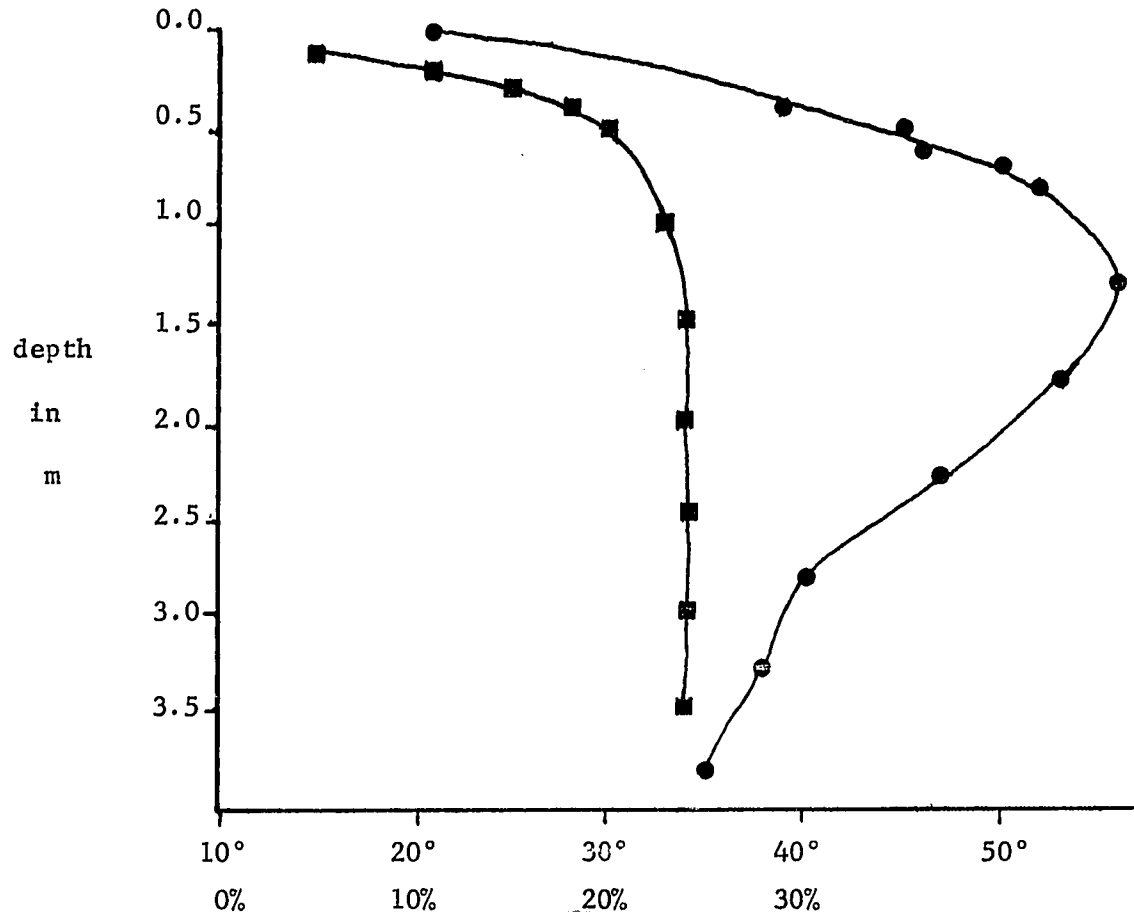

Fig. II.1. Temperature and salt profiles of Lake Medve, July 23, 1901. (Temperature in C° (●——●——●). NaCl concentration in % by weight (■——■——■). Data from Kalecsinsky (3))

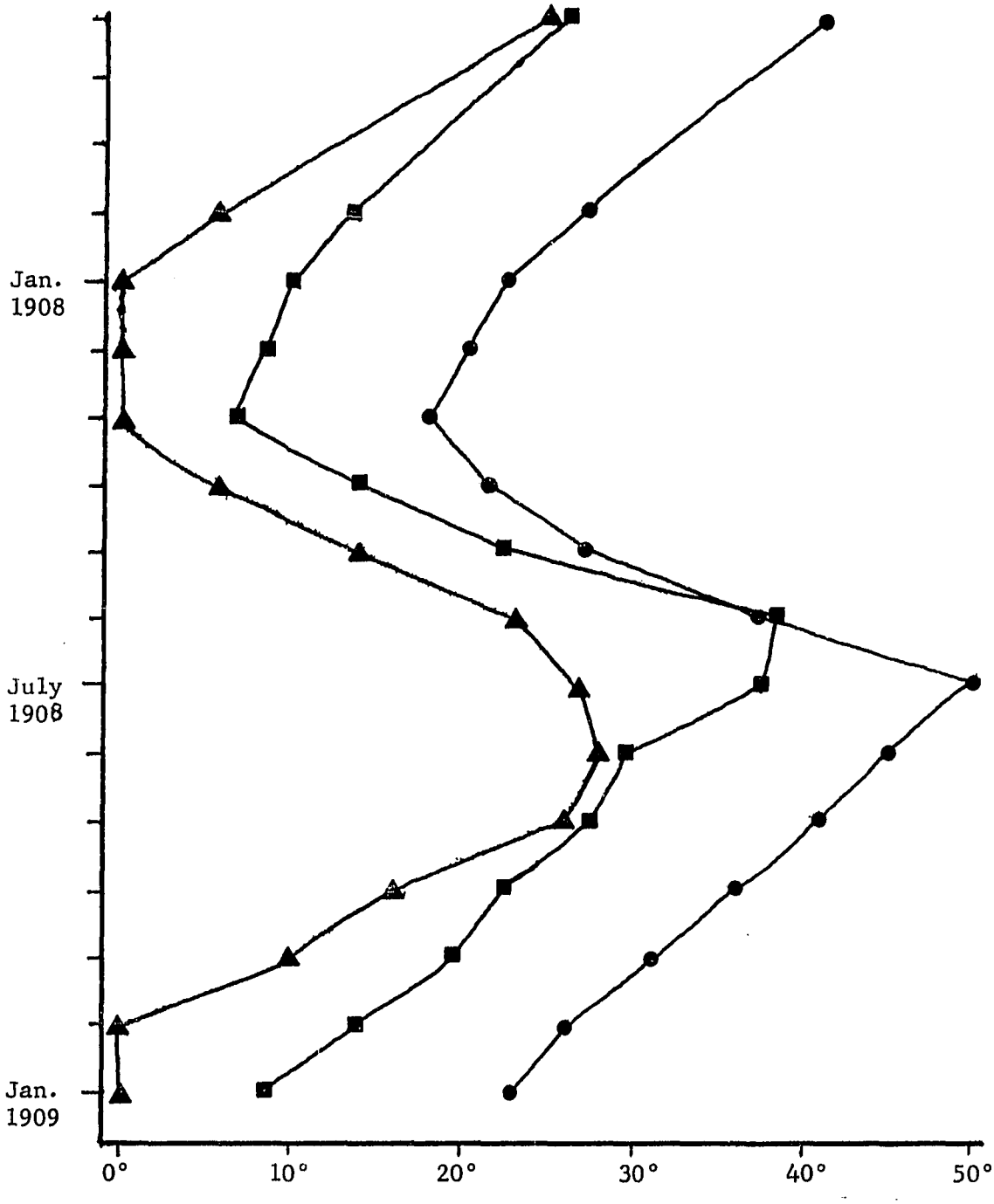

Fig. II.2. Seasonal temperature variation at several depths for Lake Bären. (All temperatures in C°. Temperature at surface-(▲). Temperature at 1 m-(■). Temperature at 2 m-(●). Data from Rozsa (4))

Bonney, located at the foot of Taylor glacier (77° 43' S, 162° 26' E), is approximately 5.4 km long, 1.1 km wide and has a maximum depth of 31 m. Lake Vanda (77° 32' S, 161° 34' E), about 50 km from the ocean at Gneiss Point, is about 6.5 km long, 1.8 km wide, and has a maximum depth of 66 m. Each lake is covered with 3.4-4.2 m of permanent ice. The seasonal partial thawing and refreezing of the bottom portion of the ice cover produces the salt concentration gradient which prevents convection in the upper part of the lakes. In Lake Bonney the temperature reaches a maximum of about 7° C toward the bottom of the gradient 15 m below the surface. Shirtcliffe (11) used steady state heat flow analysis to show that this temperature behavior is well-explained by the salt gradient and the radiation penetrating the ice cover. Temperature and salinity profiles for Lake Bonney are shown in Fig. II.3. Lake Vanda exhibits similar temperature behavior towards its surface and in addition has a larger salt concentration gradient at the bottom of the lake. This second salt gradient effectively traps heat from a geothermal source below the lake. Temperature and salinity profiles for Lake Vanda are given in Fig. II.4.

B. Work in Israel

The first artificial solar ponds were built in Israel beginning in 1958. Rudolf Bloch, who had visited the Hungarian solar lakes as a boy, had proposed using artificial solar ponds for producing heat as early as 1948 (12). Under the guidance of H. Tabor, old salt evaporation pans near the Dead Sea were converted into solar ponds. These ponds had no convective layer, but instead had a salt density gradient continuously

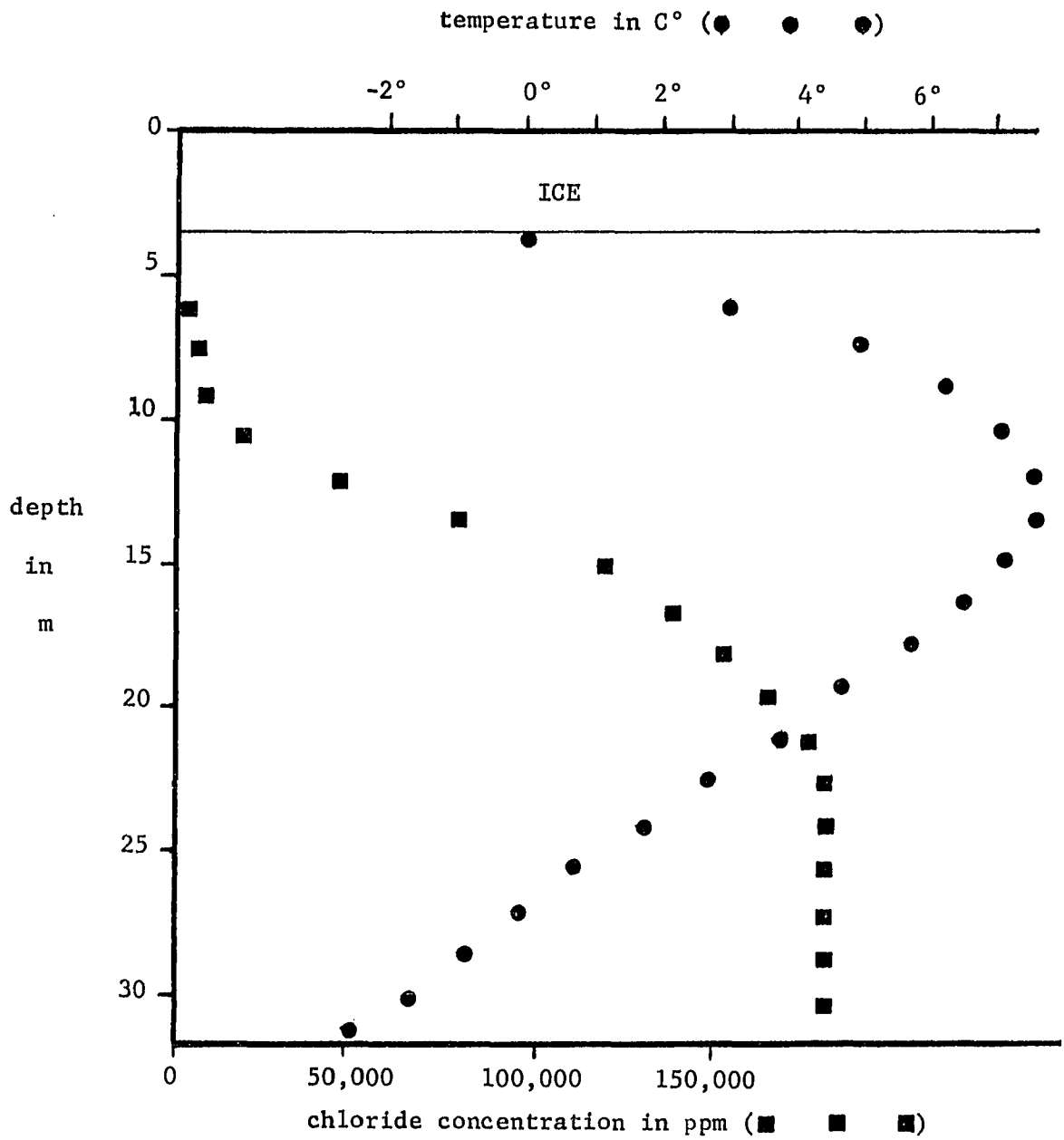

Fig. II.3. Temperature and salinity as a function of depth in Lake Bonney, Antarctica (undated). (Adapted from Shirtcliffe (11))

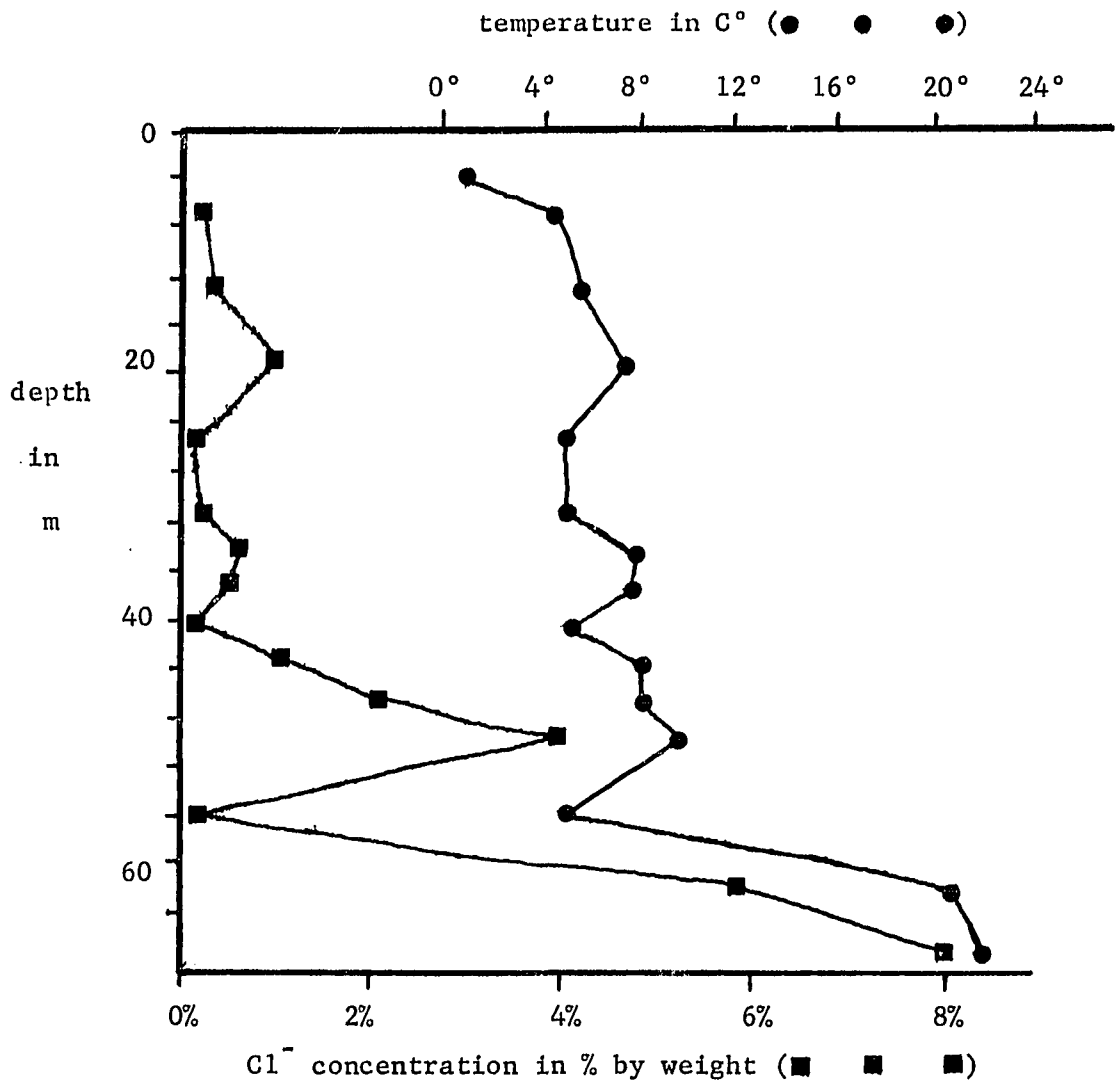

Fig. II.4. Temperature and salinity as a function of depth in Lake Vanda, Antarctica, Jan. 20-26, 1961. (From Armitage and House (7))

running the entire depth of the pond. The most successful pond used $MgCl_2$ as a salt, had a surface area of 625 m^2, and reached a maximum temperature of 96° C (13). This pond was abandoned after a year due to decay of the structural walls. The largest pond had a surface area of 1375 m^2, but had been built over a marsh. When the pond reached 74° C, bubbles from bacterial decay in the soil under the pond floated upwards, destroying the salt gradient (14).

The original motivation for solar pond work in Israel was the production of low cost power (15,16). The proposed scheme was to use the solar pond to produce water at a temperature close to boiling. This water would be flash evaporated (boiled by reducing the surrounding air pressure) and used to run a conventional steam turbine. The temperature difference and hence the Carnot efficiency would be low, but at that time Israel was short of financing capital and had many hectares of free salt. It was estimated that even at 1-3% conversion efficiency, solar ponds would produce electricity at a cost comparable to electricity production costs from fossil fuels (16). Power production potential is large. Hirshmann (17) estimates that utilization of salt flats in Chile would produce 100 times the power consumed by the South American continent. Lake Erie has a mean insolation of 3×10^{20} J/yr. If Lake Erie were a solar pond producing electricity at 2% efficiency, it would supply about 25% of this country's current electricity needs. The Great Salt Lake is a more natural candidate for a solar pond than Lake Erie. At 2% conversion efficiency the Great Salt Lake could generate about 10^{18} J/yr of electrical energy, about 5% of current U.S. electrical consumption.

Drumheller et al. (18) has shown that a large cost in such a power production scheme is the huge turbine required to operate at low temperature and estimates electricity production costs to be several times those occurring with fossil fuels. Solar pond work in Israel stopped in 1966 when it was estimated that such ponds could not compete with cheap oil available at that time; however, it appears that Israel is currently reconsidering solar ponds for several purposes. Recently an Israeli study (19) has proposed using solar ponds for low temperature industrial heat, especially in multi-effect water distillation plants operating at 75° C. There has even been a study on converting the Dead Sea into a Solar Lake (20); and there is renewed interest in generating electricity from solar ponds, but using commercial freon Rankine cycle engines rather than turbines (21). This eliminates the need for evaporating fluid and may be cost effective (22).

Starting from a theoretical analysis of fresh water lakes (23), Weinberger (24) developed a mathematical model of the Israeli style solar pond. Weinberger used Fresnel's equations to calculate how much the direct and diffuse components of solar radiation would penetrate the surface of a pond as a function of time. He noted that absorption of light by salt solutions in distilled water did not differ significantly from that of distilled water alone, but that natural ocean waters had large differences in absorptivity. In his mathematical model he assumed that the solar pond would have an absorptivity identical to that measured for sea water over the continental shelf adjacent to the pond site.

Weinberger noted the important effects that ground water movement would have on heat loss in solar ponds. He found the time dependent temperature distribution in the pond by solving the one-dimensional heat diffusion equation, assuming thermal conductivity, heat capacity, and density all to be constant. He also assumed that the surface temperature was always equal to the ambient temperature and that the solution was everywhere nonconvective. He used his results to calculate the most efficient pond size for heat extraction at any given temperature from an Israeli type pond.

Weinberger was very concerned about the thermal stability of the solar pond. He found that while a positive density gradient was sufficient to stop ordinary convection, a stronger salt density gradient was necessary to prevent the growth of oscillatory motion. He concluded that a 0.34 gm/cm^4 $MgCl_2$ salt gradient was necessary to prevent convection and that a NaCl pond would be unstable if left alone. As discussed later in this chapter, his conclusion regarding the NaCl type pond has been shown experimentally to be too pessimistic.

C. Rabl and Nielsen

Solar pond research in this country started with the work of Rabl and Nielsen (25). They suggested inserting a homogeneous convecting layer of concentrated salt solution beneath the salt gradient for the purpose of heat storage and extended Weinberger's theoretical work to model this more general design. Their mathematical model is an exact solution to the one-dimensional (depth) heat equation assuming 1) time independent absorption varying with depth and 2) insolation and ambient

temperatures to be constants plus annually periodic sinusoidal terms. The pond steady state temperature for a given solar pond design is then given by a constant plus a sinusoidal term of yearly period whose amplitude and phase are determined by the amplitudes and phases of both the insolation and ambient temperature. They found a solution for the case of 1) complete insulation of the solar pond from the ground and 2) infinite ground storage, i.e. the pond, and the ground extending to an infinite distance from the pond, is considered to be in thermal isolation from the environment except for the surface of the pond; and heat is allowed to be exchanged between the pond and the ground according to the thermal conductivity and heat capacity of the ground. More recently Nielsen and Rabl (26) and Rabl (27) have studied the time dependence of convective instabilities in solar ponds. They apply Reynolds and Chilton-Colburn analogies together with Weinberger's stability criterion to determine conditions for growth and shrinkage of convective layers at the boundary with nonconvective thermohaline layers. More details of Rabl and Nielsen's theoretical analysis are given in Chapters III, IV, and V.

In June, 1974 Rabl and Nielsen (28) constructed this country's first experimental solar pond at Ohio State University in Columbus. Since then Nielsen has solved many of the practical problems associated with managing a solar pond. The first effort was a circular plastic backyard swimming pool with surface area of 24 m^2 which was converted into a solar pond. His method of filling this pond was to mix salt solution of the appropriate concentration in a small tank at the side of the pond. This solution was allowed to flow through a hose over a board that floated on

the surface of the pond. As the pond filled, the salt concentration was made smaller to obtain the correct density gradient. Flow over the board assures that the incoming water does not mix with the saltier water already in the pond.

In this small solar pond Nielsen would occasionally pump out water at various depths through a large hose to filter out leaves and other debris. After filtering, the water would be pumped back in at the depth it had been withdrawn. Occasionally this filtering process would cause the onset of small internal convection layers in the insulating layer of the pond (29,30). These internal convection layers do not appear naturally. The easiest method for dealing with an internal convection layer is to withdraw all of the fluid at that level, add enough salt to make it stay on the bottom of the pond, and inject it into the convecting layer. Once the thickness of the internal convecting layer is reduced to 2-3 cm, it disappears. A more unstable method is to pump high salinity liquid into the bottom of the internal convecting layer. Mixing of the injected liquid with the material of the layer occurs, resulting in part of the layer being replaced by gradient stabilized material (see Fig. II.5). One could also inject liquid of lower salinity into the upper part of the internal convecting layer with the same effect.

A common problem with solar ponds is the bloom of algae near the surface, which interferes with the transmission of sunlight to the bottom. Nielsen has found that copper sulfate solution sprayed over the surface of the pond adequately checks algae growth.

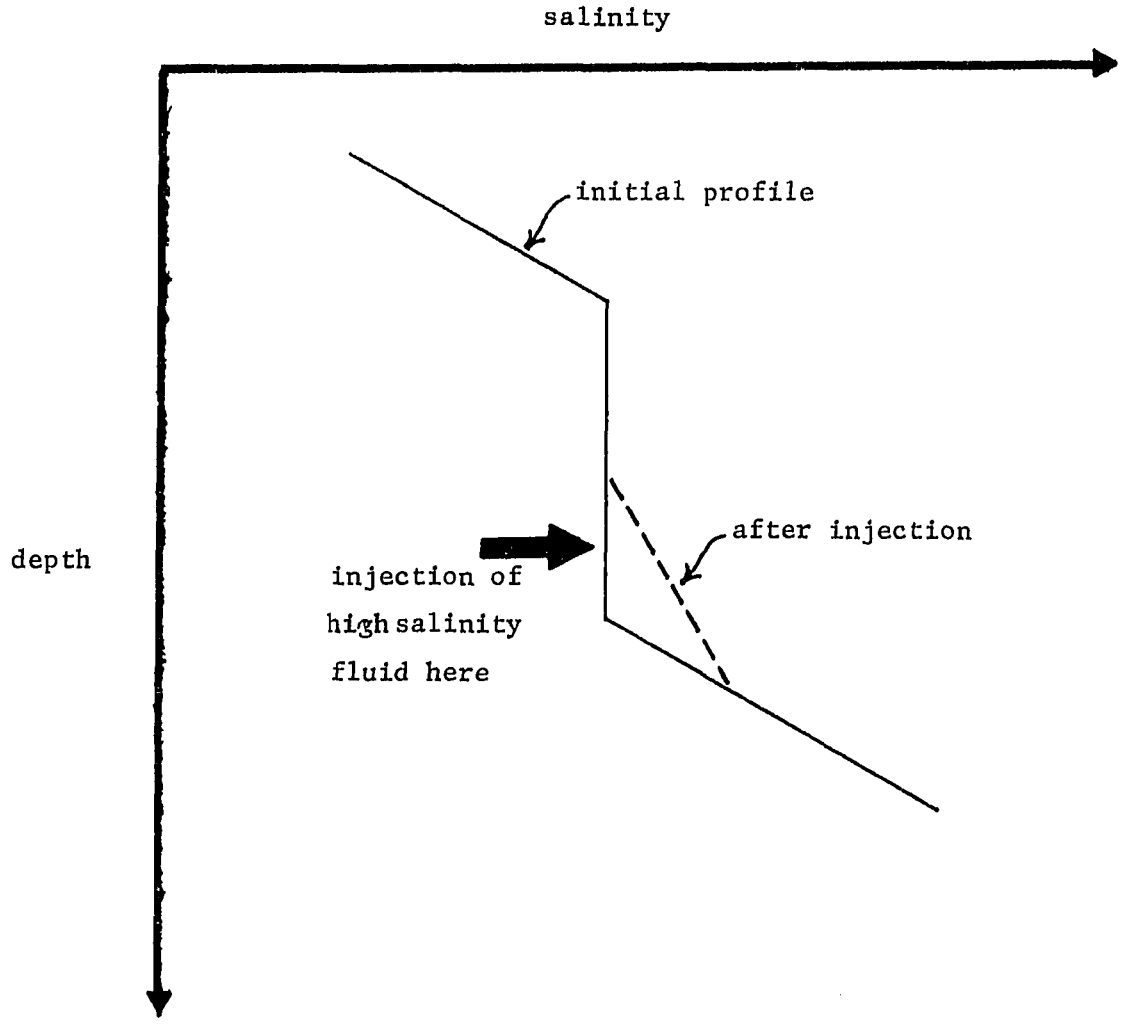

Fig. II.5. Effect of injection into an internal convection layer. Adapted from Nielsen (30).

Since the summer of 1975, Nielsen has also operated a 200 m^2 surface area solar pond at Ohio State. This solar pond was made by digging a hole in the ground, with the sides of the hole sloping at 45°. A black plastic liner was then laid over the hole, and the edges of the liner were buried in the ground around the hole. The pond was then filled with salt solution in the same way as the smaller pond. The sloping north wall of this type of pond often absorbs sunlight at almost normal incidence. This causes local hot spots and small local convection areas that disappear at night. The largest effect this has is a marked increase in salt transport from the convecting layer to the surface along this north wall. This could be eliminated by shading the north wall or by making that part of the liner more reflective. Since Nielsen has been primarily interested in internal convection layers, he has not tried to obtain maximum temperatures. Nevertheless the temperature in the convecting layer of this solar pond reached 62° C in June, 1976 and 69° C in August, 1977.

Nielsen has studied equilibrium thickness of the insulating layer, which is governed by the balance between salt diffusion upward and erosion at the boundary from fluid movement in the adjacent convecting layer (31). He has discovered an empirical relation between the temperature gradient G_T and the salt gradient G_C for layers at equilibrium, namely G_T/G_C^2 = constant (32). Nielsen has also shown that the lower boundary of the insulating layer will lower until it coincides with the depth of any heat exchanger that is removing heat from the convecting layer.

D. Other Solar Pond Research

Recently the most thermally successful solar pond has been one located at the University of New Mexico in Albuquerque, which was filled in November, 1975 (33). This pond is identical in design to Nielsen's 200 m^2 pond, but has a surface area of 175 m^2. The pond obtained a maximum temperature of 93° C in late August, 1977. During the winter of 1977-8, heat was extracted from the pond to simulate heating a typical Albuquerque home.

A solar pond has been operated at Wooster, Ohio to provide heat for a greenhouse (34,35). This pond is 8.5 m wide, 18.3 m long, and has straight wooden sides which make the pond 3.6 m deep. The pond walls and bottom were initially in direct contact with the ground, and the pond was only able to obtain a temperature of 46° C due to heat loss to underground water flow. The pond liner hung on the vertical walls and started leaking salt water to the ground. The pond was rebuilt with styrofoam insulation underneath the pond bottom and a drainage tile leading to a sump underneath the insulation to detect any further salt leakage (36).

Publicized work on solar ponds in the U.S.S.R. has consisted of some theoretical analysis and experimental results from small laboratory $MgCl_2$ ponds during the period 1969-73. The theoretical work consisted of a review paper (37), a study of spectral transmittances of $MgCl_2$ solutions (38,39), and a study of thermal behavior in ponds (40). The optical work is interesting in that it reports a significant increase in radiation absorption with increasing $MgCl_2$ concentration, whereas

NaCl solution concentration has little effect on absorption. The study on thermal behavior used a one-dimensional heat conduction equation model which was solved by the method of finite differences. This model also attempted to take account of the surface heat losses from convection, evaporation and radiation. The first experimental pond was a 40x40x50 cm insulated tank, which used a xenon lamp as a heat source to verify the theoretical model of thermal performance (41). The second experimental pond had a surface area of 4.8 m^2 and was 18 cm deep. This also used a xenon lamp as a heat source, but this pond was placed in the ground to check the theoretical model for the case when ground storage was desirable (42). The Russian work concluded that solar ponds could easily be modeled with finite difference methods.

A solar pond operated successfully at a salt works in India during the period 1970-2 (43). This pond was 55x22x1 m and was filled with bitterns (salt produced by the stage evaporation of sea water or brine after NaCl has been removed from the solution). The sides were brick masonry covered with gypsum. The bottom earth was covered with polyethylene film. This pond was estimated to collect solar energy at over 20% efficiency. After the pond reached a temperature of 80° C in April, 1972, heat was extracted from it at various intervals. The maximum temperature achieved in 1972 was 84° C.

Dake (44) at the University of Zambia in Lusaka was the first to attempt an analytical expression for the time dependent temperature behavior of a solar pond with a convective layer on the bottom. He was also aware of the need to treat the top part of the pond as a convective

layer. His solution assumed constant solar insolation and constant surface heat loss, which is reasonable for tropical locations such as Zambia.

In 1974 a solar pond was successfully field tested at the Brace Research Institute in Canada (45). This pond was 3.66 m in diameter, 75 cm deep, had 13 cm of urethane insulation sprayed on the steel walls of the tank, and had 30 cm styrofoam blocks beneath the tank. The pond was covered with two plastic membranes, one floating on the surface of the water, and one covering the entire pond. After filling was completed on July 4, the temperature at the bottom of the pond reached 78° C after 17 days and was 19° C the following November.

The first commercial user of a solar pond was John Shuette of Columbus, Ohio (46). He first used his 8x25 m solar pond to help heat his house during the winter of 1976-7. In August, 1978 the city of Miamisburg, Ohio finished filling a 2000 m^2 solar pond to heat water in an outdoor swimming pool in the summer and to provide heat to an adjoining public recreational building all year long (47).

A small laboratory solar pond has been successfully operated using KNO_3 as a salt (48-50). KNO_3 differs from NaCl or $MgCl_2$ in that its solubility increases dramatically with temperature. This means that a totally saturated KNO_3 solution would be naturally stable in a solar pond. The hotter bottom layers would always be denser than the cooler layers above them, since more KNO_3 would be dissolved in the hotter layers. As long as the bottom layers remained hotter than the upper layers, the pond would be naturally stable. Unfortunately the solubility

of KNO_3 at 100° C is 2.47 gm/cm^3 which means a large quantity of salt would be needed to achieve saturation, making the cost prohibitive.

The problem of stability in the insulating layer is important. A large percentage of the cost of solar ponds is in the initial cost of the salt. The lower the concentration of salt in the convecting layer, the lower the cost of the pond. As mentioned above, Weinberger's work indicated that even a saturated NaCl solution gradient might not be stable at high temperatures. Experimental NaCl ponds have shown this not to be the case. Recent work by Elwell et al. (51) suggests that maximum NaCl concentrations as low as 12% will maintain a stable insulating layer with temperatures as high as 100° C. This calculation includes the variation of the salt's physical parameters (viscosity, density, and thermal conductivity) with both temperature and concentration. Weinberger had assumed these parameters to be constant.

E. Market Penetration

Experimental work on solar ponds to date has consisted of building and testing prototype models. Most of these prototype ponds have been successful. As discussed above, solar ponds are starting to appear in use by the consumer public and have been suggested for climates as diverse as Israel and England (52). Although low temperature heat production costs from solar ponds is already economically competitive with other processes, the land space requirements, large edge surface area, and unfamiliarity of the device make it currently unattractive to most homeowners. Solar ponds have the best chance of market penetration in rural areas and as heat sources for clusters of residential units,

where larger ponds will make any side losses small, and maintenance can either be shared collectively or done professionally. Another commercial possibility would be for a utility to operate a large solar pond and charge phase change salt canisters in the bottom convecting layer. This would keep the convecting layer temperature down to that of the temperature of the phase change, reduce the temperature gradient, thereby lowering the amount of heat escaping through the insulating layer, and improving the thermal efficiency of the pond. The canisters could be sold to customers throughout the winter. Such a scheme would probably be most commercially feasible in an area where salt was readily available, such as the Great Salt Lake in Utah.

Another barrier to market penetration is the expense of filling the pond. Several methods have been devised to eliminate the separate mixing tank. A method developed by Zangrando and Bryant (33) is to fill the pond half way with concentrated salt solution. On top of this, fresh water is gently poured. Next, solutions are withdrawn from both the upper and lower layers, mixed in a Y hose fitting, and injected back into the pond between the previous two layers. This results in three layers: the concentrated salt solution on the bottom, a layer of half concentrated salt solution on top of this, and the fresh water layer at the top of the pond. The process is repeated between any two layers to produce as many layers as desirable. Initially there are a number of distinct layers, but after a few weeks, salt diffusion produces a continuous gradient. This method eliminates the need for a separate mixing tank, but still requires a large time investment. Most of the ponds to date

have taken several weeks to complete filling, with the majority of this time spent in dissolving the salt. If solar ponds are to become commercially viable, a filling technique must be devised that does not require a large outlay of either time or manpower.

A more serious problem for the commercialization of solar ponds is the possibility of salt contamination of the environment. Normal salt runoff from the surface of the pond, as well as irresponsible solar pond decommissionings, both are potentially large sources of salt pollution. The major danger of salt pollution is the detrimental effect of salt in drinking water to people susceptible to hypertension and other salt related diseases, and the damage to vegetation caused by overly salty soil. Salt damage may not show up until several years after the salt application, due to the slow movement and persistence of sodium in soils. It is estimated that in 1971 approximately 10^{10} kg of sodium chloride was placed on the highways of the U.S. (53). In some locations 10^{5} kg/lane km were applied. In places of high salt application, groundwater salt concentration was often so high that municipal water wells were contaminated and roadside vegetation killed (53,54). With the density of sodium chloride in solar ponds on the order of 500 kg/m^2, salt leakage from solar ponds can only exacerbate this problem. The problem of salt runoff can be dealt with by having it flow through an evaporating tank, but these costs, and any other associated environmental costs must be included in any economical analysis of solar ponds.

F. Other Types of "Solar Ponds"

Several other configurations have been suggested as alternatives to a salt gradient solar pond. A very similar concept to the salt gradient pond is that of a gel pond (18). In a gel pond the insulating layer is a gel substance which floats on top of the bottom convecting layer. The gel is a substance which is transparent to visible light and is viscous enough that convection does not occur. To date no experimental gel pond has been built.

A different type of collection and annual storage device is the underground pool connected to a traditional collector. An example of such a device is the one constructed in 1976 at the University of Virginia (55). This device consists of a tank of water buried in the ground. A large number of styrofoam beads float on the surface of the water. A flat plate collector is placed above the tank, and when the sun is shining, water is pumped from the tank and allowed to trickle down over the plate of the collector. The heated water then falls down through the styrofoam beads back into the tank.

In the literature plastic covered shallow water trenches are often referred to as "solar ponds" or "shallow solar ponds" (56). These ponds, often suggested as devices for supplying low temperature heat, should not be confused with salt gradient solar ponds; they use fresh water, or circulate brine in a tube at the bottom of fresh water, and do not use a salt gradient to suppress convection. Heat collected is used on a short term basis with no seasonal storage.

III. MATHEMATICAL MODEL OF SOLAR POND THERMAL BEHAVIOR

A. Introduction

In this chapter the physical concepts necessary to adequately predict the thermal performance of solar ponds are developed. As mentioned in Chapter II, Weinberger (24) and later Rabl and Nielsen (25) found exact solutions to solar pond heat flow in several limiting cases. This chapter borrows heavily from their results, but departs from their approach of finding an exact solution. Rather, the mathematical model is developed to the point where the solar pond heat flow can be adequately expressed by a simple iterative computer program. This approach results in the ability to predict the thermal behavior of solar ponds in a wide variety of circumstances and applications.

B. Solar Radiation Input

1. Penetration of the surface

Solar radiation incident on a horizontal portion of the earth's surface, which has been and is being measured at many geographical locations, is an input parameter to the solar pond model. The amount of this radiant energy penetrating the air/water interface at the surface of the pond varies with the angle of incidence according to Fresnel's equations (57). As shown in Fig. III.1 below, the incident wave is polarized with the electric field vector either parallel or perpendicular to the plane of incidence. The energy transmission coefficient for an incident plane wave polarized with its electric field vector parallel to the plane of incidence is

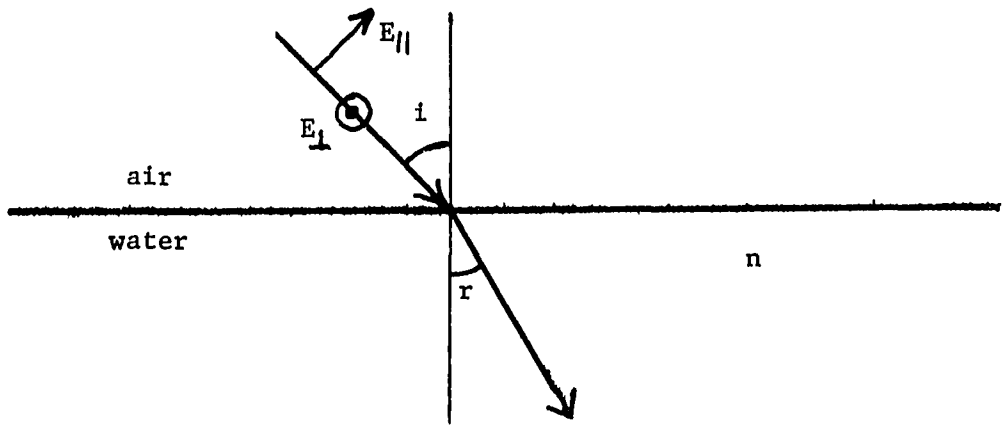

Fig. III.1. Schematic of solar pond air/water interface. ↗ represents the electric field parallel to the plane of incidence. ⊙ represents the electric field perpendicular to the plane of incidence.

$$T_{\parallel} = \frac{4n \cos i \cos r}{(\cos i + n \cos r)^2}, \qquad \text{(III.1)}$$

where n is the index of refraction of water, i is the angle of incidence, and r is the angle of refraction. i and r are related by Snell's law

$$\sin i = n \sin r. \qquad \text{(III.2)}$$

The energy transmission coefficient for an incident plane wave polarized with its electric field vector normal to the plane of incidence is

$$T_{\perp} = \frac{4n \cos i \cos r}{(n \cos i + \cos r)^2}. \qquad \text{(III.3)}$$

Direct insolation at the earth's surface is unpolarized, and hence (III.1) and (III.3) may be combined to get a total transmission coefficient for direct insolation

$$\tau = 2n\,(a^2 + b^2) \cos i \cos r, \qquad \text{(III.4)}$$

where

$$a = 1/(\cos r + n \cos i), \tag{III.5}$$

and

$$b = 1/(\cos i + n \cos r). \tag{III.6}$$

The angle of incidence i for direct insolation is derived simply:

$$\vec{x}_{pond} = (\cos L,\ 0,\ \sin L),$$

$$\vec{x}_{sun} = (\cos D \cos(2\pi t_h/24),\ \cos D \sin(2\pi t_h/24),\ \sin D),$$

where $\vec{x}_{pond}$ and $\vec{x}_{sun}$ are unit position vectors of the pond and sun respectively in a coordinate system with origin at the center of the earth, with the earth's axis in the $\hat{z}$-direction, and the solar pond longitude in the $\hat{x}$-direction as shown in Fig. III.2. L is the latitude of the solar pond, D is the declination of the sun, and t_h is the time in hours with noon = 0.

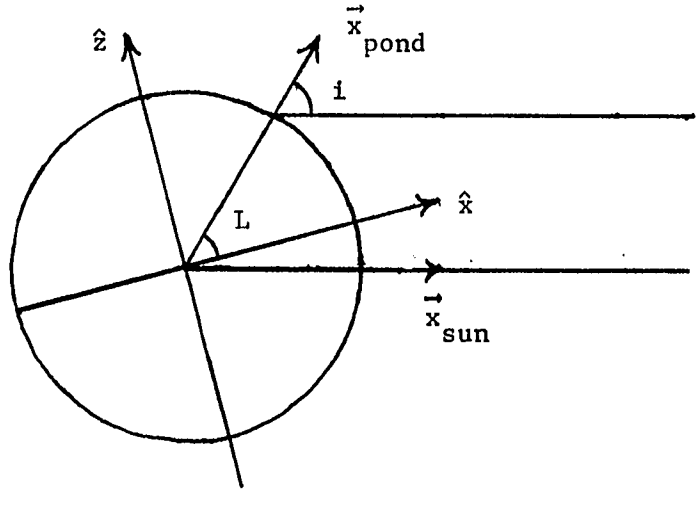

Fig. III.2. Coordinate system to calculate the angle of incidence of direct insolation for the solar pond.

The earth's orbit about the sun is an ellipse, but it is almost circular, so that a useful approximation for the declination D of the sun is (24)

$$\sin D = \sin(23^\circ\ 27')\ \cos(2\pi t/365),$$

where t is the time in days from June 21.

The angle of incidence i may be calculated from

$$\cos i = \vec{x}_{pond} \cdot \vec{x}_{sun}$$

$$= \cos L\ \cos D\ \cos(2\pi t_h/24) + \sin L\ \sin D. \qquad \text{(III.7)}$$

Wave action at the surface will change the angle of incidence over the surface of the wave. However, the deviation from the Fresnel formula in these cases appears to be small when time averaged (58).

Diffuse sky radiation is due to scattering of both direct and ground reflected solar radiation by air molecules and dust particles in the atmosphere. The ratio of daily diffuse radiation to the daily total radiation on a horizontal surface varies from a maximum 1.0 for a completely overcast day when all the radiation received is entirely diffuse radiation, to a minimum of 0.16 for a clear day (59). Since few data exist for diffuse radiation, the amount of diffuse radiation is estimated from total radiation and cloud indices when such information is available, and ignored when such information is not. The spatial dependence of diffuse radiation varies considerably, depending on atmospheric conditions, position of the sun, azimuth angle of observation, and wavelength of radiation. Most researchers assume it to be isotropic, and that is what is done here.

2. Absorption in salt water

The solar radiation penetrating the surface of the solar pond will be absorbed by various amounts at different depths depending on the angle of incidence, wavelength of radiation, and the dispersion of living organisms and "junk" throughout the pond. Absorption of light by organisms and junk greatly degrades the thermal performance of the pond, but both are easily controlled, and their effect will be assumed negligible.

The spectral distribution of solar radiant flux at the pond surface will in general depend upon the state of the sun and prevailing atmospheric conditions. Sunspot activity changes slightly the spectral distribution of light emitted from the sun. The presence of water vapor causes changes in the amount of light absorbed in the atmosphere for certain wavelengths. Dust and cloud cover change the percent of diffuse radiation. If the spectral distribution at the surface is known, one may use this data as input into the solar pond model. Usually however, the only solar radiation data available is the total insolation on a horizontal surface. In this case one assumes the spectral distribution to have the same form as the standard solar irradiance curve (60) as shown in Fig. III.3 below.

Radiant energy when passing through water is attenuated by absorption and scattering. Scattering is insignificant in attenuation compared to absorption. Down to several meters below the surface, a beam of light is reduced about an order of magnitude in intensity 3° from the central beam and more than two orders of magnitude at 9° from the central

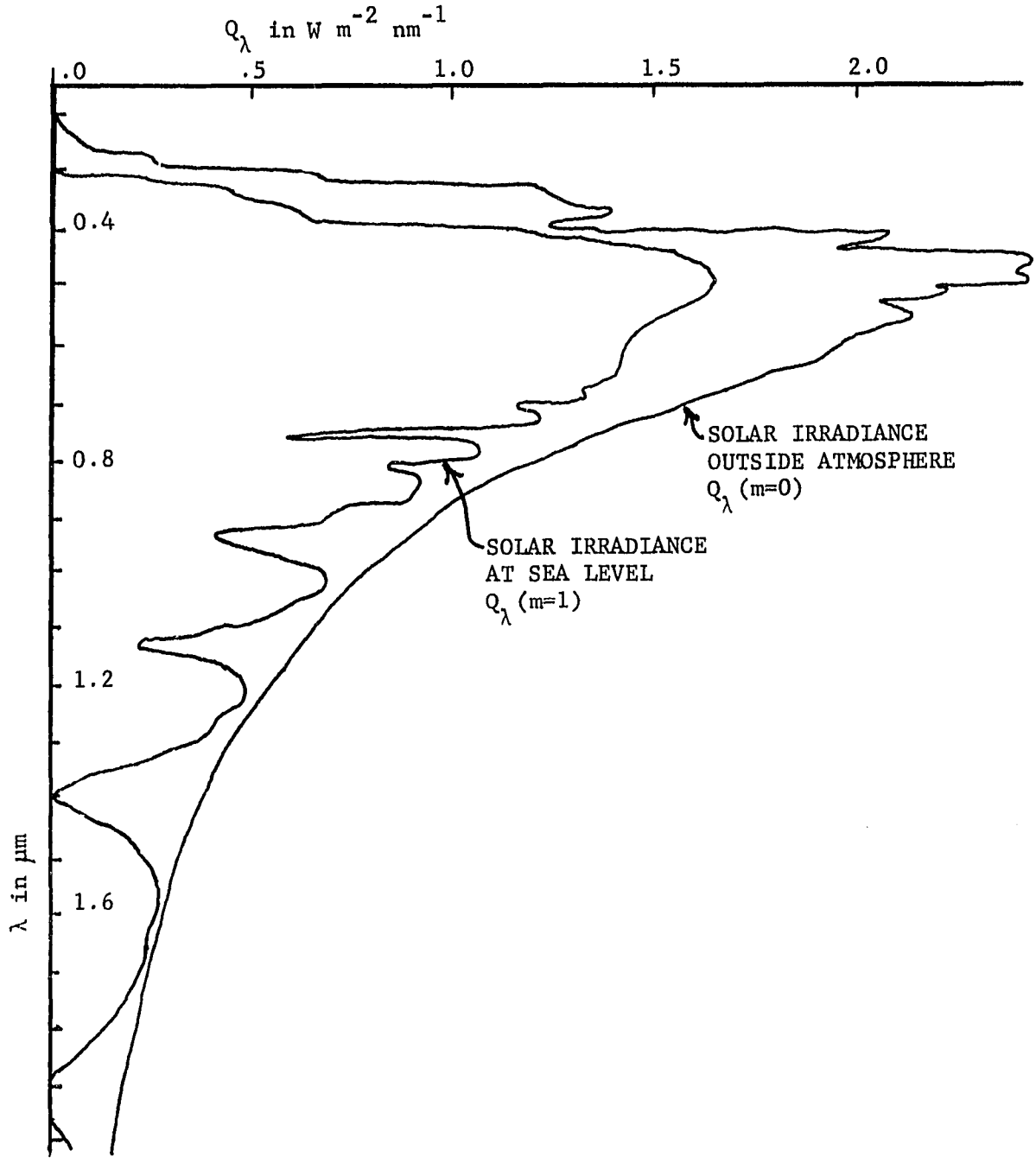

Fig. III.3. Spectral distribution of solar irradiance. Adapted from Thekaekara (60).

beam (61).

The intensity of a beam of radiation at a fixed wavelength λ at any depth is

$$I_\lambda(x) = I_\lambda(0)\, e^{-x/\delta}$$

or

$$I_\lambda(x) = I_\lambda(0)\, e^{-\mu x}$$

where $I_\lambda(x)$ is the intensity of the beam for wavelength λ, x is the distance the beam has traveled in water, $I_\lambda(0)$ is the beam intensity that penetrates the surface, δ is the characteristic attenuation length, and $\mu = 1/\delta$ is the effective attenuation coefficient.

Differences in scattering between pure water and sea water are small (62). The attenuation of electromagnetic energy in sea water is shown in Fig. III.4. One of the unique characteristics of water is that water is most transparent in the part of the spectrum where the sun's radiation is most intense, and drastically more opaque in nearby regions of the spectrum. A detailed graph of pure water electromagnetic energy attenuation at wavelengths where solar radiation is appreciable is shown in Fig. III.5. The measurement is difficult in the most transparent part of the spectrum, and there is some disagreement between experiments there. Following the recommendation of Jerlov (61), I have chosen the results of Clarke and James (63) for the region $325 \leq \lambda \leq 800$ nm and the results of Curcio and Petty (64) for the region $800 \leq \lambda \leq 1300$ nm.

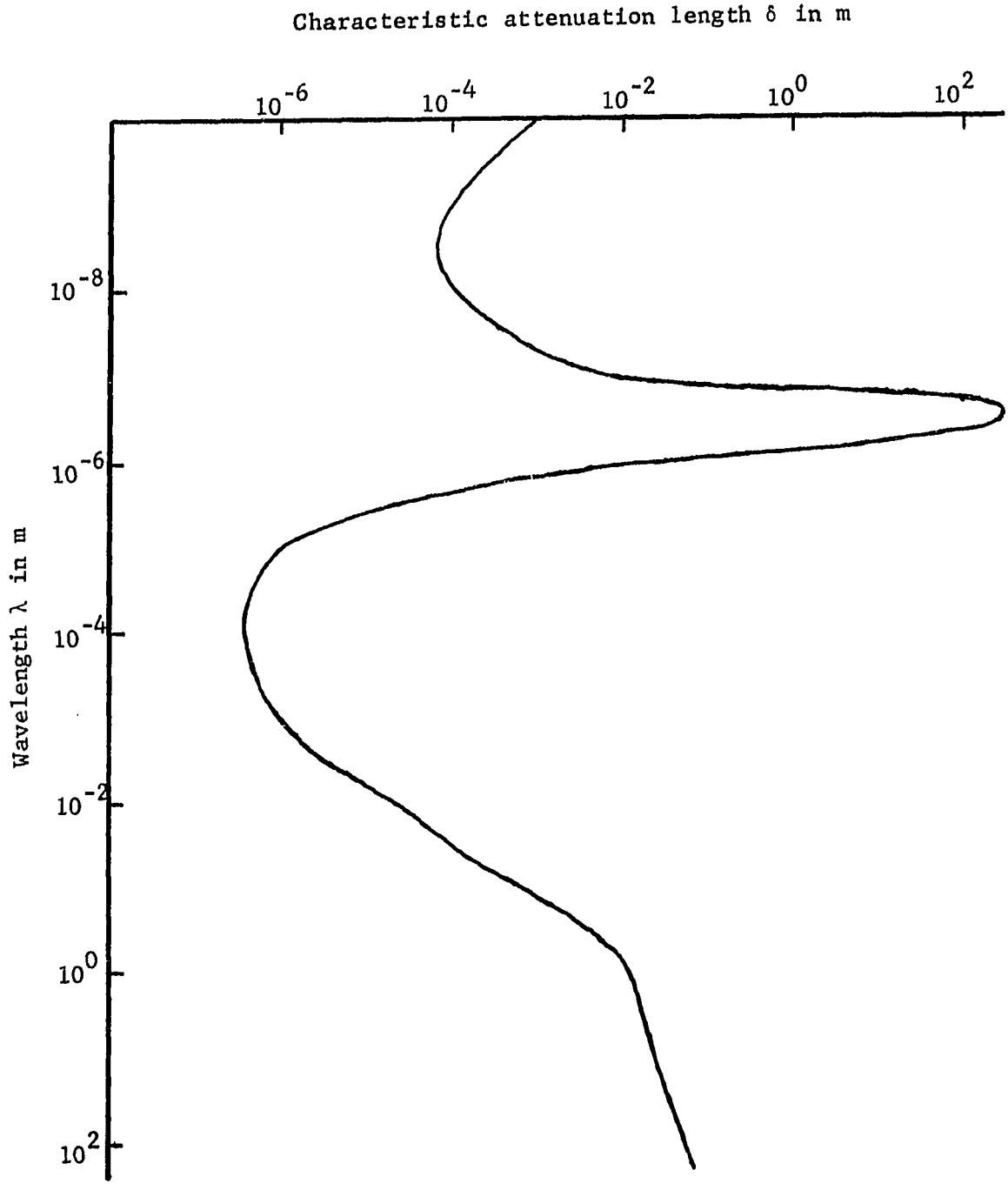

Fig. III.4. Attenuation of electromagnetic energy in seawater (61).

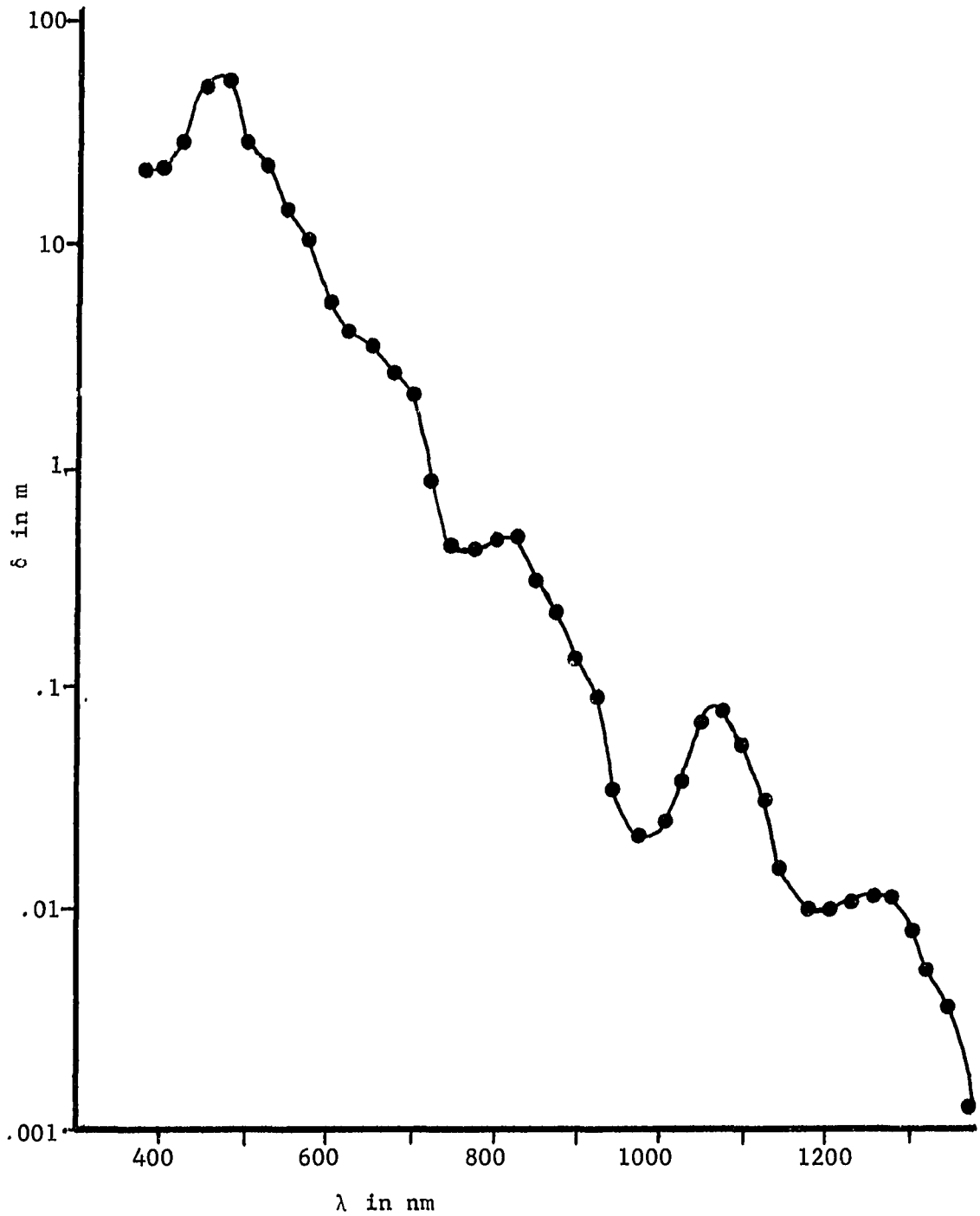

Fig. III.5. Characteristic absorption length δ versus wavelength λ for pure water.

We may combine the data in Fig. III.3 and Fig. III.5 to get the total intensity of a direct solar beam integrated over all wavelengths I(x) at any path length x. I(x) is calculated as follows: All radiation with $\lambda \geq 1312.5$ nm is assumed absorbed at the surface. The rest of the spectrum is divided into 25 nm bins with the first of 40 bins centered at λ = 325 nm, and the last bin centered at λ = 1300 nm. $I_\lambda(0)$ is calculated from Fig. III.3 as the value Q_λ for the wavelength at the center of each bin. $I_\lambda(x)$ is then calculated for each of the λ and for each x of interest. I(x) is the sum over all λ of $I_\lambda(x)$. The results are shown in Table III.1. I(x) is normalized so that I(0) = 1.0.

Table III.1. Energy transmission as a function of path length for pure water.

path length (m)	Fraction transmitted
0.0	1.000
0.1	.649
0.2	.599
0.3	.568
0.4	.545
0.5	.526
0.6	.511
0.7	.498
0.8	.487
0.9	.477
1.0	.468
1.2	.453
1.4	.440
1.6	.428
1.8	.418
2.0	.408
2.2	.399
2.4	.391
2.6	.383
2.8	.376
3.0	.369
3.2	.363

In solar pond modeling we assume that the transmission of sunlight through a sodium chloride solution is the same as that through pure water. This assumption is somewhat questionable, since measurements of the absorption coefficient in magnesium chloride solutions (39) show a strong increase in absorption with increasing magnesium chloride concentration, especially in the visible, where most of the available solar pond energy is. However, as mentioned above, there is little difference in the absorption coefficients of pure water and sea water. The salt in sea water is mostly sodium chloride, and so it is likely that a sodium chloride solution will have nearly the same transparency as that of pure water. Until measurements of the absorption coefficient for sodium chloride solutions are made, the assumption we have adopted is probably the best one.

C. Heat Flow within the Solar Pond

1. Radiation

The temperature at which a solar pond boils is a boundary condition on any model and must be avoided in a real pond to prevent convection. The boiling point of a saturated NaCl solution at sea level is 108.7° C, while that of a saturated $MgCl_2$ solution is 125.5° C (see Sec. F of Appendix A). Thus the maximum water temperature is less than 400° K. The blackbody radiation from the pond is hence in the infrared, which is completely and immediately reabsorbed by the water.

Wien's law gives us the wavelength of the radiation

$$\lambda_{max} = b/T,$$

where λ_{max} is the wavelength of the maximum radiation from a black body

at absolute temperature T and

$$b = 2.9 \times 10^{-3} \text{ m K°}.$$

For T = 400° K, $\lambda_{max} = 6.75 \times 10^{-6}$ m. From Fig. III.4 we see that most of this radiation is absorbed 10^{-4} m to 10^{-6} m from its source.

We can calculate the heat energy transferred by radiation over this distance by taking the spatial derivative of Stefan's law

$$dP/dx = 4\sigma T^3 \, dT/dx,$$

where dP is the power per unit area transferred by the radiation, T is the absolute temperature, and

$$\sigma = 5.67 \times 10^{-8} \text{ W m}^{-2} \text{ K°}^{-4}.$$

In a solar pond

$$dP = 4\sigma T^3 \, \Delta x \, dT/dx,$$

which, if we choose $\Delta x = 10^{-4}$ m and T = 373° K, becomes

$$dP = (.0012 \text{ W m}^{-1} \text{ K°}^{-1}) \, dT/dx.$$

We may compare this to the energy transferred by conduction using the heat conduction equation

$$dP = k \, dT/dx = (.587 \text{ W m}^{-1} \text{ K°}^{-1}) \, dT/dx.$$

These calculations indicate that for the purposes of the model, it can be assumed that infrared radiation is negligible in the interior of the solar pond.

2. Convection

It is assumed that the salt gradient is stable and sufficient to prevent heat transfer by convection in the insulating layer. This is necessary for the successful operation of the solar pond. Stability of the salt gradient is discussed in Chapter V.

In the convective layer, water heated at the bottom of the pond will rise until it reaches the salt gradient. This produces a stagnant temperature inversion, with the top of the convecting layer possibly at most 5° C warmer than the bottom of the pond (30). This inversion could probably be eliminated when heat is extracted at the top of the convecting layer. At any rate, a difference of several degrees is small when compared with other uncertainties of the model, e.g. the transparency of the water. In the mathematical model it is assumed that the entire convecting layer is of uniform temperature. Heat extraction is assumed to be small enough that no significant local temperature changes occur.

3. Conduction

Conduction is the mechanism by which most of the heat is transferred within the solar pond. The direction of this transfer is in general upwards from the convecting layer to the surface through the insulating layer. The computer model (see Chapter IV) handles this transfer by dividing the insulating layer into thin sublayers that are assumed to be of uniform temperature. The temperature of the sublayer is assigned to the sublayer's nodal point, located at the physical center of the sublayer. The conduction of heat between two adjacent sublayers, ΔH, in time Δt, is given by

$$\Delta H = K_w A(\Delta T/\Delta x)\Delta t, \qquad \text{(III.8)}$$

where K_w is the thermal conductivity of water, a function of both temperature and salinity, A is the area of the sublayer, ΔT is the temperature difference between the adjacent sublayers, and Δx is the distance between the nodes of the adjacent sublayers.

As described in the next chapter, this approximation is reasonable when there are enough sublayers to give an adequate temperature profile of the insulating layer, and the time interval of the iteration step is small enough that the sublayer temperature change per iteration is smaller than the temperature difference between sublayers.

D. Heat Flow Out of the Solar Pond

Heat is conducted through the bottom and side walls of the solar pond. Usually the walls of the pond will be surrounded by earth, and if there is little ground water flow, then that earth may be used as additional heat storage. Conduction through the walls is handled similarly to conduction in the insulating layer with (III.8), except that $\Delta T(z) = T_p(z) - T_g(z)$ where $T_p(z)$ is the temperature of the pond at depth z, and $T_g(z)$ is the corresponding ground temperature. This time in (III.8) Δx is the width of the wall, and K_w is now the thermal conductivity of the wall instead of water.

Since the solar pond at Living History Farms is located in an area of high water table and large ground water flow, a ground storage option was not incorporated into the model. Any heat passing from the pond through the insulation to the ground water is assumed lost. The ground water temperature is assumed constant, since it varies by only a few degrees throughout the year at the depth equivalent to the bottom of the pond. The thermal mass of the pond walls and insulation is negligible compared with that of the rest of the pond and is ignored in the model. For cases where ground storage is possible, additional sublayers would have to be added to the model. The sublayers would have to be placed

below and to the side of the water sublayers and would have the physical parameters of the surrounding soil. Heat would flow vertically and horizontally between all adjacent sublayers in each iteration step.

Heat may be removed from the convecting layer through a heat exchanger to deliver heat to a load, e.g. to provide space heating or to dry grain. It is assumed that the heat exchanger can remove as much heat as it needs at any given time. In real situations this would be true if the heat exchanger were connected to a heat pump, but would be limited to extracting heat only when the pond temperature was above some critical temperature, if a simple circulating loop were used. As in the case of conduction between sublayers in the insulating layer, one must be careful that the heat load is not so high as to draw down the temperature of the convecting layer too fast between iteration steps.

Heat may also flow out of the pond at the pond surface. Heat is lost from the surface primarily by evaporation, wind convection, and far infrared radiation to the sky. Since in general the physics of the air/water interface is complex and is not well-understood (65,66), many simplifying assumptions are made to make the interface tractable. Some formulations for this heat flow have been attempted (e.g. (40)), but they usually depend on weather data, such as humidity and cloud cover type, that are usually not readily available.

Weinberger (24) makes the following argument to determine the solar pond surface temperature: Experimentally it is known that the mean daily temperature of the sea is generally a few degrees warmer than the mean daily ambient air temperature. However, heat lost at the surface of the

sea is rapidly replenished from below via both conduction and convection, while in solar ponds, heat lost from the surface is only replenished via conduction. Therefore, one expects the surface of a solar pond to be slightly colder than the surface of the sea, and it is then quite reasonable to assume that the solar pond surface temperature is equal to that of the ambient air. Other researchers (25,33) also make this assumption.

The large surface absorption of sunlight during the day and surface radiation to the night sky cause a large daily temperature swing in the top few centimeters of the solar pond. This, together with wind mixing, causes a convection layer at the top of the pond that extends downward about 10 cm below the surface. Detailed modeling of such behavior would be difficult. In the computer program, we follow the example of other researchers and let the surface temperature equal that of the ambient air. Any heat reaching the surface is then permanently lost to the system. The temperature fluctuations at the surface have little effect on the long term heat flow through the insulating layer, hence it is justifiable to use the average temperature of the top sublayer. If anything, this assumption probably leads to a slight underestimate of the thermal performance of the solar pond.

So far all solar ponds in this country have formed surface ice in the winter (29,33). This degrades the thermal performance of the solar pond; since the thermal conductivity of ice is about 3.7 times that of water, the heat capacity of ice is about half that of water, and ice is much less transparent to visible radiation than water. In practice the ice thickness is always less than that on a fresh water pond, and

there is not yet enough data available to successfully predict ice formation and ice thickness in solar ponds as a function of time and/or immediate weather conditions. In addition, when ice forms, its transparency varies considerably depending on the conditions of formation. If ice thickness and transparency are known, then they can be incorporated into the model by suitable changes in the physical parameters (e.g. thermal conductivity and transparency) of the upper sublayers. If it is not known, the computer model escapes dealing with the problem by pretending that the ice is not there. This assumption is probably not too bad as far as radiation input is concerned, since insolation is low, and Fresnel reflection losses are high during those times that ice formation is likely. However, the assumption certainly leads to an overestimate of the thermal performance of the pond somewhat in the winter.

A transparent plastic membrane is often suggested for the top of solar ponds. A cover has the advantage of eliminating evaporation and wind convection and adds about 5% to the thermal resistance of the insulating layer. It has the disadvantage of reducing the input radiation by at least 5%, and, as shown in Chapter V, does not stop the formation of the surface convective sublayer. A cover could be included in the model by including an additional sublayer at the top of the pond with the correct thermal conductivity and heat capacity. The radiation input to the pond would have to be reduced by an additional set of Fresnel reflections, as well as additional absorption by the cover. Due to the questionable economic feasibility of a cover, this option has been left out of the computer model.

IV. COMPUTER MODEL OF SOLAR POND THERMAL BEHAVIOR

A. General Features

The mathematical model of solar pond thermal behavior which was detailed in the last chapter has been implemented in a PL-1 iterative computer program. In this model the solar pond is divided into horizontal sublayers. The convecting layer is one complete sublayer, while the insulating layer is divided into a number (user specified) of sublayers, each of a user specified depth. Each sublayer is in thermal contact with each adjacent sublayer and with the surrounding environment. A thermal network diagram of this model is given in Fig. IV.1 below.

The computer program starts with an initial temperature distribution at some fixed date; and given typical insolation and ambient temperature data for the location considered, calculates the heat exchanged between adjacent sublayers and between the sublayers and the surroundings and predicts the temperature at all levels in the pond at any time for any heat withdrawal scheme. The general features of the computer model are discussed in this section, and a current listing of the program is given in Appendix B. Section B discusses the viability of a few variations and simplifications to the program and compares the program to some other theoretical models of solar pond thermal behavior. In Section C an example of the use of the program in the solar pond design for Living History Farms is discussed. In Section D the computer model is used to discuss the potential of the solar pond as a heat source for grain drying.

The logic flow of the computer program is given in Fig. IV.2 below. The first major section is input of data parameters. First, the solar

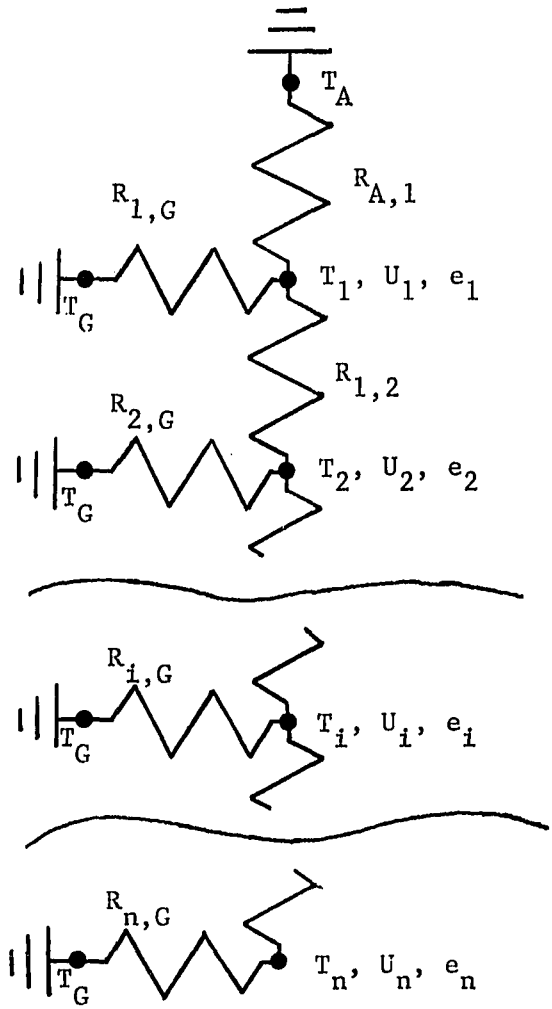

Fig. IV.1. Thermal network diagram of solar pond computer model. T is the temperature at each node. U is the heat energy stored at each node. e is the solar energy absorbed or energy taken away by the load at each node. $R_{i,j}$ is the thermal resistance between adjacent nodes i and j.

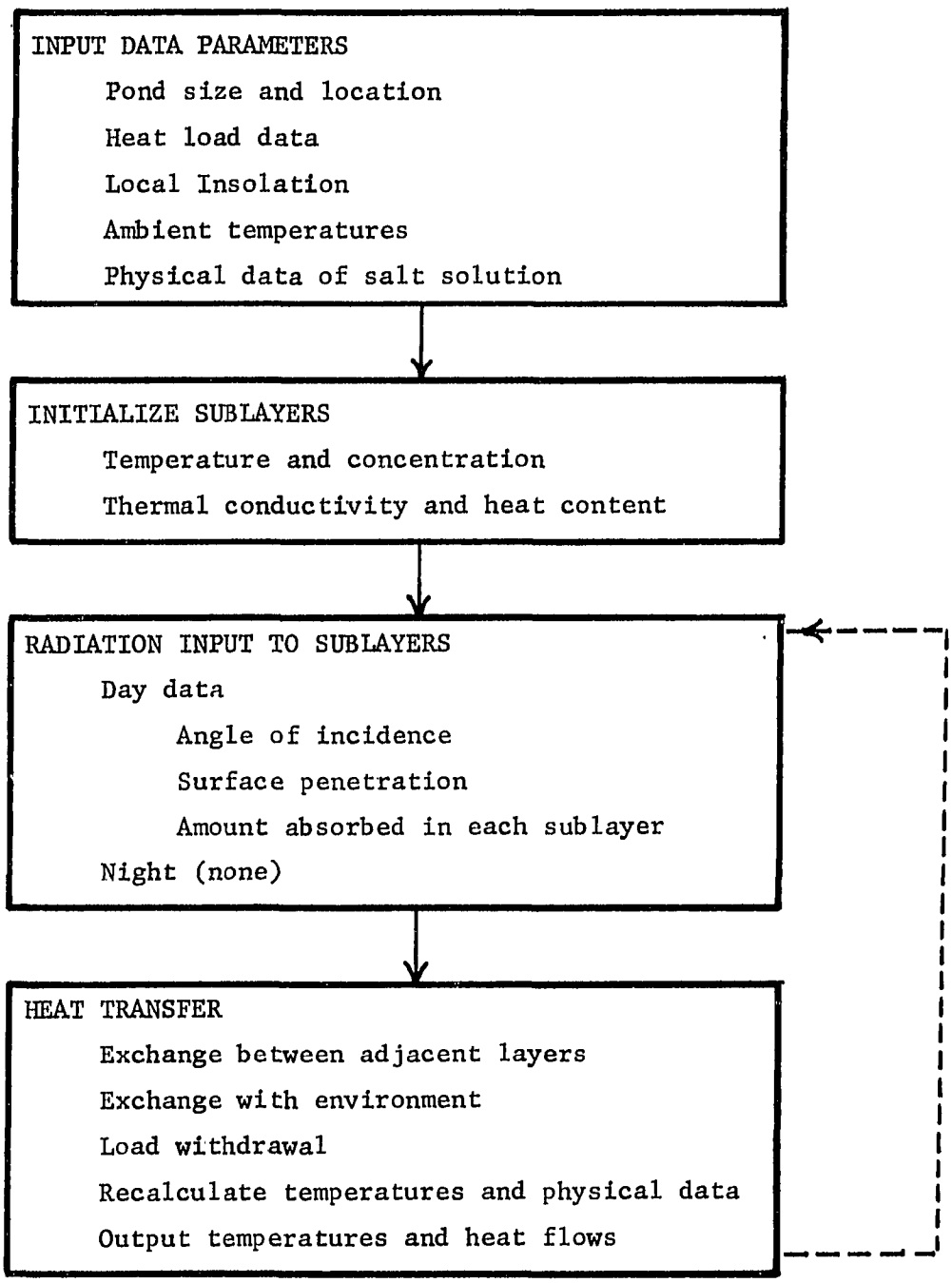

Fig. IV.2. General logic flow of solar pond computer model.

pond design parameters of surface area, number and depth of insulating layer sublayers, depth of the convecting layer, thickness and thermal conductivity of the sides, and type of salt used are specified. Next, the environmental conditions are specified. These include the latitude, load temperature, heat load in W/C°, ground temperature, hourly ambient temperature, and insolation data. Then the initial temperature and salt concentration of each solar pond sublayer are specified. The last data input is the physical parameters of salt solutions, which includes density, thermal conductivity, and heat capacity.

The second section of the program is the initialization of each solar pond sublayer. The program calculates the salt solution physical parameters and initializes the heat content of each sublayer. After initialization, the program begins an iterative loop to calculate heat transfer both within the solar pond and in exchange with the environment. The iteration loop comprises sections three and four of the program. Each iteration represents one hour in real time.

The third major section of the program calculates the radiation input to each of the sublayers. This is done with the hourly insolation data and the angle of incidence of direct radiation using the procedure of the last chapter. All sunlight is assumed to be direct. Time is reckoned in days from January 1 and in hours from midnight. The hourly insolation data for Ames was obtained from data taken in 1969, which was available on punched cards. These data are usually considered to be low due to instrumentation calibration error (67). The data were uniformly adjusted upward by about 9% to compensate for this error.

The fourth section of the program is the heat transfer iteration. Each sublayer exchanges heat with each adjacent sublayer and tc the environment immediately surrounding the sublayer. For the case of the convecting layer, this includes the ground underneath the pond, as well as the side walls. For the case of the uppermost insulation layer sublayer, heat exchange also occurs with the ambient air. Heat is stored only in the liquid sublayers of the pond. Surrounding ground and ambient air temperatures are given by the input data only. The ground and air are assumed to be infinite sources or sinks of heat. Since the solar pond is almost always warmer than its surroundings, the ground and air usually act as heat sinks. The solar pond is assumed to be cylindrical in shape for purposes of calculating the area of the side walls for each sublayer. The convecting layer also suffers heat loss due to the load. The manner in which this is done varies with the application. For typical residential space heating, the load is a constant times the difference between the ambient temperature and the desired temperature of the space to be heated. After the new heat content of each sublayer is established, the new sublayer temperatures are calculated. After the new temperatures are calculated, the physical parameters for each sublayer are recalculated. The iteration step is completed, and the program loops back to the beginning of section three. The salt concentration of each sublayer is always assumed to be constant.

The last section of the program outputs the solar pond thermal behavior. Although the temperature of each sublayer is calculated each hour, it is usually only printed out twice a day, once in the morning

(5 A.M.), and once in the evening (7 P.M.). Initial runs with hourly temperature printouts indicated that this is usually when the daily temperature extrema occur. Also, an accumulative record of major categories of heat input and output to the system are given. These include energy out the sides, bottom, and top, as well as radiation heat input, and total heat energy supplied to the load.

B. Possible Variations and Simplifications

The listing of the computer program in Appendix B evolved from more humble beginnings. The goal from the outset was to produce code that would accurately predict the thermal performance of a solar pond, given sufficient design and environmental information. At the time the program was written (1975-6), there was a scarcity of available experimental solar pond data, and so the computer model was tested against the mathematical model of Rabl and Nielsen (25) with good success. Even today it is difficult to adequately test the computer program against experimental data, since heat loss to the ground in experimental solar ponds is not well-known. The computer model was also tested against experimental insulation layer temperature profiles, again with good success. As the program evolved, many of the assumptions of the Rabl and Nielsen mathematical model, as well as other simplifications, were tested. As discussed below, it was found that most common sense simplifications and long term averaging schemes work fairly well.

Hourly local temperature and insolation data were available in suitable format for a complete year, so initial iteration steps of one hour were chosen. The insulation layer was initially divided into 10 cm

sublayers, since this would give enough points to establish an adequate temperature profile to compare against experimental ponds. Since optimization of computer time was not a goal, an increase in the value of either of these parameters was not tested. Both the iteration time and the sublayer depth were separately reduced by a factor of two to test for accuracy. In neither case were the results significantly different. Another factor which suggested the adequacy of these parameters was that the temperature change in each sublayer was always less than 10% of the temperature difference between adjacent sublayers.

The first success of the computer code was agreement with the Rabl and Nielsen model (25). Their model made the following assumptions:

1. Twenty-four hr. insolation varying sinusoidally with a yearly period about a constant value, with maximum insolation on June 21.
2. Ambient temperature varying sinusoidally with a yearly period about a constant value, with the time of maximum temperature usually sometime later than the time of maximum insolation.
3. All insolation direct, with angle of incidence fixed and equal to that at 2 P.M. on an equinox.
4. The pond is infinitely insulated and there are no side losses.

Rabl and Nielsen also did calculations for infinite ground storage. This is one place where the computer model can be more useful than the Rabl and Nielsen model, since the program can incorporate any amount of heat loss to the ground.

5. The heat load is 550 W/C° at a load temperature of 18.3° C.

6. Whenever the ambient temperature is warmer than the load temperature, heat is pumped into the solar pond convecting layer. Since the temperature of the solar pond is much warmer than the ambient in the summer, this is a very inefficient way of air conditioning. In their numerical calculations Rabl and Nielsen avoid this problem by decreasing the oscillation amplitude of the ambient air so that the maximum ambient temperature is that of the load. This does not change the average solar pond convecting layer temperature, but probably distorts the temperature variations, especially in warmer climates. This is another place where the computer program is more desirable, since the program can accommodate any scheme of heat withdrawal.

7. The Rabl and Nielsen model breaks the solar spectrum up into four regions of wavelength and assigns a single absorption coefficient to each region. The absorption coefficients are chosen to give the best fit to transmission of light in water data. The computer model breaks the spectrum into 40 regions as discussed in the previous chapter.

The Rabl and Nielsen model predicts the temperature distribution in the solar pond for the steady state. When comparing convecting layer temperature calculations, it is important that the program is also at a steady state solution for the comparison to be valid. A good way to do this is to calculate an initial temperature distribution using the method of Rabl and Nielsen (25). Another way steady state is assured is if the temperature distribution at the end of the year is the same as at the beginning of the year.

Two tests were made comparing calculations for a 140 m^2 pond at Columbus, Ohio. In the first the insulating layer was 1.0 m, and the convecting layer was 3.0 m. In the second the insulating layer was 1.2 m, and the convecting layer was 1.8 m. In both cases the average convecting layer temperature calculated by the computer program agreed with that calculated by the Rabl and Nielsen model to within a few degrees. For several times during the year, an insulating layer temperature profile was calculated using the Rabl and Nielsen model. When compared with computer generated profiles for the same time, agreement was again within several degrees at all depths in the insulating layer. The computer generated insulating layer profiles also corresponded in shape favorably with published experimental insulating layer profiles (30,33). The program also predicted a period of about 2-3 weeks in which the convective layer temperature was within 0.5° C of the maximum temperature and a similar period about the minimum temperature. These periods easily overlapped the times for maximum and minimum convective layer temperatures predicted by the Rabl and Nielsen model. In these tests both the radiation input and ambient temperature were allowed to vary sinusoidally over the course of the year. Both were held constant for each 24 hr period corresponding to a day, with both given the value at the beginning of the day.

So far, the computer model had incorporated the same assumptions as the Rabl and Nielsen mathematical model. At this point the program was modifed to try and model the ambient temperature more accurately. The year was divided into weekly segments, with each segment assigned an

average temperature and daily temperature swing amplitude. The ambient temperature was then allowed to vary sinusoidally with this amplitude about the average over the course of the day. The average temperatures and daily amplitudes were adapted from weather bureau data (68). It was discovered that if the total yearly heating and cooling degree days were the same, the solar pond temperatures of this variation at any given time never varied by more than a few degrees from the previous version of the program.

The next series of variations tested different radiation input schemes. First, the program was modified to use weekly radiation averages, which were available for both Columbus and Ames. This was first implemented by calculating the daily radiation input from the weekly average. The radiation was assumed constant 24 hr a day for the entire week. A second implementation assumed that the same total daily insolation was available for only 12 hr a day. The daily temperature variations in the solar pond of this second implementation differed from the first by a few degrees, but the seasonal variation of the two implementations, compared at the same hour of the day, were nearly identical. Using weekly radiation averages gives the same general solar pond thermal behavior as using a sinusoidal radiation input of yearly period. If the total yearly insolation is the same, then the minimum and maximum temperatures of the two versions are within a few degrees of each other and occur within a few weeks of each other. The weekly radiation averages do not in general vary sinusoidally, and at a few times during the year, the temperatures of the two versions may differ by about 5 degrees.

The next version of radiation input used actual hourly insolation data, which was made available to me in punched card format by Prof. Gene Takle of the Iowa State University Meteorology Department. This data was for the calendar year 1969 and is possibly a worst case year. Fig. IV.3 below compares each monthly average of the 1969 radiation data to the corresponding monthly average radiation of the years 1959-1970 (68). As shown in Fig. IV.3, the 1969 insolation is lower than average during most of the year and is especially so during some months. The 1969 yearly average was 309 langleys/day, while the 1959-1970 average was 341 langleys/day. As mentioned earlier in this chapter, the hourly data was uniformly adjusted upward to correct for calibration error. When this version of the program was compared to a yearly varying sinusoidal input of equal yearly total energy, the results were similar to that using weekly radiation averages. When the total yearly insolation was the same, the temperature extrema and extrema dates were about the same, but at some times during the year, say after a few weeks of cloudy weather or after a long period of clear weather, the temperatures of the two versions might differ by as much as 5 degrees.

The next version of radiation input allowed the angle of incidence to vary on an hourly basis. In all previous versions the angle of incidence was fixed through the year as that at 2 P.M. on an equinox. In the final version of the program, the angle of incidence is calculated for the middle of each hour using the procedure developed in the last chapter. Allowing the angle of incidence to vary each hour results in somewhat degraded thermal performance of the solar pond when compared with the

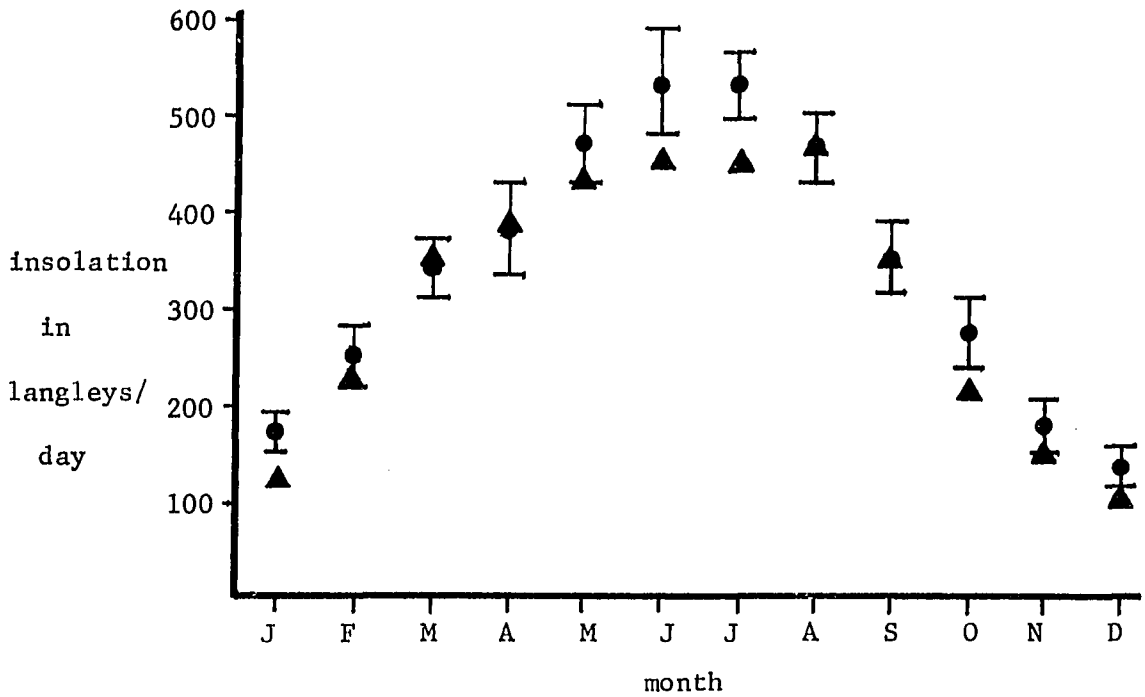

Fig. IV.3. Comparison of monthly average Ames insolation between the year 1969 (▲) and the average of the years 1959-1970 (⧳). The error bars represent one standard deviation in the averages for each month.

fixed angle of incidence version. When initial temperature profiles of the two versions were the same at the beginning of the year, the version that varied the angle of incidence ended the year with a convecting layer temperature that was 3.2° C lower than the version with a fixed angle of incidence. A closer inspection of the two versions showed that the colder version had less penetration of light into the bottom of the pond. This suggests that the fixed angle of incidence in the Rabl and Nielsen model should be increased slightly. To make the amount of energy going into the bottom of the pond in the fixed angle of incidence version equal to that of the varying version, the fixed angle of incidence had to be increased 11° to that of 3:17 P.M. on an equinox. This angle of incidence also had identical temperatures at the end of the year to that of the varying version, and had maximum and minimum temperatures that were within 1° C, and occurred on the same date as in the varying version.

The most significant difference between the final computer model and the Rabl and Nielsen model was obtained when the absorption constants of the water were revised. Rabl and Nielsen used absorption constant data that was taken about 1900. The absorption data that the computer model used (see Fig. III.5) were more recent. Using the newer absorption data in the computer model gave a temperature at the end of the year that was 16° C higher than with the previous version. This occurred because water transparency is higher in the more recent data. A comparison of total energy transmission for the two schemes is given in Fig. IV.4 below.

While the final computer version is most accurate in determining radiation transmission through pure water, it is desirable to have a

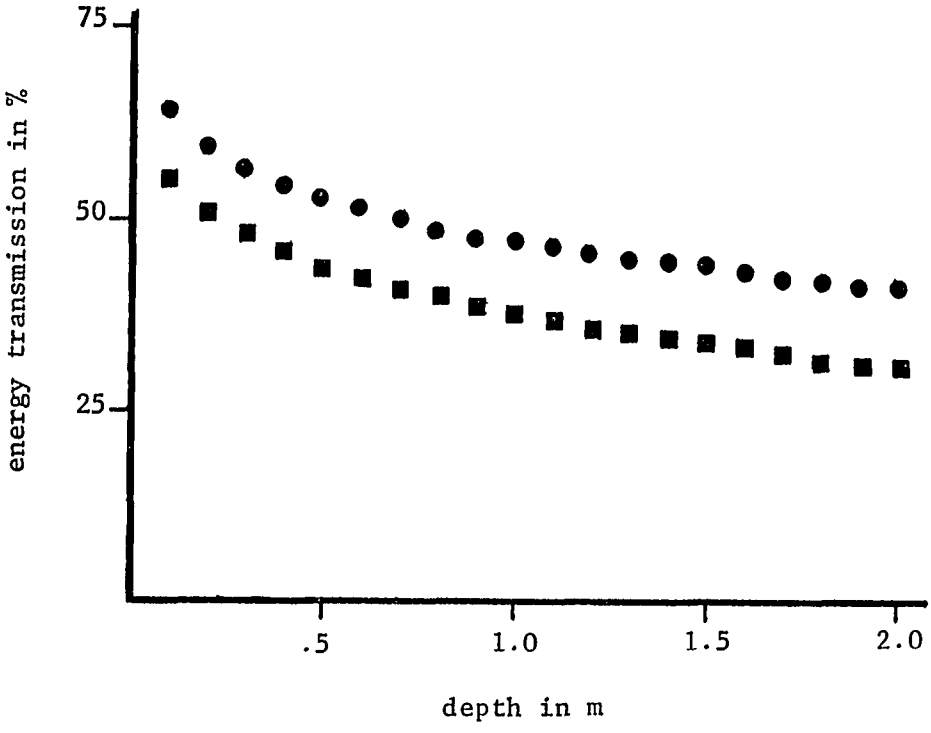

Fig. IV.4. Comparison of energy transmission through pure water using data of Fig. III.5 (●) and the Rabl and Nielsen parameterization (■).

simpler function for cases where either the computer is not available, or else computer time is precious. An 8 parameter function analogous to the Rabl and Nielsen (RN) model function was fitted to the more recent absorption data. The transmission in percent was calculated for the data of Fig. III.5 at 10 cm intervals from 10 cm to 2 m. An error of 1% in transmission was arbitrarily assigned to each of the 20 points. Each point was then considered to be "data". The RN function for energy transmission in water

$$T = \sum_{i=1}^{4} \eta_i \exp(-\mu_i z) \qquad \text{(IV.1)}$$

where z is the depth in m, and η_i and μ_i are parameters, was fitted to to this data. The 8 parameters are adjusted until the χ^2 between T and the data is minimized. The result of this fit is shown in Table IV.1 below. The value of χ^2 for this fit was 0.4, and the transmission calculated from the 8 parameter fit never differed from the data transmission by more than 1% over the entire 2 m interval.

Table IV.1. 8 parameter fit of Rabl and Nielsen function (IV.1) to absorption data to a depth of 2 m.

i	η_i	μ_i (m^{-1})
1	.190	20.0
2	.230	1.75
3	.301	.0656
4	.141	.0102

A very good fit to the old Rabl and Nielsen model transmission function was found by Bryant and Colbeck (52) to be

$$T = .73 - .08 \ln(x), \qquad \text{(IV.2)}$$

where x is the depth in cm. The Bryant transmission function never differs from the old Rabl and Nielsen transmission function by more than 1% of transmission down to a depth of 5 m. A Bryant type of transmission function

$$T = a - b \ln (c\, z) \qquad \text{(IV.3)}$$

was fitted to the absorption data of Fig. III.5 in 10 cm intervals from 10 cm to 2 m of depth. The best fit obtained had a χ^2 of 4.9. The values of the parameters for this fit are given in Table IV.2. A comparison of the RN function fit and the Bryant function fit to the data is shown in Fig. IV.4.

Table IV.2. Bryant function (IV.3) 3 parameter fit to absorption data of Fig. III.5 to a depth of 2 m.

a	.727
b	.056
c	100.0 m^{-1}

While actual transmission will vary from pond to pond depending on water type and maintenance standards, the data of Fig. III.5 probably represent the best transmission obtainable in a salt and water pond. The RN function with parameters from Table IV.1 is an excellent approximation to this transmission. The Bryant function, while simpler, is not

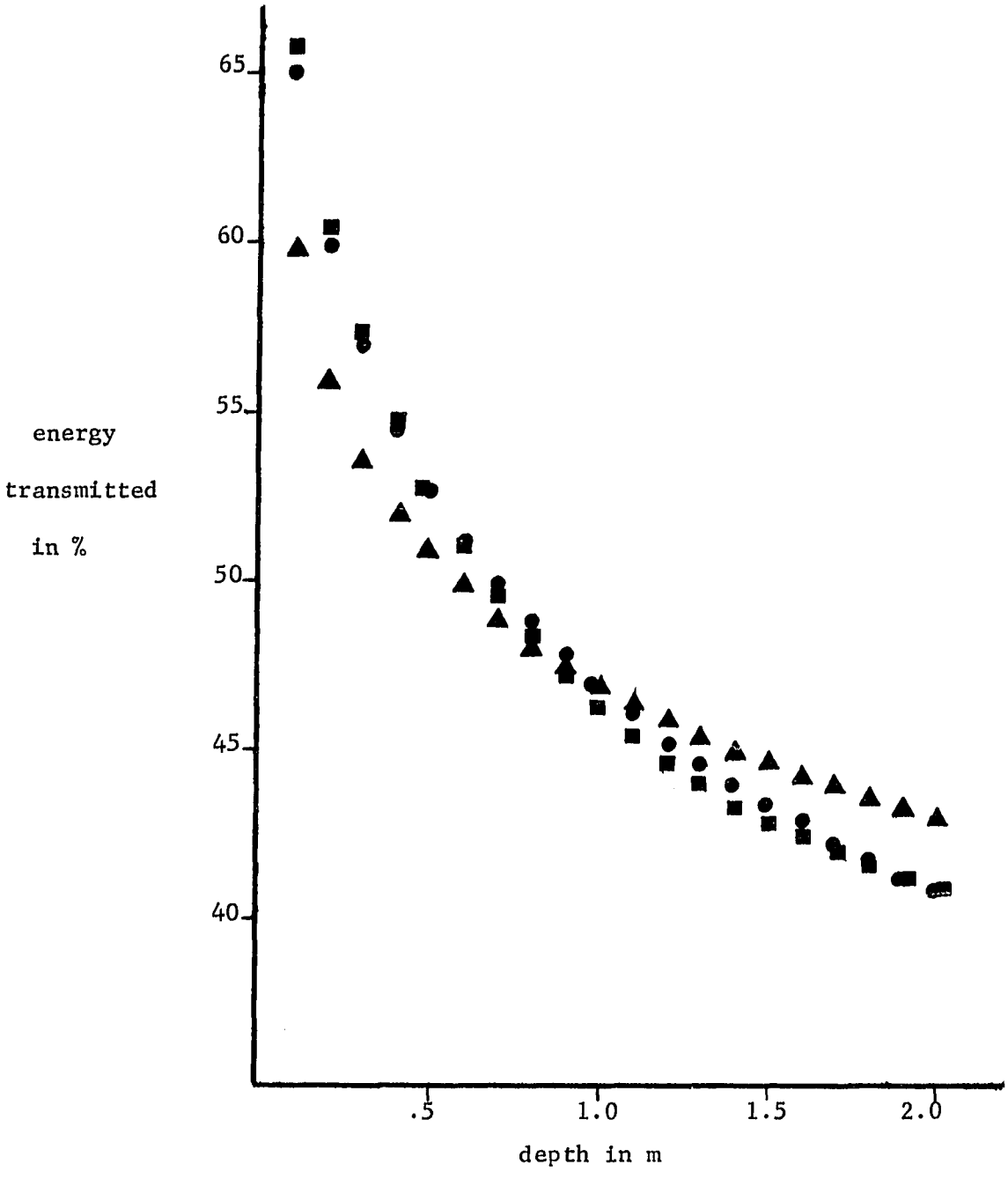

Fig. IV.5. Comparison of energy transmission through pure water using data of Fig. III.5 (●), the Rabl and Nielsen function parameterization (■), and the Bryant function parameterization (▲).

as good an approximation as the RN function. The Bryant function is uniquely interesting however, in that the argument of the natural logarithm is exactly the depth in centimeters.

C. Solar Pond Design for Living History Farms

As a first example of how the computer model developed in the last two sections can be used in solar pond design, we examine its application to the design of the solar pond at Living History Farms. The "Farm of Today and Tomorrow" at Living History Farms is to include a solar residence that will draw auxiliary heat from an adjacent solar pond. This residence is discussed in more detail in Chapter VI. The input parameters to the model were the residence heat load and the pond surface area. The model was to aid in deciding the depth of the insulating layer, the depth of the convecting layer, and the amount of bottom and side insulation.

Architectural considerations fixed the pond surface as a circle of 9.1 m diameter. The solar residence heat load was calculated as 410 W/C° with a base temperature of 18.3° C. The residence will achieve part of its heat via its passive solar system. Since a good model for the type of passive system used in the residence does not at present exist, a conservative approach was taken, and it was assumed that the house would draw heat from the solar pond during any hour for which there was no recorded insolation and for which the ambient temperature was less than the base temperature. If, as expected, the passive system could supply part of this nighttime heat, then the excess heat stored in the solar pond would be used for domestic hot water heating.

In general, the deeper the insulating layer, the higher is the average temperature; and the deeper the convecting layer, the smaller is the difference between the minimum and maximum temperatures. These depths should be kept as small as possible for economic reasons. The minimum pond temperature that heat can be extracted from the pond for space heating without using a heat pump is about 35-40° C. The maximum pond temperature is of course about 100° C (varying somewhat with salt concentration and elevation). The first step is then to set the side (which includes the bottom) insulation to infinity and then to adjust the insulating layer depth until an average temperature of 65-70° C is obtained. Then the convecting layer depth is adjusted until a minimum of 35-40° C is obtained.

The next step is to determine how much side and bottom insulation is needed. From our infinite insulation case we have a good idea how much heat is going into the pond, how much is actually used for house heating, and how much heat is going back out the top of the pond. We then decrease the insulation until the heat going out of the sides is some percent of one of the above amounts, or until the pond temperature falls to an unacceptable level. Decreasing the insulation decreases the thermal performance of the pond, and the entire procedure may have to be repeated for different insulation values, until adequate performance is obtained. In the case of the solar pond at Living History Farms, an insulating layer of depth 1.4 m gives an average temperature of 66° C, a convecting layer depth of 2.8 m gives a maximum temperature deviation from average of 34° C, and side insulation that is the equivalent of

64 cm of styrofoam allows 20% of the energy penetrating the surface of the pond to escape out the sides.

D. Solar Ponds for Grain Drying

As a second example of applying the computer program to solar pond design, we consider the case of grain drying. Grain drying usually begins at harvest time in early fall when the grain may have a moisture content as high as 25%. For shelled grain to be stored for long periods of time, moisture content must be reduced to about 15% in a period of about 50 days. Air at about 4° C above ambient is passed through the grain, which removes moisture. At this temperature rise, approximately 1.3×10^7 J of energy applied over the 50 day period is needed to adequately dry 1 bushel of grain from 25% moisture content to 15% moisture content (69).

Grain drying is one of the most efficient applications for a solar pond. The pond may be started in the spring and be totally depleted of heat at the end of fall. The pond does not then lose heat during the winter when both ambient temperatures and insolation are low.

We assume that we have an area of 180 m^2, that we initiate the solar pond on March 29, and that we will increase the load to dry as much grain as possible. The pond will be considered to no longer be able to dry grain when its temperature falls below 10° C. We increase the heat load until the pond reaches 10° C after 49 days of drying. The pond starts to dry the grain on October 4. The heat load is then continuous.

We notice that as we increase the depth of the convecting layer, the maximum temperature of the pond decreases, but the amount of heat energy retained increases. This is due to the decrease in temperature gradient, and hence decreased heat flow across the insulating layer. Also the amount of salt necessary to establish the gradient is decreased. For example, a pond with infinite insulation, an insulating layer depth of 1.4 m, and a convecting layer depth of 3.0 m yields a maximum temperature of 105° C and 3.1×10^{11} J of usable heat. If we increase the convecting layer depth to 9.0 m, we obtain a maximum temperature of 56° C but 4.1×10^{11} J of usable heat, enough to dry about 3×10^{4} bushels of grain.

In practice, rather than digging a deeper hole, it would probably be more practical to place an equivalent amount of heat storage, in the form of phase change material, at the bottom of the pond. The cost of the phase change material would be at least partially offset by the decreased cost of the salt and insulation. As discussed in Sec. E of Ch. II, a similar procedure could be used in space heating or domestic hot water heating. The phase change material could be selected with a transition temperature equal to the lowest temperature that would adequately transfer heat to the load.

V. THEORY OF STABILITY IN THE SOLAR POND SALT GRADIENT

A. Introduction

If solar ponds are to work properly, one must constantly maintain the nonconvecting status of the insulating layer. This system, where a destabilizing temperature gradient is balanced by a stabilizing salt gradient, is not unique to solar pond studies, but has been intensively investigated by oceanography and limnology researchers. Related effects have also been observed in the laboratory when two solutes are used and when metal alloys are solidified (70). The term "double-diffusive convection" is used to describe the general phenomena, while "thermohaline" or "thermosolutal" convection has been used to describe the phenomena associated with solar ponds.

There have been two major approaches to solar pond stability analysis. The major effort has followed the linear stability method developed by Rayleigh (71), which calculates conditions for the onset of convection. This method will be discussed in some detail below. The second approach, first applied to thermohaline convection by Turner (72), considers the growth of convection layers with time using a one-dimensional heat diffusion equation. Rabl (73) and Nielsen (30) combine Turner's results with the stability criteria of Weinberger (24) to establish the time dependent growth and shrinkage conditions of small convection layers located within the salt gradient.

A related phenomenon in thermohaline convection is the "salt fountain", first described by Stommel, Arons, and Blanchard (74). If a long vertical tube with conducting walls is placed in the ocean so that its

bottom is exposed to cold fresh water and its top to warm salty water, a continuous motion (ascending or descending) can be maintained after priming the fountain. The ascending (or descending) water in the tube exchanges heat but not salt with the otherwise nonconvectively stable ambient ocean and is accelerated due to its deficit (surplus) in salt and density relative to that of the ocean at the same level. As described by Stern (75), nature provides her own convective fountains, since the molecular diffusivity of salt ($k_S = 1.3 \times 10^{-9}$ m^2/s) is much smaller than the molecular diffusivity of temperature ($k_T = 1.5 \times 10^{-7}$ m^2/s). This type of behavior is in the so called thermohaline "salt finger" regime, whose stability has been investigated by Stern (76).

The large difference between the salt and temperature diffusivities is also responsible for the "overstability" regime of thermohaline convection. Consider a particle of fluid in an otherwise stable solar pond insulating layer. If the particle is displaced upwards, it finds itself warmer and saltier than its surroundings. Its temperature decreases rapidly to that of the surroundings, but its salt content only slowly decreases. Being saltier, and hence denser, than its surroundings, the buoyancy force acts to restore it to its original level. When it reaches its starting position, it is about as salty as its surroundings but colder, and so it overshoots its original position and goes lower in the pond. At this position the particle takes on heat faster than it does salt. The result is oscillations of increasing amplitude leading to convection for certain salt and temperature gradient combinations. These combinations comprise the "overstability" regime.

Two other methods of initiating convection in an otherwise stable solar pond insulating layer are spontaneously occurring convective motion from infinitesimal disturbances and convection initiated by finite amplitude steady motions. The latter has been extensively studied by Veronis (77,78). The former is solved by the linear stability analysis techniques originally developed to describe the Benard convection problem. As pointed out by Nield (79), it is now known that surface tension effects, and not buoyancy, were dominant in Benard's experiments. A number of researchers (80-82) have used the linear stability analysis to analyze the case of a fluid slab with free kinematic boundaries, which is the most tractable case. Nield (79), using numerical techniques, provides solutions for several other boundary conditions. Fig. V.1 in Section C shows the different thermohaline regimes in terms of the salt and thermal Rayleigh numbers.

The rest of this chapter will discuss the linear stability analysis. In Section B the basic hydrodynamic equations of the Boussinesq approximation are established. In Section C the perturbation equations without a radiation term are solved and discussed. In Section D, using the results of Section C, the perturbation equations including a radiation term are solved. In Section E the results of Section D are discussed regarding their application to solar pond design.

B. Basic Hydrodynamic Equations

The basic hydrodynamic equations necessary for understanding linear stability analysis can be found in most fluid mechanics textbooks such as Yih (83) or Sissom and Pitts (84). Here we consider the basic

equations describing a Newtonian fluid particle that is absorbing radiation incident from above. These equations are:

1. Equation of state

$$p = p_m(1 - \alpha T + \beta S), \tag{V.1}$$

where p is the density, p_m is the mean density, T is the temperature in C°, S is the solute concentration,

$$\alpha = (-\frac{1}{p}\frac{\partial p}{\partial T})_{S,P}, \text{ and } \beta = (-\frac{1}{p}\frac{\partial p}{\partial S})_{T,P},$$

where P is the isotropic pressure.

2. Incompressibility

$$\partial u_j/\partial x_j = 0, \tag{V.2}$$

where x_j is the spatial coordinate, and $u_j = \partial x_j/\partial t$, where t is the time.

3. Conservation of mass

$$\frac{\partial p}{\partial t} + u_j \frac{\partial p}{\partial x_j} = 0. \tag{V.3}$$

4. Conservation of solute

$$\frac{\partial S}{\partial t} + u_j \frac{\partial S}{\partial x_j} = \frac{\partial}{\partial x_j}(K_S \frac{\partial S}{\partial x_j}), \tag{V.4}$$

where K_S is the coefficient of solute diffusivity. The second term on the left represents the amount of solute carried into the fluid particle by convection. The term on the right represents the amount of solute diffusing across the boundary of the fluid particle.

5. Conservation of momentum

$$\frac{d}{dt}(p\, u_i) = p\, X_i + \frac{\partial P_{ij}}{\partial x_j}, \tag{V.5}$$

where X_i are the external body forces, and P_{ij} is the stress tensor.

In a Newtonian fluid, stress is related to strain e_{ij} in the following way:

$$P_{ij} = -P\,\delta_{ij} + 2\nu\, e_{ij} - \frac{2}{3}\nu\,\delta_{ij}\, e_{kk}, \qquad (V.6)$$

where δ_{ij} is the Kronecker delta function, ν is the absolute viscosity, and

$$e_{ij} = \tfrac{1}{2}\left(\frac{\partial u_i}{\partial x_j} + \frac{\partial u_j}{\partial x_i}\right). \qquad (V.7)$$

(V.5) reduces to

$$p\frac{\partial u_i}{\partial t} + p\, u_j \frac{\partial u_i}{\partial x_j} = pX_i - \frac{\partial P}{\partial x_i} + \nu\frac{\partial^2 u_i}{\partial x_j \partial x_j} + \frac{\partial \nu}{\partial x_j}\left(\frac{\partial u_i}{\partial x_j} + \frac{\partial u_j}{\partial x_i}\right). \qquad (V.8)$$

ν is assumed to be a constant, and the last term in (V.8) is 0.

6. Conservation of energy

$$p\frac{\partial (C_V\, T)}{\partial t} + p\, u_j \frac{\partial}{\partial x_j}(C_V\, T) = \frac{\partial}{\partial x_j}\left(k\,\frac{\partial T}{\partial x_j}\right) + \Phi$$

$$+ \int d\lambda\, H(\lambda)\, \mu(\lambda)\, \exp(-\mu(\lambda)\, z), \qquad (V.9)$$

where C_V is the heat capacity at constant volume, k is the thermal conductivity,

$$\Phi = P_{ij}\frac{\partial u_i}{\partial x_j},$$

$$= 4\nu(e_{12}^2 + e_{13}^2 + e_{23}^2),$$

is the rate at which kinetic energy is dissipated by viscosity, which (since e_{ij} is second order in the velocity, an infinitesimal) is small and ignored in our application, and the last term on the right is the radiant energy absorbed by the fluid particle. It is assumed that the radiant energy flow per unit area, I, is given by

$$I = \int d\lambda\ H(\lambda)\ \exp(-\mu(\lambda)\ z),$$

where λ is the radiation wavelength, $H(\lambda)$ is the surface flux that is not reflected, $\mu(\lambda)$ is the absorption coefficient, and z is the distance from the surface of the pond and is positive downward. The amount of radiant energy absorbed by a fluid particle of unit area and depth dz is just -dI/dz, which is the last term on the right in (V.9).

In the study of convection, the Boussinesq approximation is often used and will be followed in the results below. In the Boussinesq approximation, the parameters such as viscosity ν, thermal diffusivity K_T, thermal conductivity k, solute diffusivity K_S, heat capacity C_V, and the density expansion coefficients α and β are assumed to be constant. Furthermore, density is assumed to be constant except in the body force term of the conservation of momentum equation, where it is given by the equation of state. It should be pointed out that these parameters are not constant. Even the assumption of incompressibility is invalid if the temperature is allowed to change. However, over the range of conditions found in the onset of convection in solar ponds, the changes in these parameters are small, and their effects on the results are small, especially when compared to density change effects in the body force term. Hence we may make the Boussinesq approximation and treat these parameters as constants. If the equation of state (V.1) is substituted into the body force term of (V.8), we get

$$\frac{\partial u_i}{\partial t} + u_j \frac{\partial u_i}{\partial x_j} = -\frac{1}{\rho_m} \frac{\partial P}{\partial x_i} + \left(1+\frac{\delta P}{\rho_m}\right) X_i + \nu' \nabla^2 u_i, \qquad \text{(V.10)}$$

where $\delta\rho = \rho_m(-\alpha T + \beta S)$, and $\nu' = \nu/\rho_m$ is the kinematic viscosity. In the work that follows we shall omit the prime from the kinematic viscosity. (V.4) becomes

$$\frac{\partial S}{\partial t} + u_j \frac{\partial S}{\partial x_j} = K_S \nabla^2 S. \tag{V.11}$$

(V.9) becomes

$$\frac{\partial T}{\partial t} + u_j \frac{\partial T}{\partial x_j} = K_T \nabla^2 T + \frac{1}{\rho_m C_v} \int d\lambda \; H(\lambda) \, \mu(\lambda) \exp(-\mu(\lambda) \, z). \tag{V.12}$$

C. Basic Perturbation Equations

In this section we consider the case of a fluid slab of depth d that does not absorb radiation and is initially stagnant. The temperature and salinity at the boundaries are held constant and in both cases are lower at the top of the slab than at the bottom. The boundaries are dynamically free, i.e., will support no stress and are assumed to be infinite conductors of both heat and salt. We write

$$z = 0; \qquad T = T_o, \qquad S = S_o,$$

$$z = d; \qquad T = T_d, \qquad S = S_d.$$

The pertinent equations are (V.2,10-12) except that the last term in (V .12), the radiation absorption term, is set to 0. The body force X_i in (V.10) is simply the force of gravity

$$X_i = -\rho_m g \, \delta_{i3},$$

where g is the acceleration of gravity. The solution follows along lines similar to that of references (77-82). We solve these equations first for the case $u_i = 0$, the unperturbed state.

(V .11) becomes

$$\nabla^2 S = 0,$$

$$S(z) = S_o + (\Delta S/d)\ z, \qquad (V.13)$$

where $\Delta S = S_d - S_o$. (V.12) becomes

$$\nabla^2 T = 0,$$

$$T(z) = T_o + (\Delta T/d)\ z, \qquad (V.14)$$

where $\Delta T = T_d - T_o$. The steady state p(z) is now given by substituting (V.13,14) into (V.1). (V.10) becomes

$$\partial P/\partial z = p_m\ g\ (1 - \alpha T(z) + \beta S(z)).$$

This can be solved for P(z), but the result is not important here.

We now introduce infinitesimal perturbations to the variables, denoting the unperturbed variables by * and the perturbed variables by '.

$$T = T^* + T',$$

$$P = P^* + P',$$

$$p = p^* + p' = p_m + \delta p + p',$$

$$S = S^* + S',$$

$$u_i = u_i'.$$

The basic hydrodynamic equations become

$$\frac{\partial u_j'}{\partial x_j} = 0,$$

$$\frac{\partial u_i'}{\partial t} + u_j' \frac{\partial u_i'}{\partial x_j} = -\frac{1}{p_m}\frac{\partial P^*}{\partial x_i} - \frac{1}{p_m}\frac{\partial P'}{\partial x_i} + \left(1 + \frac{\delta p}{p_m}\right) g\, \delta_{i3} + \frac{p'}{p_m} g\, \delta_{i3} + \nu\, \nabla^2 u_i',$$

$$\frac{\partial T^*}{\partial t} + \frac{\partial T'}{\partial t} + u_j' \frac{\partial T^*}{\partial x_j} + u_j' \frac{\partial T'}{\partial x_j} = K_T\, \nabla^2 T^* + K_T\, \nabla^2 T',$$

$$\frac{\partial S^*}{\partial t} + \frac{\partial S'}{\partial t} + u_j' \frac{\partial S^*}{\partial x_j} + u_j' \frac{\partial S'}{\partial x_j} = K_S\, \nabla^2 S^* + K_S\, \nabla^2 S',$$

with $p' = p_m(-\alpha T' + \beta S')$. The zero order terms cancel out, and we keep only the first order terms in what remains. We write the resulting equations, dropping the primes on the perturbed variables.

$$\frac{\partial u_j}{\partial x_j} = 0, \tag{V.15}$$

$$\frac{\partial u_i}{\partial t} = -\frac{1}{p_m}\frac{\partial P}{\partial x_i} - g\,(\alpha T - \beta S)\,\delta_{i3} + \nu\, \nabla^2 u_i, \tag{V.16}$$

$$\frac{\partial T}{\partial t} + u_z\,(\Delta T/d) = K_T\, \nabla^2 T, \tag{V.17}$$

$$\frac{\partial S}{\partial t} + u_z\,(\Delta S/d) = K_S\, \nabla^2 S. \tag{V.18}$$

To make these equations compatible with each other, we make all the terms nondimensional by constructing new variables, which we denote by *, as follows: $x_i = d\, x_i^*$, $t = (d^2/K_T)\, t^*$, $u_i = (K_T/d)\, u_i^*$, $T = (\Delta T)\, T^*$, $S = (\Delta S)\, S^*$, and $P = (p_m\, \nu\, K_T/d^2)\, P^*$.

The equations then become

$$\frac{\partial u_j}{\partial x_j} = 0, \tag{V.19}$$

$$\frac{1}{\sigma}\frac{\partial u_i}{\partial t} = -\frac{\partial P}{\partial x_i} - (R_T\, T - R_S\, S)\,\delta_{i3} + \nabla^2 u_i, \tag{V.20}$$

$$\frac{\partial T}{\partial t} + u_z = \nabla^2 T, \tag{V.21}$$

$$\frac{\partial S}{\partial t} + u_z = \tau\,\nabla^2 S, \tag{V.22}$$

where the * has been dropped from the new variables, and where $\tau = K_S/K_T$, $\sigma = \nu/K_T$, $R_T = (g\,\alpha\,\Delta T\,d^3)/(\nu\,K_T)$ and is called the thermal Rayleigh number, and $R_S = (g\,\beta\,\Delta S\,d^3)/(\nu\,K_T)$ and is called the salinity Rayleigh number. For convenience we assume $u_y = 0$. Equations (V.19-22) (two components for (V.20)) then give us five equations for our five unknown perturbed parameters P, S, T, u_x, u_z. At both boundaries all perturbed parameters must be zero, so as a solution, we try

$$T = T\, e^{ik_x x}\, e^{ik_z z}\, e^{nt},$$

$$S = S\, e^{ik_x x}\, e^{ik_z z}\, e^{nt},$$

$$P = P\, e^{ik_x x}\, e^{ik_z z}\, e^{nt},$$

$$u_x = u_x\, e^{ik_x x}\, e^{ik_z z}\, e^{nt},$$

$$u_z = u_z\, e^{ik_x x}\, e^{ik_z z}\, e^{nt},$$

where in each case the leading terms on the right are constants,

$$k = \sqrt{k_x^2 + k_z^2},$$

is the wavenumber of the disturbance, and n is the time constant (which may be complex). The sign of the real part of this time constant

determines the stability of the system. When n is positive, infinitesimal disturbances grow in time and are unstable. When n is negative, the disturbances shrink in time and are stable. Substituting our trial solutions into (V.19-22), we obtain

$$ik_x u_x + ik_z u_z = 0, \tag{V.23}$$

$$(n/\sigma + k^2)\, u_x + ik_x P = 0, \tag{V.24}$$

$$(n/\sigma + k^2)\, u_z + ik_z P + R_T T - R_S S = 0, \tag{V.25}$$

$$u_z + (n + k^2)\, T = 0, \tag{V.26}$$

$$u_z + (n + \tau k^2)\, S = 0. \tag{V.27}$$

From equations (V.23-27), by setting the determinant of the coefficients to 0, we can derive the characteristic equation

$$\frac{n^3}{\sigma} + n^2 k^2 \left(1 + \frac{1+\tau}{\sigma}\right) + n\left\{k^4 \left(1 + \tau + \frac{\tau}{\sigma}\right) + \frac{k_x^2}{k^2}(R_S - R_T)\right\}$$
$$+ \left\{\tau k^6 + k_x^2 (R_S - \tau R_T)\right\} = 0. \tag{V.28}$$

(V.28) is dependent on the wave number k. A discussion of the general solution benefits from dropping this dependence. We make the substitution $n = k^2 q$, $R_T' = k_x^2 R_T/k^6$, and $R_S' = k_x^2 R_S/k^6$ to obtain

$$\frac{q^3}{\sigma} + q^2 \left(1 + \frac{1+\tau}{\sigma}\right) + q\left(1 + \tau + \frac{\tau}{\sigma} + R_S' - R_T'\right)$$
$$+ (\tau + R_S' - \tau R_T') = 0. \tag{V.29}$$

The general form of a cubic equation is $ax^3 + bx^2 + cx + d = 0$ and is usually solved in the manner shown below to derive Cardan's formulas (85). First a reduced cubic equation is derived by eliminating the x^2

term with the substitution $x = y - b/3a$. We now have the equation

$$y^3 + y\,(c/a - b^2/3a^2) + (d/a - bc/3a^2 + 2b^3/27a^3) = 0,$$

or the reduced cubic equation $y^3 + Cy + D = 0$, where $C = c/a - b^2/3a^2$, and $D = d/a - bc/3a^2 + 2b^3/27a^3$. The reduced cubic equation is solved with the substitution $y = u + v$, which results in

$$u^3 + v^3 + (C + 3uv)\,(u + v) + D = 0, \qquad \text{(V.30)}$$

which is indeterminate unless we impose an additional restriction on u and v. A convenient restriction is to choose the auxiliary equation $3uv + C = 0$, or $uv = -C/3$, which eliminates the middle term in (V.30). Taking the cube of the auxiliary equation, we have

$$u^3 + v^3 = -D \text{ and } u^3v^3 = -C/27. \qquad \text{(V.31)}$$

Since we know the sum and the product of the unknowns u^3 and v^3, they must be the roots of the quadratic equation $t^2 + Dt - C^3/27 = 0$. This equation has the solution

$$A = -D/2 + \sqrt{D^2/4 + C^3/27}$$

and

$$B = -D/2 - \sqrt{D^2/4 + C^3/27}.$$

Since the equations are symmetrical with respect to u and v, we are at liberty to set $u^3 = A$ and $v^3 = B$. However y must satisfy (V.31). $A^{1/3}$ has three roots, and we are free to choose which one we want. Then $B^{1/3}$ is determined by the second equation of (V.31). The three roots of y are then constrained to be

$$y_1 = A^{1/3} + B^{1/3},\ y_2 = \omega A^{1/3} + \omega^2 B^{1/3},\ y_3 = \omega^2 A^{1/3} + \omega B^{1/3},$$

where $\omega = (-1 + i\sqrt{3})/2$.

The nature of the roots depends on the discriminant of the quadratic equation for t. This can be described by the function $\Delta = 4C^3 + 27D^2$, which will be positive, negative, or zero. We examine each of the three cases in turn.

1. $\Delta > 0$

In this case the determinate is real, and A and B are not equal. The three roots for y become

$$y_1 = A^{1/3} + B^{1/3},$$
$$y_2 = -(A^{1/3} + B^{1/3})/2 + i\sqrt{3}(A^{1/3} - B^{1/3})/2,$$
$$y_3 = -(A^{1/3} + B^{1/3})/2 - i\sqrt{3}(A^{1/3} - B^{1/3})/2.$$

Note that y_1 is a real root, and y_2 and y_3 are unequal complex conjugate roots.

2. $\Delta < 0$

In this case the determinate is pure imaginary. If we let $A^{1/3} = \alpha + i\beta$, then since $A^{1/3}B^{1/3} = -C/3$, a real number, we must have $B^{1/3} = \alpha - i\beta$. The three roots for y are then

$$y_1 = 2\alpha,\ y_2 = -\alpha + \sqrt{3}\beta,\ y_3 = -\alpha - \sqrt{3}\beta.$$

These are three real and unequal roots.

3. $\Delta = 0$

This case can be derived from either case 1 or case 2 above. Starting with the latter, we have $A = B = \alpha$. The three real roots, two of them equal are

$$y_1 = 2\alpha,\ y_2 = y_3 = -\alpha.$$

To examine the structure of (V.29), we need to find the values for R_S' and R_T' when $\Delta = 0$ and again when the real part of $q = 0$. This will break the $R_S'R_T'$ plane up into regions of different stability. Veronis (77) first solved for the former conditions. If q is pure imaginary, then $q = ip$. Substituting this into (V.29) and equating the real and imaginary parts to 0, we obtain

$$p\{-p^2 + \sigma(1 + \tau + \frac{\tau}{\sigma} + R_S' - R_T')\} = 0, \tag{V.32}$$

$$-p^2 (1 + \frac{1 + \tau}{\sigma}) + (\tau + R_S' - \tau R_T') = 0. \tag{V.33}$$

When $p = 0$ (everywhere, since there is always one real root), we have

$$R_T' = (1/\tau) R_S' + 1. \tag{V.34}$$

When $p \neq 0$ (i.e. $\Delta > 0$), we can solve (V.32) for p^2 and substitute the result into (V.33). We then have

$$R_T' = \frac{\sigma + \tau}{\sigma + 1} R_S' + \frac{1}{\sigma} (1 + \tau)(\sigma + \tau). \tag{V.35}$$

The roots for $\Delta = 0$ may be solved for by Newton's method of successive approximation on the computer. Values for σ and τ for a given S and T may be computed from the saline water thermal constants given by Elwell et al. (51). A brief table of values for σ and τ for several values of S and T are given in Table V.1.

Table V.1. Values of σ and τ for several values of S and T.

T (C°)	S (%)	σ	τ
8	0	10	.007
20	0	7.0	.010
30	5	5.5	.011
60	15	3.5	.020
90	20	2.6	.031

The results for T = 8° C, S = 0 are shown in Fig. V.1. The solid line ZY represents (V.34). The solid line WX represents (V.35). The dotted line represents the roots of the equation $\Delta = 0$. Δ is positive in the region VXU and below STU. Δ is negative elsewhere. The solution divides the $R_S'R_T'$ plane into six regions. In region I, composed of UXW and ZTU, there is one real root and two complex roots. The real part of each root is negative, and the solution is stable. In region II, bounded by UTX, there are three real negative roots, and the solution is stable. In region III, bounded by VXW, there are two complex roots and one real root. The real root is negative, but the real part of each complex root is positive. The solution is unstable to growing oscillations. In region IV, bounded by VXY, there are two positive real roots and one negative real root. The solution is unstable to convection from infinitesimal disturbances. In region V, bounded by STY, there are two negative real roots and one positive real root. The solution is again unstable to convection from infinitesimal disturbances. In

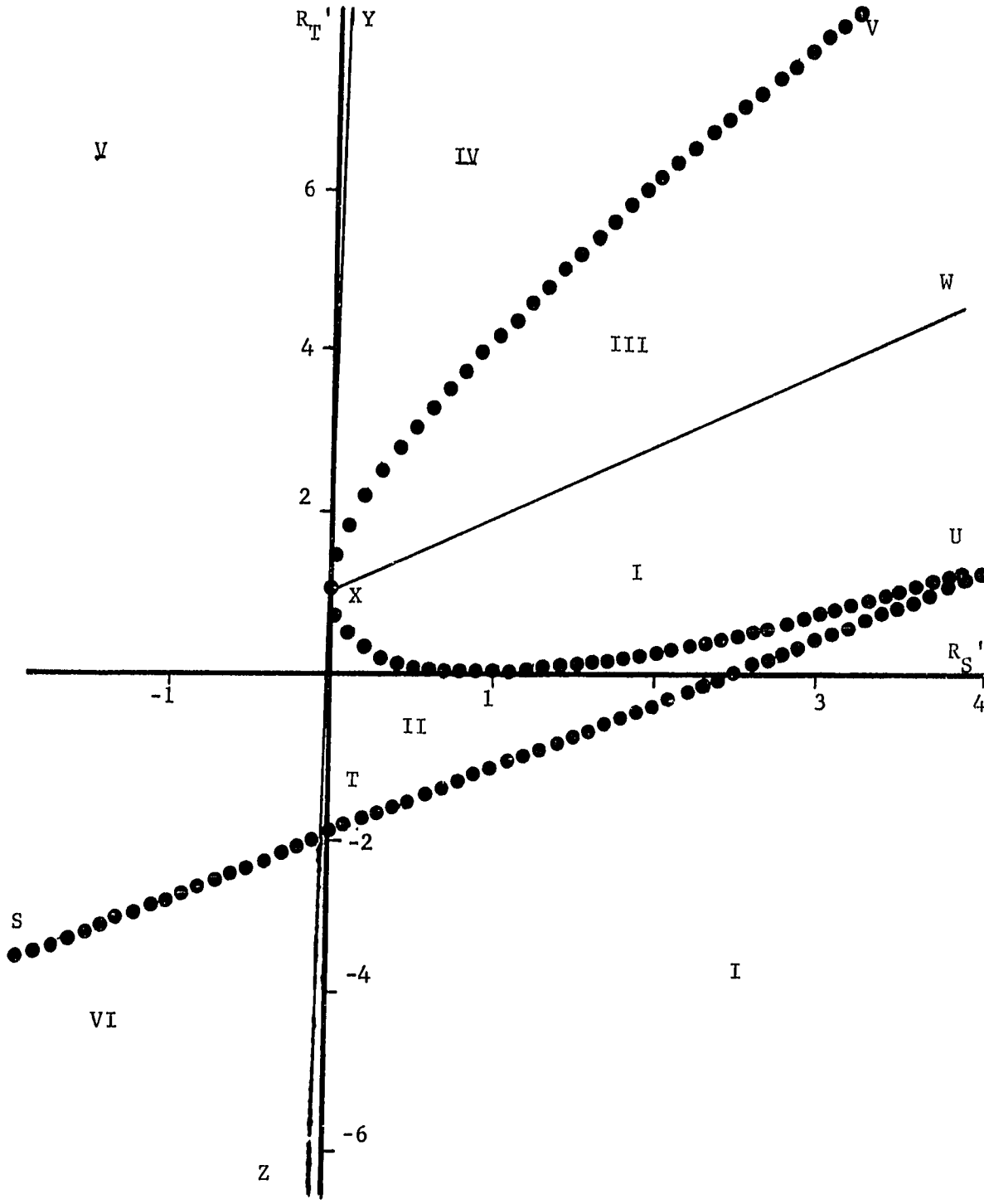

Fig. V.1. Solution plane of convective stability characteristic equation.

region VI, bounded by STZ, there are two complex roots and one real root. The real part of each complex root is negative, but the real root is positive. The solution here is also unstable to convection from infinitesimal disturbances. The solution is then composed of three regimes. Regions I and II make up the stable regime. Region III is the overstable regime. Regions IV, V, and VI make up the unstable direct regime.

Fig. V.1 is representative of the solution for virtually all values of T and S. The slope WX is slightly smaller, and the area of region II is slightly less for higher values of T.

We are chiefly interested in the boundary of the stable regime, the lines ST, TX, and XW, for physical values of R_T and R_S where R_T' is positive. To determine this, we need to establish the dependence of the solution on wavenumbers k and k_x. We invert the substitutions that led to (V.29) from (V.28). Then (V.34) and (V.35) become respectively

$$R_T = \frac{1}{\tau} R_S + \frac{k^6}{k_x^2} , \tag{V.36}$$

$$R_T = \frac{\sigma + \tau}{\sigma + 1} R_S + \frac{1}{\sigma} (1 + \tau) (\sigma + \tau) \frac{k^6}{k_x^2} . \tag{V.37}$$

For a given R_S we are interested in the smallest R_T that is possible for all allowable wavenumbers. $k^2 = k_x^2 + k_z^2$. R_T will be smallest for the smallest allowed k_z. To satisfy a zero perturbation at the boundaries, $k_z = m\pi$, where m is an integer. If we are to have a disturbance at all, then m must be at least 1. Therefore the smallest value of R_T is given when $k_z^2 = \pi^2$. To find the minimum with respect to k_x,

we take $\partial R_T/\partial(k_x^2)$, obtaining $k_x^2 = \frac{1}{2}\pi^2$. k^6/k_x^2 in (V.36) and (V.37) then becomes $27\pi^4/4 = 658$. Since $\tau \ll \sigma$, the region of stability, i.e. the area below WX, is approximately given by

$$R_T \lesssim \frac{\sigma}{\sigma + 1} R_S + \frac{27\pi^4}{4} . \qquad (V.38)$$

If we established a salt gradient ranging from S = 0 to S = 20% over a depth of 1.5 m, then $R_S \approx 3.5 \times 10^{13}$. Since we are so far from the origin, we may write $R_T \lesssim \sigma/(\sigma+1)\ R_S$ or

$$\Delta T \lesssim \frac{\sigma}{\sigma + 1} \frac{\beta}{\alpha} \Delta S. \qquad (V.39)$$

D. Perturbation Equations with Radiation Term

In this section we consider the case of a fluid slab of depth d that absorbs radiation incident from above and is initially stagnant. The boundary conditions and the procedure are the same as in Section C, except that here, the radiation term is included in (V.12). In the unperturbed case we have a change in the solution for T(z). (V.12) becomes

$$\nabla^2 T = - \frac{1}{p_m C_V K_T} \int d\lambda\ H(\lambda)\ \mu(\lambda)\ \exp(-\mu(\lambda)\ z)$$

$$T(z) = T_o + \{\frac{1}{K} \int d\lambda\ \frac{H(\lambda)}{\mu(\lambda)}\} + \{\frac{\Delta T}{d} - \frac{1}{K\,d} \int d\lambda\ \frac{H(\lambda)}{\mu(\lambda)}\ (1 - \exp(-\mu(\lambda)\ d))\}\ z$$

$$- \frac{1}{K} \int d\lambda\ \frac{H(\lambda)}{\mu(\lambda)} \exp(-\mu(\lambda)\ z), \qquad (V.40)$$

where $K = p_m C_V K_T$. (V.40) is typical of the temperature profile in solar pond insulating layers.

When we introduce infinitesimal perturbations to the variables, we get the same results as Section C, except that (V.17) becomes

$$\frac{\partial T}{\partial z} + u_z \left\{\frac{\Delta T}{d} - \frac{1}{K\,d}\int d\lambda\, \frac{H(\lambda)}{\mu(\lambda)}\,(1 - \mu(\lambda)\, d\, \exp(-\mu(\lambda)\, z) - \exp(-\mu(\lambda)\, d))\right\}$$
$$= K_T\, \nabla^2 T. \qquad (V.41)$$

The term in brackets is simply $\partial T/\partial z$ from (V.40). It is important to recognize this, because it implies that the radiation dependence of the stability conditions at any given point are dependent only on $\partial T/\partial z$, which can often be determined experimentally. We now define the radiative temperature correction term as

$$dT_R = -\frac{1}{K}\int d\lambda\, \frac{H(\lambda)}{\mu(\lambda)}\,(1 - \mu(\lambda)\, d\, \exp(-\mu(\lambda)\, z) - \exp(-\mu(\lambda)\, d)), \qquad (V.42)$$

which is a function of z. We also define the radiation thermal Rayleigh number as

$$R_{TR}(z) = (\Delta T + dT_R)\,\frac{g\,\alpha\, d^3}{\nu\, K_T}. \qquad (V.43)$$

We substitute $\Delta T/d + dT_R/d$ for $\Delta T/d$ in (V.17), substitute $R_{TR}(z)$ for R_T, and once again carry out the procedure of Section C. With these substitutions, all the results of Section C, especially Fig. V.1 and (V.34-38), will also be valid for the case where the incident radiation term is included. (V.39) is now rewritten

$$dT_R < -\Delta T + \frac{\sigma\,\beta}{(\sigma + 1)\,\alpha}\,\Delta S. \qquad (V.44)$$

E. Implications for Solar Pond Design

The radiative correction term dT_R has been calculated using the absorption coefficients of Fig. III.5 and the air mass 1 spectral irradiance data of Fig. III.3, adjusted for a total insolation of 100 W/m^2. The results for several insulation layer depths are given in Table V.2 below. All radiation with $\lambda > 1325$ nm has been assumed to be totally absorbed in the first millimeter below the surface.

Since solar pond temperatures are relatively slow to change over the course of the day, and it is the average insolation that produces $\partial T/\partial z$, the 24 hr average insolation should be used. The 100 W/m^2 is the insolation that actually penetrates the surface, and Fresnel losses must first be accounted for when considering measured surface insolation values. The implication of (V.42), as illustrated by the values of dT_R in Table V.2, is that there will always be a steep temperature gradient at the top of the solar pond insulating layer whenever the average insolation is high. The high temperature gradient makes that part of the pond very susceptible to convective instability. Providing a cover would not eliminate the instability, unless it selectively absorbed almost all of the longwave radiation, while transmitting all of the shortwave radiation. It should be recognized that the top few cm of the solar pond undergoes significant temperature fluctuations on a daily basis. These daily fluctuations increase the chances of the onset of convection. However daily effects at deeper levels, several dm below the surface, are small compared with long term effects.

Table V.2. Radiative temperature correction term dT_R (C°) as a function of slab depth h and depth below the top surface of the slab z for a surface penetrating insolation of 100 W/m^2.

z(m)\h(m)	.4	.8	1.2	1.6	2.0	2.4
.01	12.08	31.22	53.28	77.28	102.79	129.55
.02	9.21	25.49	44.69	65.83	88.47	112.37
.03	7.45	21.98	39.42	58.79	79.67	101.82
.04	6.21	19.48	35.68	53.80	73.44	94.34
.05	5.23	17.54	32.75	49.91	68.57	88.50
.06	4.43	15.93	30.34	46.69	64.55	83.66
.07	3.74	14.55	28.27	43.93	61.10	79.53
.08	3.13	13.33	26.45	41.51	58.07	75.90
.09	2.59	12.25	24.83	39.35	55.37	72.65
.10	2.10	11.28	23.27	37.39	52.92	69.72
.12	1.24	9.56	20.79	33.95	48.62	64.56
.14	.50	8.07	18.56	30.99	44.92	60.11
.16	-.15	6.77	16.60	28.37	41.65	56.19
.18	-.74	5.60	14.84	26.03	38.72	52.68
.20	-1.27	4.53	13.25	23.90	36.06	49.49
.25	-2.42	2.23	9.80	19.31	30.32	42.59
.30	-3.38	.31	6.91	15.45	25.50	36.81
.35	-4.21	-1.35	4.42	12.14	21.36	31.84
.40	-4.94	-2.80	2.25	9.23	17.72	27.48
.45		-4.10	.31	6.64	14.49	23.60
.50		-5.26	-1.44	4.32	11.58	20.11
.55		-6.31	-3.02	2.21	8.94	16.94
.60		-7.28	-4.47	.28	6.53	14.05
.65		-8.17	-5.80	-1.50	4.31	11.38
.70		-8.99	-7.04	-3.15	2.25	8.94
.75		-9.76	-8.19	-4.68	.33	6.61

Since salt is a major cost of solar ponds, there is economic pressure to use as little salt as possible. Since the top of the pond is likely to convect anyway, a good scheme to minimize salt use would be to keep the surface of the pond flooded with fresh water, so that the entire salt gradient is completely below the top convecting layer. The radiation penetrating through the insulating layer would be decreased only slightly by this technique.

As an example of the use of Table V.2 in solar pond design, consider a 1.6 m deep insulating layer that supports ΔT = 60° C and ΔS = 10%. Assume that the average penetrating insolation is 250 W/m^2, the temperature in the top of the pond is 40° C, and the salt concentration is a few percent. We then have σ = 4.3 and β/α = 16.5. From (V.44) the maximum allowable radiative temperature correction term is then

$$dT_R = -60 + (4.3/5.3)\ (16.5)\ (10) = 72°\ C.$$

The number to look for in Table V.2 is then (72° C) (100/250) = 28.8° C, which occurs between .14 and .16 m. If a minimum salt strategy is being used, the insulating layer should then be covered with .16 m of fresh water at this time of intense insolation.

VI. EXPERIMENTAL PROJECT AT LIVING HISTORY FARMS

A. Introduction to Project

In conjunction with the modeling of solar pond thermal behavior and theoretical analysis of convective instability reported in the previous three chapters, an experimental solar pond project has been conducted in collaboration with Living History Farms, a historical museum, and an architecturaldesign team under the direction of Ray D. Crites. The project consists of designing, constructing and monitoring the thermal performance of a solar residence and salt gradient solar pond combined system. A brief report of the preliminary results of this project was presented at the 2nd National Passive Solar Conference in March, 1978 (86).

Living History Farms was formed in 1967 as a nonprofit, educational, historical foundation to buy land and develop and operate three farms which tell the story of Midwestern agricultural development. The three farms are located on a 500 acre site on Interstates 80 and 35, northwest of Des Moines, Iowa at Exit 32. The three farms include a Pioneer Farm of 1840 and a Horse Farm of 1900, which are both operating, and a Farm of Today and Tomorrow which is currently being developed. The farms are open daily for visitors and serve over 100,000 people yearly, of which 40,000 are school children. Crafts, grain harvest, and corn picking festivals are held each year. Living History Farms operates from contributions and fees and is a nonprofit organization. Over $3,000,000 has been contributed to date.

The Farm of Today and Tomorrow will include a hybrid solar residence, crop museum, and several small-scale prototype farming operations. The farm will utilize current advanced farming techniques, as well as prototypical future systems for poultry layers, poultry broilers, swine, dairying, beef, sheep production, grain processing, and grain handling. The farm intends to develop an integrated program utilizing energy conservation and solar energy whenever possible.

Ray D. Crites, F.A.I.A., is Professor of Architecture at Iowa State University and is senior partner in the Ames Design Collaborative, an architectural design firm. He has been active in energy conserving and solar design work for the past five years and has designed a number of solar residences throughout Iowa.

The solar project was initially funded by a $17,000 grant from the Iowa Energy Policy Council (IEPC) to Living History Farms in 1975. This grant was used to fund the conceptual design of the residence, build the model from which the picture for Fig. VI.1 below was taken, and purchase two radiation pyranometers and 38 thermocouples for instrumentation of the solar pond. In addition the IEPC grant sponsored a solar pond conference in Ames in December, 1975, featuring invited speakers Carl Nielsen from Ohio State University, David Styris from Battelle Northwest Laboratories, and Ari Rabl from Argonne National Laboratory.

Starting at the same time as the IEPC grant, the Energy and Mineral Resources Research Institute (EMRRI) at Iowa State University provided computer time and the services of myself in developing a computer model of the solar pond and in designing the solar pond at Living History Farms.

This EMRRI support has continued up to the present time. During 1977 EMRRI also provided part time services of Paul Sidles and Professor Laurent Hodges as advisors to this project.

In 1977 IEPC provided an additional $12,000 to help monitor the thermal performance of the house and the solar pond. $771.40 of this amount was used to purchase additional thermocouples which were to be placed in the ground around the solar pond. The remainder of the IEPC grant reverted back to the IEPC when Department of Energy (DOE) funding of this project was announced.

In September, 1977 the U.S. DOE awarded a research grant of $54,500 to Ray D. Crites and the Ames Design Collaborative for this project. These funds were to be used to provide detailed architectural drawings of the solar pond and solar pond heat exchange system, help construct the solar pond, instrument the pond and house, collect and analyze data from the instruments, provide a computer model of the house-pond system, and report on the thermal performance of the system and the results of the system model.

B. Hybrid Solar Residence

The solar heated residence for the Farm of Today and Tomorrow, designed by Ray D. Crites and the Ames Design Collaborative and currently under construction, will incorporate many energy conserving and passive solar principles. A passive solar device is defined as a solar device in which the flow of heat is completely by natural means, as opposed to an active device in which the flow of heat is by mechanical means (e.g. using

air fans or water pumps). A greenhouse is incorporated into the residence, and the house is covered by large amounts of earth insulation. Although most of the heat in the residence will move by natural means, the house is called a hybrid solar residence, since small fans will occasionally be used to move heat. This will improve both the efficiency of the solar system and the comfort level of the house. A small adjacent salt gradient solar pond will supply supplemental space heat to the 262 m^2 of heated area in the structure and will preheat domestic hot water.

A model of the hybrid solar residence and solar pond is shown in Fig. VI.1 below. A floor plan of the residence is shown in Figs. VI.2 and VI.3. Extensive use is made of south facing windows which, during the day, admit solar energy which will be absorbed by the massive concrete structure of the house and stored for use at night. Insulating drapery will reduce heat loss through these windows at night and on cloudy days. A roof overhang over the south windows is designed to provide appropriate shading of direct sunlight during the summer while allowing extensive penetration of direct sunlight during the winter. Solar gain through the south windows will be enhanced in the winter due to sunlight reflecting off the farm pond immediately to the south of the house.

Greenhouse space, incorporated into the residence on both sides of the living space, also collects solar energy, provides some food, absorbs CO_2 and generates O_2, and additionally provides beneficial visual and emotional effects derived from living with plants.

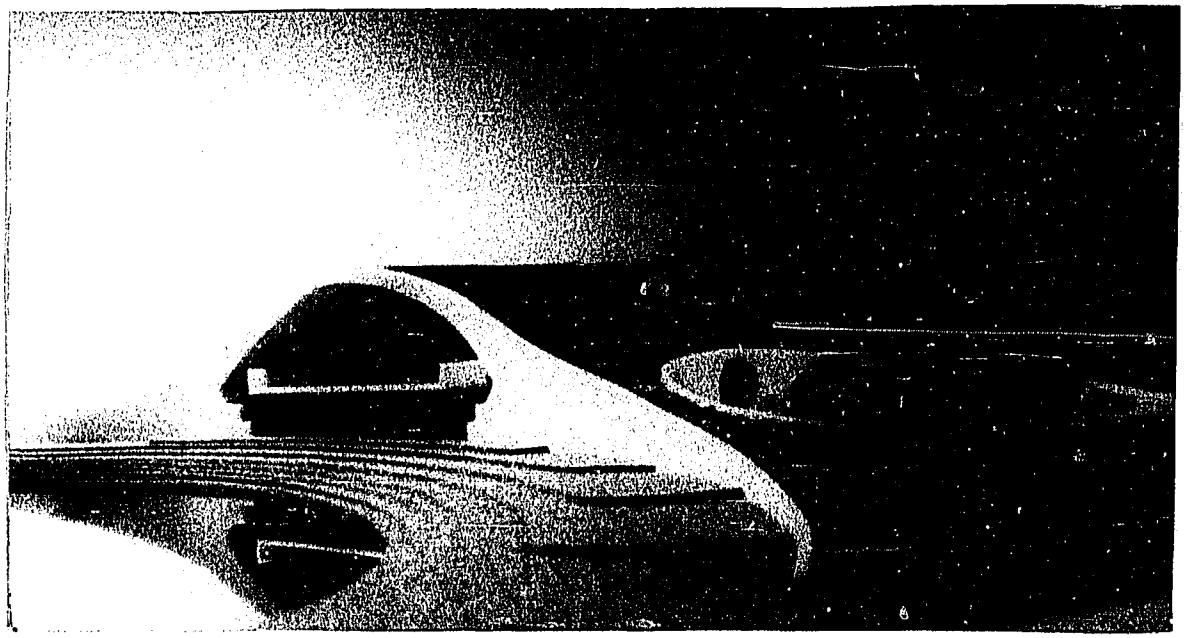

Fig. VI.1. Model of house and solar pond.

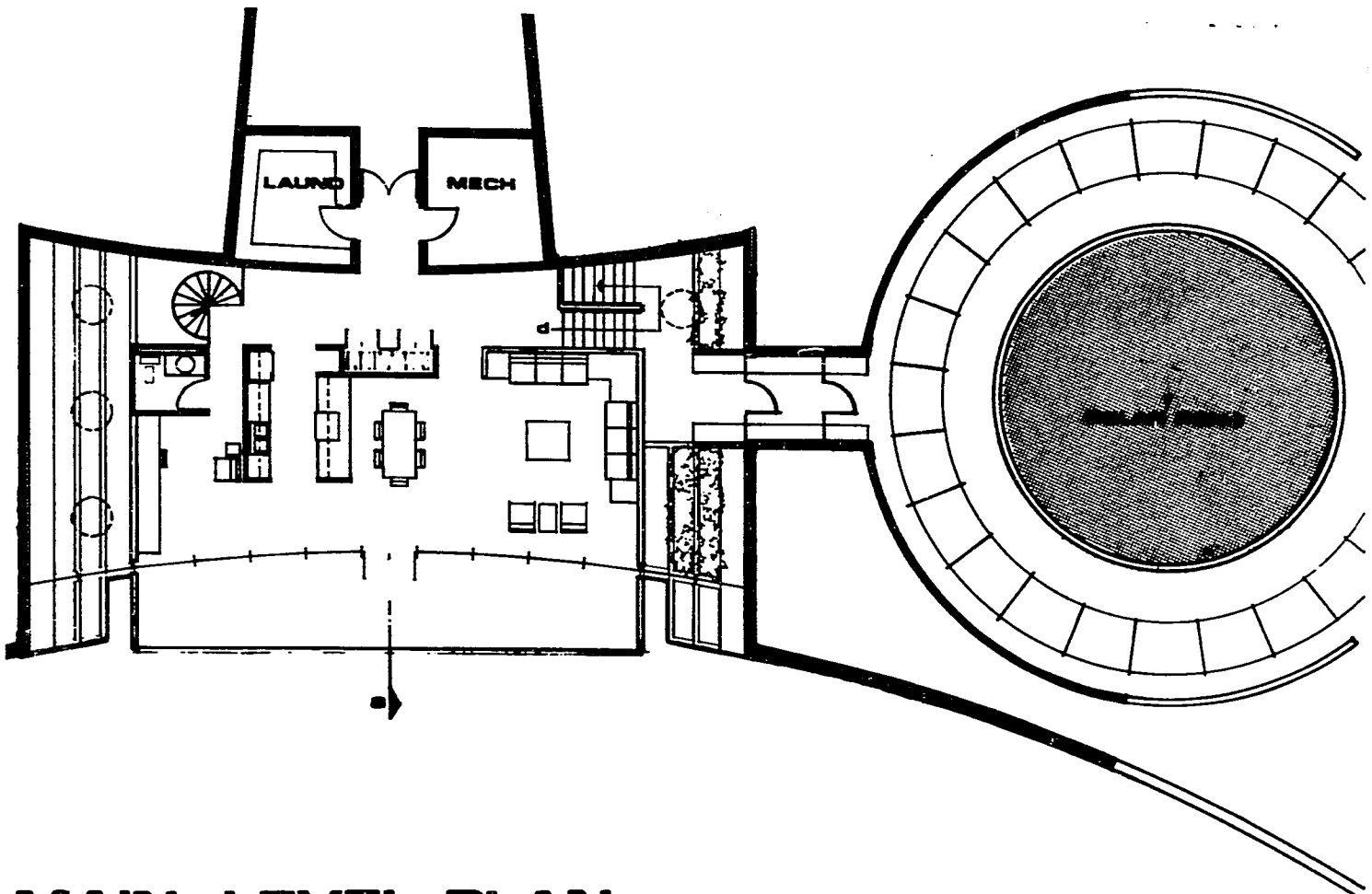

Fig. VI.2. Main level plan of house.

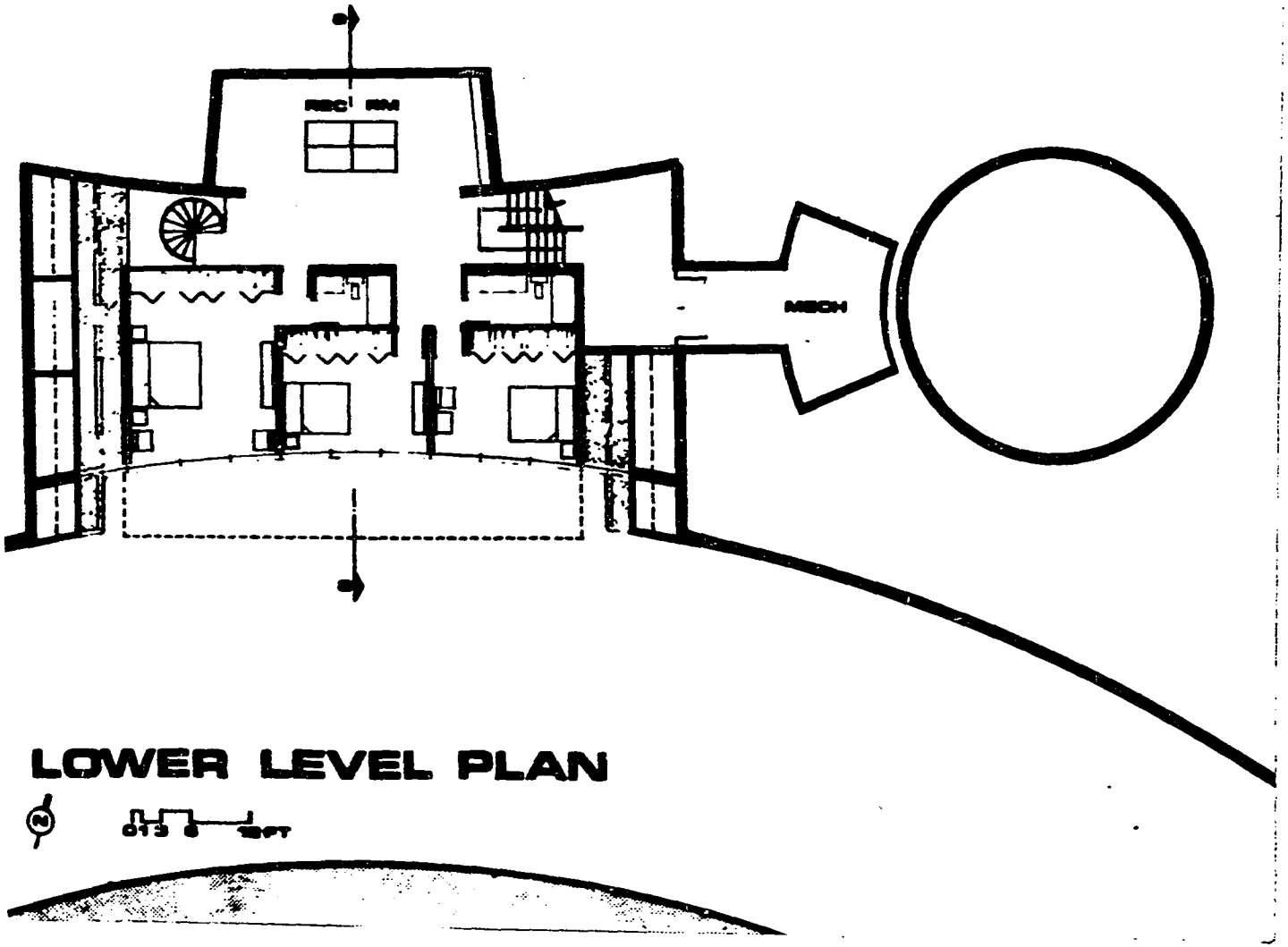

Fig. VI.3. Lower level plan of house.

The top, east, and west sides of the house will be completely covered by 1 to 3 meters of earth, which helps reduce heat losses, provides some additional thermal mass, and makes the passive solar system feasible. Earth underneath the lower concrete slab cannot be used as heat storage due to the high water table in the area. As in the case with the solar pond, underground water movement below the house constitutes a very large heat sink. Soil samples of the building site, as well as water leaking into the solar pond excavation, indicate several slow moving sand-water streams. Heat losses will be controlled by insulation under the lower slab and by careful drainage of the house and solar pond site.

Much of the collected heat will tend to migrate via natural convection toward the ceiling of the upper level. When the air temperature near the ceiling of the upper level is sufficiently great, a small fan will transport the stratified warm air near the underside of the roof to the lower level, where it will be introduced into the bedrooms and be allowed to return through the greenhouse to be recycled.

A connected hydronic network of water pipes, embedded in the concrete slab of both the upper and lower floors, will provide an uniform floor temperature throughout the house. During the heating season, the upper floor will receive most of the incoming solar radiation, and the top part of the upper-level floor slab will be covered with ceramic floor tile, which will heat up quickly. When the temperature difference between the upper-level floor slab and the lower-level floor slab becomes sufficiently great, a pump will operate, and water will circulate in the hydronic network, carrying heat from the upper slab to the lower slab.

During the night this heat will radiate and naturally convect into the living space.

When sufficient sunlight is not available, and when heat from the thermal mass of the house has been depleted, heat will be withdrawn from the solar pond through a liquid to liquid heat exchanger and circulated through the hydronic network of the floor slabs. It is estimated that except for small amounts of electrical energy needed to operate fans and water pumps, the passive solar system and the solar pond will provide 100% of the space heating needs of the house; however, a liquid to air heat pump that operates off of the fresh water farm pond will provide emergency backup heating and summer cooling for the latent cooling load.

During the cooling season, the house will operate partially in the passive mode. The roof overhang will intercept the incoming radiation, and most of the diffuse radiation can be reflected by the insulating drapes. The surrounding earth, at a lower temperature than the house, will absorb some of the heat. Water from the bottom of the farm pond will be circulated in the liquid floor panels to compensate for sensible heat gain. The heat pump will provide auxiliary cooling and dehumidification.

To date the only construction work completed on the house has been the pouring of the concrete walls and ceiling of the mechanical room adjacent to the solar pond in September, 1978. One function of this mechanical room is to house the data recording instruments used to monitor the thermal performance of the residence and solar pond.

C. Solar Pond

The design of the solar pond at Living History Farms has been discussed previously in Chapter IV, Section C of this thesis. The solar pond was intended to provide all of the auxiliary space heat for the hybrid solar residence. The amount of auxiliary heat required over the course of the year was difficult to calculate, since the performance efficiency of the passive solar system of the house, being of unique design, was uncertain. A conservative design strategy was selected. It was assumed that the house could supply 100% of its heat needs during the time when the sun was above the horizon, but none of its heat needs when the sun was below the horizon. The heat load for the house was calculated by standard architectural techniques to be 410 W/C° with a load temperature of 18.3° C. Using this heat load, the average weekly temperature data for the area, and the computer program as described in Chapter IV, the surface area, depth of the insulating layer, depth of the convecting layer, and amount of wall insulation was determined. It was also assumed that any heat entering the ground water either from the solar pond or the house would be immediately lost to the system. It is hoped that drainage tiles around the pond site will improve the groundwater situation, and that some ground storage will become available. But for the initial design, the worst case situation was assumed.

The solar pond at Living History Farms is a steel reinforced concrete cylinder that is sunk into the ground adjacent to the solar residence site. The open top has a radius of 4.8 m. The cylinder is 4.5 m deep. The concrete vertical walls and circular bottom are 21 cm thick.

Approximately 30 cm of polyurethane insulation will be sprayed on the interior walls to thermally insulate the pond from the environment and protect the concrete walls from vertical thermal stress. The urethane insulation will be covered with a water impermeable membrane to protect the integrity of the insulation and prevent salt leakage. The bottom convecting layer will be approximately 2.8 m deep and will consist of a 20% salt solution. The insulating layer, which contains the salt gradient, will be approximately 1.4 m deep.

A copper or stainless steel heat exchange coil will be placed at the top of the convecting layer. Fresh water will be circulated through the heat exchanger, picking up heat in the solar pond and losing heat to the house load, either in the hydronic floor network or in a domestic hot water heat exchanger.

Although an air inflated plastic cover is shown in the model in Fig. VI.1, it is most likely that such a cover will not be employed. Although such a cover is architecturally pleasing and keeps leaves and other debris out of the pond, it degrades the performance of the pond slightly from both a thermal and economical standpoint.

Construction progress to date (October, 1978) is that a hole has been excavated, the concrete walls and floor have been poured, and earth has been filled back in around the outside of the pond. The polyurethane insulation has yet to be installed.

An array of thermocouples have been placed in the ground around the solar pond. Additional thermocouples have been attached to the inside wall of the pond to monitor the temperature in the urethane

insulation. The physical location of the thermocouples with respect to the solar pond is shown in Fig. VI.5. These thermocouples are made of iron-constantan and are enclosed in a stainless steel sheath. Connecting wire leads from the thermocouples through PVC pipe into the mechanical room. The thermocouples shown in Fig. VI.5 have all been installed. An additional array of thermocouples will be placed in the pond salt solution after it is filled.

It is anticipated that construction of the pond will finish during the fall of 1978. Filling and operation of the pond should commence in the early spring of 1979. It is anticipated that the pond will deliver 7.4×10^{10} J of usable heat. The predicted convecting layer temperature as a function of time is shown in Fig. IV.4.

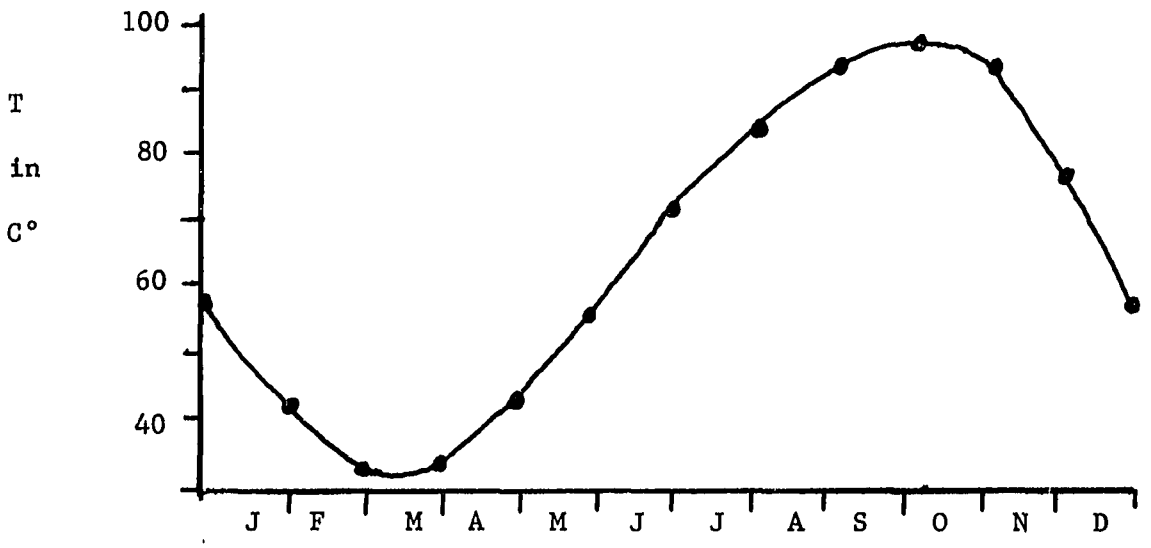

Fig. IV.4. Predicted convective layer temperature as a function of time for the solar pond at Living History Farms.

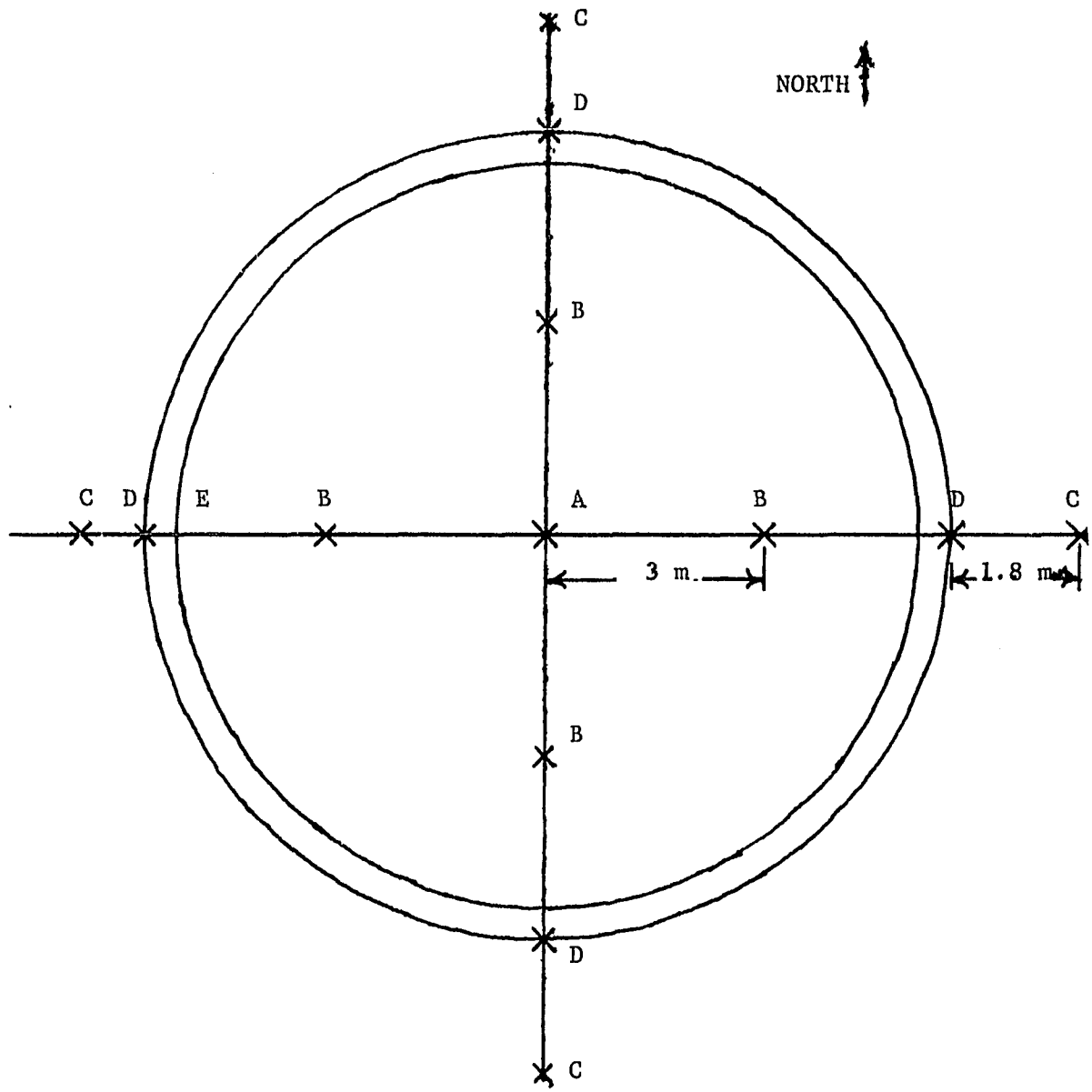

A-3,4,5,6,7,8,9,10,11; B-4,7,9; C-1,2,7; D-1,2,7;
E-3 at 1, 3 at 2, in side insulation;
where, measured up from the bottom of the pond floor slab:
1 = 2.8 m; 2 = 1.2 m; 3 = .35 m; 4 = .25 m; 5 = .15 m; 6 = 0 m;
7 = -.5 m; 8 = -1 m; 9 = -1.5 m; 10 = -2 m; 11 = -2.5 m.

Fig. VI.5. Location of fixed solar pond thermocouple array.

VII. REFERENCES CITED

1. E. Cook, Sci. Am. 224, 135 (Sept., 1971).

2. G. F. Montgomery, Sci. Am. 237, 52 (Dec., 1977).

3. A. v. Kalecsinsky, Ann. Physik IV 7, 408 (1902).

4. M. Rozsa, Physik. Zeitschr. 16, 108 (1915).

5. E. E. Angino, K. B. Armitage, and J. C. Tash, Limnology and Oceanography 9, 207 (1964).

6. E. E. Angino and K. B. Armitage, J. of Geology 71, 89 (1963).

7. K. B. Armitage and H. B. House, Limnology and Oceanography 7, 36 (1962).

8. R. A. Hoare et al., Nature 202, 886 (1964).

9. T. G. L. Shirtcliffe and R. F. Benseman, J. of Geophys. Res. 69, 3355 (1964).

10. A. T. Wilson and H. W. Wellman, Nature 196, 1171 (1962).

11. T. G. L. Shirtcliffe, J. of Geophys. Res. 69, 5257 (1965).

12. H. Tabor, Electronics and Power 10, 296 (1966).

13. H. Z. Tabor, Science Journal 2, No. 6, 66 (June, 1966).

14. H. Tabor and R. Matz, Solar Energy 9, 177 (1965).

15. H. Tabor, Solar Energy 3, 189 (1959).

16. H. Tabor, Solar Energy 7, 189 (1963).

17. J. R. Hirshmann, Solar Energy 13, 83 (1970).

18. K. Drumheller et al., Battelle Pacific Northwest Laboratories Report No. BNWL-1951 (1975).

19. H. Tabor, Desalination 17, 289 (1975).

20. G. Assaf, Solar Energy 18, 293 (1976).

21. G. Rambach, Nonconvecting Pond Review (1978) (unpublished).

22. T. Taylor, Solar Age 3, No. 8, 22 (August, 1978).

23. R. Emden, Helvetica Physica Acta 13, 396 (1940).

24. H. Weinberger, Solar Energy 8, 45 (1964).

25. A. Rabl and C. E. Nielsen, Solar Energy 17, 1 (1975).

26. C. E. Nielsen and A. Rabl, Proc. AS of ISES and SES of Canada 5, 183 (1976).

27. A. Rabl, Solar Energy Research Institute, private communication.

28. A. Rabl and C. E. Nielsen, Chemtech 5, 608 (1975).

29. C. E. Nielsen and A. Rabl, ISES, Extended abstract 35/5 (1975).

30. C. E. Nielsen, Proc. AS of ISES and SES of Canada 5, 169 (1976).

31. C. E. Nielsen, ISES, Paper 1203 (1978).

32. C. E. Nielsen, AS of ISES, 932 (1978).

33. F. Zangrando and H. C. Bryant, Solar Age 3, No. 4, 21 (April, 1978).

34. T. H. Short, P. C. Badger, and W. L. Roller, Proc. Conf. on Solar Energy for Heating Greenhouses and Greenhouse-Residence Combinations, 220 (1977).

35. P. C. Badger et al., AS of ISES (1977).

36. T. H. Short, P. C. Badger, and W. L. Roller, Proc. Conf. on Solar Energy for Heating Greenhouses and Greenhouse-Residence Combinations (1978).

37. Yu. U. Usmanov, G. Ya. Umarov, and R. A. Zakhidov, Geliotekhnica 5, No. 2, 49 (1969).

38. Yu. Usmanov, V. Eliseev, and G. Umarov, Geliotekhnica 7, No. 1, 28 (1971).

39. Yu. Usmanov, V. Eliseev, and G. Ya. Umarov, Geliotekhnica 7, No. 3, 78 (1971).

40. V. N. Eliseev, Yu. U. Usmanov, and L. N. Teslenko, Geliotekhnica 7, No. 4, 17 (1971).

41. Yu. U. Usmanov, V. N. Eliseev, and G. Ya. Umarov, Geliotekhnica 7, No. 4, 24 (1971).

42. Yu. U. Usmanov et al., Geliotekhnica 9, No. 2, 60 (1973).

43. G. C. Jain, The Paris Congress on Solar Energy, Paper EH61 (1973).

44. J. M. K. Dake, The Paris Congress on Solar Energy, Paper E17 (1973).

45. B. Saulnier et al., ISES, Extended abstract 35/1 (1975).

46. E. Nelson, Popular Science 211, No. 6, 30 (1977).

47. L. J. Wittenberg, Nonconvecting Pond Review (1978) (unpublished).

48. D. L. Styris, R. J. Zaworski, and O. K. Harling, Battelle Pacific Nortwest Laboratories, Report No. BNWL-1891 (1975).

49. D. L. Styris et al., ISES, Extended abstract 35/2 (1975).

50. J. P. Leshuk et al., AS of ISES and SES of Canada 5. 188 (1976).

51. D. L. Elwell, T. H. Short, and P. C. Badger, AS of ISES (1977).

52. H. C. Bryant, and I. Colbeck, Solar Energy 19, 321 (1977).

53. Environmental Protection Agency, Water Pollution Control Research Series 11040 GKK (1971).

54. R. C. Terry Jr., Road Salt, Drinking Water, and Safety (Ballinger Publishing Co., Cambridge, Mass., 1974).

55. J. T. Beard et al., NTIS report ORO/5136-77/2 (1977).

56. W. C. Dickinson et al., Solar Energy 18, 1 (1976).

57. D. Corson and P. Lorrain, Introduction to Electromagnetic Fields and Waves (W. H. Freeman, San Francisco, 1962), Chapter 11.

58. R. J. List, Smithsonian Miscellaneous Collection 116, 444 (1968).

59. B. Y. H. Liu and R. C. Jordan, Solar Energy 7, 53 (1962).

60. M. P. Thekaekara, Solar Energy 9, 7 (1965).

61. N. G. Jerlov, Optical Oceanography (Elsevier, Amsterdam, 1968), p. 47.

62. J. Williams, Optical Properties of the Sea (U.S. Naval Institute, Annapolis, 1970).

63. G. L. Clarke and H. R. James, J. Opt. Soc. Am. 29, 43 (1939).

64. J. A. Curcio and C. C. Petty, J. Opt. Soc. Am. 41, 302 (1951).

65. S. A. Kitaigorodskii, The Physics of Air-Sea Interaction (Gidrometeorologicheskoe Izdatelstvo, Leningrad, 1970).

66. E. B. Kraus, Atmosphere-Ocean Interaction (Clarendon Press, Oxford, 1972).

67. D. G. Baker and D. A. Haines, Northcentral Regional Research Publication 195 (1969).

68. U.S. Environmental Data Service and U.S. Weather Bureau, Climatological Data, Vols. 1-27.

69. G. C. Shove, in Grain Storage: Part of a System, edited by R. N. Sinha and W. E. Muir (Avi Publishing, Westport, CO., 1973), p. 209.

70. J. S. Turner, Buoyancy Effects in Fluids (Cambridge at the University Press, 1973), Chapter 8.

71. Lord Rayleigh, Phil. Mag. 32, 529 (1916).

72. J. S. Turner, J. Fluid Mech. 33, 183 (1968).

73. A. Rabl, Solar Energy Research Institute, private communication.

74. H. Stommel, A. B. Arons, and D. Blanchard, Deep Sea Research 3, 152 (1956).

75. M. E. Stern, Tellus 12, 172 (1960).

76. M. E. Stern, J. Fluid Mech. 35, 209 (1969).

77. G. Veronis, J. Mar. Res. 26, 49 (1966).

78. G. Veronis, J. Fluid Mech. 34, 315 (1968).

79. D. A. Nield, J. Fluid Mech. 29, 545 (1967).

80. G. Walin, Tellus 16, 389 (1964).

81. R. S. Shechter, I. Prigogine, and J. R. Hamm, Physics of Fluids 15, 379 (1972).

82. P. G. Baines and A. E. Gill, J. Fluid Mech. 37, 289 (1969).

83. C. Yih, Fluid Mechanics (McGraw-Hill, New York, 1969).

84. L. E. Sissom and D. R. Pitts, Elements of Transport Phenomena (McGraw-Hill, New York, 1972).

85. J. Uspensky, Theory of Equations (McGraw-Hill, New York, 1948).

86. R. D. Crites and J. R. Hull, Proc. 2nd National Passive Solar Conf., 266 (1978).

87. National Research Council, International critical tables..., (McGraw-Hill, New York, 1926-1930).

88. G. Neuman and W. J. Pierson Jr., Principles of Oceanography, (Prentice-Hall Inc., Englewood Cliffs, N.J., 1966), p. 47.

VIII. ACKNOWLEDGMENTS

The author wishes to express his deeply felt gratitude to Professor Laurent Hodges for his help and guidance throughout the entire project.

Many other people have also contributed to the success of this project. Paul Sidles suggested the project and has been helpful throughout. Professor Derek Pursey provided helpful insights during the first stages of the work on convective instability. Professor Ray Crites provided many interesting discussions on the design of the solar pond.

Professor Eugene Takle generously provided hourly Ames insolation data. Mal Iles provided excellent suggestions for instrumentation design. H. V. Sparks generously made available the use of his personal computer for some of the calculations. Both Mal Iles and William McClain helped install most of the thermocouples at the solar pond.

William Murray, president of Living History Farms, and the work crew at the Farm of Today and Tomorrow have cooperated magnificently in respecting the scientific goals of the project.

Finally, my wife, Amy, and son, Cotati, have provided love and understanding throughout my career as a graduate student.

IX. APPENDIX A: PHYSICAL PROPERTIES OF SALT WATER

Except where noted, all values in this appendix were taken from reference 87.

A. Thermal Conductivity

The thermal conductivity K of pure water as a function of temperature T is

$$K(T) = K(20)\ (1 + \alpha(T - 20)), \qquad 0°C < T < 80°C, \qquad (IX.1)$$

where

$$\alpha = 2.81 \times 10^{-3}\ °C^{-1},$$

and

$$K(20) = 0.587\ W\ m^{-1}\ °C^{-1}.$$

The thermal conductivity of aqueous solutions at a given temperature as a function of salt concentration q is

$$K(q) = K_w\ (1 - \beta\ q), \qquad (IX.2)$$

where K_w is the thermal conductivity of pure water at a given temperature and may be found from (IX.1), q is the concentration in grams of solute per 100 grams of solution, and β is a constant that depends on the type of salt as shown in Table IX.1 below.

Table IX.1. Thermal conductivity constant β for aqueous solutions.

Solute	β
$MgCl_2$	4.88×10^{-3}
NaCl	2.48×10^{-3}
KNO_3	3.47×10^{-3}

B. Heat Capacity

The heat capacity values given below were from the I.C.T. tables (87) for $q > 5$. Values for lower q were extrapolated to agree with that of pure water (88) for $q = 0$. q is the concentration in grams of solute per 100 grams of solution.

1. NaCl

The heat capacity of a NaCl solution at 20° C as a function of concentration, $C_{20}(q)$, is

$$C_{20}(q) = (0.6516 + (0.3475)\ (0.96285)^{q}\ )\ \text{cal gm}^{-1}\ ^{\circ}\text{C}^{-1}. \qquad \text{(IX.3)}$$

The heat capacity as a function of temperature, C(T), is

$$C(T) = C_{20} + a\ (T - 20) - b\ (T - 20)^{2}\ \text{cal gm}^{-1}\ ^{\circ}\text{C}^{-1}, \qquad \text{(IX.4)}$$

where T is the temperature in °C, C_{20} is given by (IX.3), and a and b are functions of q given by table IX.2 below. (IX.4) is good to within a few percent over the entire temperature range of liquid water and is worst at higher temperatures.

2. $MgCl_2$

The heat capacity of a $MgCl_2$ solution at 0° C as a function of concentration, $C_0(q)$, is

$$C_0(q) = 1.0158 - 0.018091\ q + 1.9734 \times 10^{-4}\ q^{2}\ \text{cal gm}^{-1}\ ^{\circ}\text{C}^{-1}. \qquad \text{(IX.5)}$$

The heat capacity as a function of temperature C(T) is

$$C(T) = C_0 + a\ T\ \text{cal gm}^{-1}\ ^{\circ}\text{C}^{-1}, \qquad \text{(IX.6)}$$

where C_0 is given by (IX.5), and a is a function of concentration given by Table IX.3 below.

Table IX.2. NaCl heat capacity constants as a function of concentration.

a is in 10^4 cal gm^{-1} $°C^{-2}$. b is in 10^6 cal gm^{-1} $°C^{-3}$.

q	0	1	2	3	4	5	6	7	8
a	0.0	0.5	1.0	1.5	1.9	2.3	2.6	2.8	3.0
b	0	0	0	0	0	0	-1	-2	-3
q	9	10	11	12	13	14	15	16	17
a	3.0	3.1	3.2	3.2	3.2	3.1	3.0	2.8	2.7
b	-4	-5	-5	-5	-6	-6	-6	-6	-6
q	18	19	20	21	22	23	24	25	
a	2.5	2.3	2.0	1.8	1.5	1.5	1.2	0.9	
b	-6	-6	-6	-6	-6	-5	-5	-5	

Table IX.3. $MgCl_2$ heat capacity constant as a function of concentration.

a is in 10^4 cal gm^{-1} $°C^{-2}$.

q	0	1	2	3	4	5	6	7	8
a	0.0	0.3	0.7	1.1	1.5	1.9	2.4	2.8	3.3
q	9	10	11	12	13	14	15	16	17
a	3.7	4.1	4.5	4.8	5.2	5.5	5.8	6.0	6.2
q	18	19	20	21	22	23	24	25	26
a	6.3	6.4	6.5	6.5	6.5	6.5	6.5	6.4	6.4

C. Density

1. NaCl

The density values given below were taken from the I.C.T. tables (87) for $q > 5$. Values for lower q were extrapolated to agree with that of Table IX.5.

The density of a NaCl solution at temperature 25° C as a function of concentration $d_{25}(q)$ is

$$d_{25}(q) = 0.99797 + 0.0070033\ q + 1.4059\times10^{-5}\ q^2 + 3.309\times10^{-7}\ q^3 \quad \text{gm/ml.} \qquad \text{(IX.7)}$$

The density of a NaCl solution as a function of temperature d(T) is

$$d(T) = d(0)/(1 + a\ T + b\ T^2 + c\ T^3)\ \text{gm/ml}, \qquad \text{(IX.8)}$$

where d(0) is the density at 0° C, and may be found from (IX.7) and (IX.8), and a, b, and c are functions of the concentration and are given in Table IX.4 below.

The density of NaCl solutions as a function of both temperature and concentration is given in Table IX.5 below. Table IX.5 may be used to corroborate Table IX.4 or be used independently. In the solar pond computer model the former method is used.

Table IX.4. NaCl density constants as a function of concentration.

a is in 10^{-4} °C^{-1}. b is in 10^{-6} °C^{-2}. c is in 10^{-9} °C^{-3}.

q	a	b	c
0	0.00	4.0	36
1	0.10	4.2	33
2	0.30	4.5	30
3	0.50	5.0	27
4	0.77	5.0	24
5	1.0685	5.1425	21.750
6	1.3380	4.7100	19.000
7	1.5879	4.1362	16.547
8	1.8235	3.9350	14.000
9	2.0394	3.6062	12.047
10	2.2409	3.3037	10.297
11	2.4472	3.0362	8.875
12	2.6001	2.7962	7.703
13	2.7613	2.5725	6.578
14	2.9260	2.2575	3.750
15	3.0629	2.0937	3.297
16	3.1936	1.9187	2.453
17	3.3127	1.7725	1.922
18	3.4253	1.6300	1.328
19	3.5290	1.5100	1.000
20	3.6237	1.4125	0.922
21	3.7129	1.3187	0.797

Table IX.5. Density of NaCl solutions in gm/ml as a function of temperature and concentration.

T	0° C	10° C	20° C	25° C	30° C
q					
1	1.00747	1.00707	1.00534	1.00409	1.00261
2	1.01509	1.01442	1.01246	1.01112	1.00957
4	1.03038	1.02920	1.02680	1.02530	1.02361
6	1.04575	1.04408	1.04127	1.03963	1.03781
8	1.06121	1.05907	1.05589	1.05412	1.05219
10	1.07677	1.07419	1.07068	1.06879	1.06676
12	1.09244	1.08946	1.08566	1.08365	1.08153
14	1.10824	1.10491	1.10085	1.09872	1.09651
16	1.12419	1.12056	1.11621	1.11401	1.11171
18	1.14031	1.13643	1.13190	1.12954	1.12715
20	1.15663	1.15254	1.14779	1.14533	1.14285
22	1.17318	1.16891	1.16395	1.16140	1.15883
24	1.18999	1.18557	1.18040	1.17776	1.17511
26	1.20709	1.20254	1.19719	1.19443	1.19170

T	40° C	50° C	60° C	80° C	100° C
q					
1	0.99908	0.99482	0.9900	0.9785	0.9651
2	1.00593	1.00161	0.9967	0.9852	0.9719
4	1.01977	1.01531	1.0103	0.9988	0.9855
6	1.03378	1.02919	1.0241	1.0125	0.9994
8	1.04798	1.04326	1.0383	1.0264	1.0134
10	1.06328	1.05753	1.0523	1.0405	1.0276
12	1.07699	1.07202	1.0667	1.0549	1.0420
14	1.09182	1.08674	1.0813	1.0694	1.0565
16	1.10688	1.10170	1.0962	1.0842	1.0713
18	1.12218	1.11691	1.1113	1.0993	1.0864
20	1.13774	1.13238	1.1268	1.1146	1.1017
22	1.15358	1.14812	1.1425	1.1303	1.1172
24	1.16971	1.16414	1.1584	1.1463	1.1331
26	1.18614	1.18045	1.1747	1.1626	1.1492

2. $MgCl_2$

The density of a $MgCl_2$ solution at 0° C as a function of concentration $d_0(q)$ is

$$d_0(q) = 0.99987 + 0.008652\ q + 1.626\times10^{-5}\ q^2 + 4.877\times10^{-7}\ q^3 \quad \text{gm/ml.} \tag{IX.9}$$

The density of a $MgCl_2$ solution as a function of temperature d(T) is

$$d(T) = d_0 - a\ T - b\ T^2 \quad \text{gm/ml,} \tag{IX.10}$$

where d_0 is given by (IX.9) above, and a and b are functions of the concentration and are given in Table IX.6 below. In addition, we have the density of $MgCl_2$ as a function of temperature and concentration in Table IX.7 below. Table IX.7 may be used to verify Table IX.6 or used independently.

Table IX.6. $MgCl_2$ density constants as a function of concentration.

a is in 10^{-6} gm ml^{-1} $°C^{-1}$. b is in gm ml^{-1} $°C^{-2}$.

q	0	1	2	3	4	5	6	7
a	-30	-15	0	15	30	50	70	95
b	4.2	4.5	5.0	5.5	5.5	5.0	4.5	4.5
q	8	9	10	11	12	13	14	15
a	105	115	145	155	172	180	197	205
b	4.5	4.5	3.5	3.5	3.1	3.0	2.6	2.5
q	16	17	18	19	20	21	22	23
a	222	230	238	247	255	258	264	280
b	2.1	2.0	1.8	1.6	1.5	1.6	1.5	1.0

Table IX.7. Density of $MgCl_2$ solutions in gm/ml as a function of temperature and concentration.

T	0° C	10° C	20° C	25° C	30° C	40° C
q						
2	1.0168	1.0163	1.0146	1.0134	1.0119	1.0084
4	1.0338	1.0330	1.0311	1.0298	1.0282	1.0248
6	1.0510	1.0499	1.0478	1.0463	1.0447	1.0413
8	1.0683	1.0669	1.0646	1.0631	1.0615	1.0580
10	1.0858	1.0840	1.0816	1.0801	1.0785	1.0749
12	1.1035	1.1014	1.0989	1.0974	1.0957	1.0921
14	1.1214	1.1190	1.1164	1.1149	1.1132	1.1095
16	1.1395	1.1369	1.1342	1.1326	1.1309	1.1272
18	1.1578	1.1551	1.1523	1.1506	1.1489	1.1452
20	1.1764	1.1735	1.1706	1.1689	1.1672	1.1635
25	1.2246	1.2216	1.2184	1.2167	1.2149	1.2111
30	1.2754	1.2722	1.2688	1.2671	1.2652	1.2614

T	50° C	60° C	70° C	80° C	90° C	100° C
q						
2	1.0043	0.9995	0.9942	0.9883	0.9820	0.9753
4	1.0207	1.0159	1.0107	1.0050	0.9988	0.9923
6	1.0372	1.0325	1.0274	1.0218	1.0158	1.0095
8	1.0539	1.0493	1.0442	1.0388	1.0330	1.0269
10	1.0708	1.0663	1.0613	1.0560	1.0504	1.0444
12	1.0880	1.0836	1.0787	1.0735	1.0680	1.0622
14	1.1055	1.1011	1.0963	1.0912	1.0859	1.0803
16	1.1232	1.1188	1.1141	1.1092	1.1041	1.0984
18	1.1412	1.1368	1.1322	1.1275	1.1225	1.1170
20	1.1595	1.1552	1.1506	1.1460	1.1412	1.1359
25	1.2072	1.2031	1.1987	1.1942	1.1896	1.1847
30	1.2575	1.2535	1.2493	1.2451	1.2406	1.2360

3. KNO_3

The density of KNO_3 solutions as a function of temperature and concentration is given in Table IX.8 below.

Table IX.8. Density of KNO_3 solutions in gm/ml as a function of temperature and concentration.

T q	0° C	10° C	20° C	25° C	30° C
1	1.00654	1.00615	1.00447	1.00324	1.00178
2	1.01326	1.01262	1.01075	1.00946	1.00794
4	1.02677	1.02566	1.02344	1.02203	1.02038
6	1.04041	1.03887	1.03632	1.03479	1.03301
8	1.05419	1.05226	1.04940	1.04775	1.04584
10	1.06812	1.06584	1.06269	1.06093	1.05889
12	1.08221	1.07963	1.07620	1.07433	1.07217
14			1.08994	1.08796	1.08569
16			1.10392	1.10183	1.09947
18			1.11814	1.11595	1.11351
20			1.13261	1.13033	1.12782
22			1.14734	1.14497	1.15726

T q	40° C	50° C	60° C	80° C	100° C
1	0.99825	0.99401	0.9890	0.9776	0.9641
2	1.00430	0.99999	0.9949	0.9834	0.9699
4	1.01652	1.01207	1.0068	0.9951	0.9816
6	1.02892	1.02432	1.0189	1.0070	0.9935
8	1.04152	1.03676	1.0313	1.0192	1.0056
10	1.05434	1.04941	1.0439	1.0316	1.0179
12	1.06740	1.06229	1.0567	1.0442	1.0304
14	1.08072	1.07542	1.0698	1.0571	1.0432
16	1.09432	1.08882	1.0831	1.0703	1.0562
18	1.10821	1.10251	1.0967	1.0837	1.0695
20	1.12240	1.11650	1.1106	1.0974	1.0831
22	1.13691	1.13080	1.1247	1.1113	1.0969

D. Viscosity

Absolute viscosity η is friction to fluid flow and is measured in poise, with 1 poise = 1 gm cm^{-1} s^{-1} = .1 kg m^{-1} s^{-1}. Viscosity is an important parameter in the study of convective stability in solar ponds. The viscosity of pure water is given in Table IX.9 below.

Table IX.9. Viscosity of pure water in millipoise as a function of temperature.

T(C°)	0	1	2	3	4	5	6	7	8	9
0	17.93	17.32	16.74	16.19	15.67	15.18	14.72	14.28	13.87	13.47
10	13.09	12.73	12.39	12.06	11.74	11.44	11.15	10.87	10.60	10.34
20	10.08	9.84	9.60	9.38	9.16	8.94	8.74	8.55	8.36	8.18
30	8.00	7.83	7.67	7.51	7.35	7.20	7.06	6.92	6.79	6.66
40	6.53	6.41	6.29	6.18	6.07	5.97	5.86	5.77	5.67	5.58
50	5.49	5.40	5.32	5.23	5.15	5.07	4.99	4.91	4.84	4.77
60	4.69	4.62	4.56	4.49	4.43	4.36	4.30	4.24	4.18	4.12
70	4.07	4.01	3.96	3.90	3.85	3.80	3.75	3.70	3.66	3.61
80	3.57	3.52	3.48	3.44	3.39	3.35	3.31	3.27	3.24	3.20
90	3.16	3.13	3.09	3.06	3.02	2.99	2.96	2.93	2.89	2.86
100	2.83	2.82	2.79	2.76	2.73	2.70	2.67	2.64	2.62	2.59

1. NaCl

The viscosity η of a NaCl solution is given by

$$\eta = a\,\eta_w, \qquad \text{(IX.11)}$$

where η_w is the viscosity of pure water from Table IX.9 above, and a is a constant from Table IX.10 below.

Table IX.10. Viscosity constant for NaCl solutions as a function of temperature and concentration.

T q	0° C	10° C	18° C	25° C	40° C	60° C	80° C	100° C
0.58	1.004	1.006	1.008	1.009	1.010	1.012	1.013	1.013
1.44	1.009	1.016	1.020	1.022	1.026	1.030	1.031	1.032
2.84	1.02	1.032	1.040	1.046	1.053	1.060	1.062	1.065
5.5	1.04	1.071	1.084	1.094	1.108	1.121	1.12	1.13
10.5	1.14	1.17	1.192	1.205	1.22	1.24	1.26	1.26
14.9	1.28	1.31	1.329	1.341	1.36	1.39	1.40	1.40
18.9	1.45	1.48	1.498	1.50	1.52	1.54	1.55	1.55
22.5		1.69	1.700	1.70	1.71	1.72		

2. $MgCl_2$

The viscosity of a $MgCl_2$ solution is also give by (IX.11), but the constant a is taken from Table IX.11 below.

Table IX.11. Viscosity constant for $MgCl_2$ solutions as a function of temperature and concentration.

T \ q	0.46	0.92	2.32	4.55	8.7	16.0	22.2
18° C	1.022	1.042	1.102	1.209			
25° C	1.016	1.034	1.093	1.200	1.468	2.23	3.36

3. KNO_3

The viscosity of KNO_3 solutions is also given by (IX.11), but the constant a is taken from Table IX.12 below.

Table IX.12. Viscosity constant of KNO_3 solutions as a function of temperature and concentration.

q \ T	10° C	40° C	50° C	60° C
1.00	0.994	0.995		
2.46	0.985	0.989		
4.8	0.974	0.982		
9.1	0.963	0.976	1.02	1.03
17.0	0.97	0.99	1.06	1.08

E. Freezing Point Depression

The freezing point depression is a useful number for studying ice formation in solar ponds. In Tables IX.13, IX.14, and IX.15 below, Δ t is the number of C° below 0° C for which the solution freezes.

Table IX.13. Freezing point depression for NaCl solutions as a function of concentration.

q	Δ t	q	Δ t
0.04	0.025	2.3	1.35
0.06	0.036	3.9	2.35
0.12	0.071	5.5	3.37
0.23	0.14	10.5	6.9
0.40	0.245	14.9	10.8
0.62	0.35	18.9	15.1
1.2	0.68	23.3	21.2

At q = 23.3, the solution becomes a eutectic mixture of ice and $NaCl \cdot 2H_2O$.

Table IX.14. Freezing point depression for $MgCl_2$ solutions as a function of concentration.

q	Δ t	q	Δ t	q	Δt
0.095	0.05	0.92	0.49	8.7	6.35
0.23	0.125	1.8	1.0	16	17.6
0.47	0.25	4.55	2.7	21.9	33.5

At q = 2.94 the solution turns into an eutectic mixture of ice and $MgCl_2 \cdot 12H_2O$.

Table IX.15. Freezing point depression of KNO_3 solutions as a function of concentration.

q	Δ t	q	Δ t
0.02	0.007	2.0	0.63
0.05	0.018	2.9	0.92
0.1	0.036	4.8	1.44
0.2	0.07	9.0	2.56
0.5	0.17	11.2	3.02
1.0	0.33		

At q = 2.41 the solution becomes a eutectic mixture of ice and KNO_3 (rhombic).

F. Boiling Point Elevation

The temperature at which the solar pond boils is a boundary condition on any model and must be avoided in a real pond to prevent convection. In Tables IX.16, IX.17, and IX.18 below, Δ t is the number of C° above 100° C of the boiling point of the solution at sea level.

Table IX.16. Boiling point elevation of NaCl solutions as a function of concentration.

q	Δ t	q	Δ t
2.8	0.47	18.9	4.35
5.5	0.96	22.5	6.0
10.5	2.02	28.4	8.7
14.9	3.2		

Table IX.17. Boiling point elevation of $MgCl_2$ solutions as a function of concentration.

q	Δ t	q	Δ t
0.92	0.12	16	4.35
1.8	0.24	27.6	13.0
4.55	0.64	36	25.5
8.7	1.59		

Table IX.18. Boiling point elevation of KNO_3 solutions as a function of concentration.

q	Δ t	q	Δ t
4.8	0.44	50	6.0
9	0.85	72	12.0
17	1.64	79	15.6
33	3.6		

G. Solubility

The solubility of the various salts is important to know, so that one may establish a sufficient salt gradient to prevent convection. Also there is the possibility of salt freezing out in the winter when the pond cools. The solubility of NaCl, $MgCl_2$, and KNO_3 as a function of temperature is given in Table IX.19 below.

Table IX.19. Solubility of NaCl, $MgCl_2$, and KNO_3 solutions as a function of temperature.

Solubility is in gm of formula weight per 1000 gm of solvent.

T(C°)	$MgCl_2$	NaCl	KNO_3
0	5.50	6.10	1.30
10		6.11	2.08
20	5.76	6.13	3.08
30		6.16	4.47
40		6.22	6.22
50		6.26	8.42
60	6.39	6.33	10.89
70		6.41	13.72
80	6.82	6.50	16.78
90		6.60	20.40
100	7.59	6.70	24.50
116.7	8.98		
120	9.07		

X. APPENDIX B: LISTING OF COMPUTER PROGRAM

On the following pages is a listing of a PL-1 computer program that calculates the thermal performance of a solar pond. A detailed discussion of this program was given in Chapter IV. The program configuration listed contains the following major features:

1. NaCl salt physical parameters are used.
2. The load withdraws heat from the convective layer only at night.
3. Ambient temperature varies sinusoidally about an average with yearly period. The value given is for Ames, Iowa.
4. The pond surface is a circle.
5. Radiation absorption is that of pure water.
6. Each iteration step represents one hour in real time.

The user is required to specify certain solar pond design parameters and several types of input data. The input requirements may be found by searching the program listing for GET statements. Data of salt physical properties may be found in Chapter IX.

```
APOND: PROC OPTIONS (MAIN);
                        /* CALCULATES THERMAL PERFORMANCE OF SOLAR    */
                        /* PONDS                                      */
              /*  INPUT SECTION  */
/* N IS THE TOTAL NUMBER OF SUBLAYERS, N-1 OF WHICH ARE OF DEPTH Z     */
/* CONVECTING LAYER IS M*Z DEEP.  HEATNEED IS IN W/DEG.  THOUSE IS     */
/* ROOM TEMPERATURE. LI=DEPTH OF INSULATING LAYER. LC IS DEPTH OF      */
/* CONVECTING LAYER. T IS THE TEMPERATURE OF EACH SUBLAYER.  LAYER     */
/* ONE IS AT THE TOP OF THE POND AND LAYER N-1 IS AT THE BOTTOM OF     */
/* THE INSULATING LAYER.  LAYER N IS THE CONVECTING LAYER.             */
     DCL (I,J,K,L,M,N,K1) FIXED BIN;
     DCL (Z,THOUSE,HEATNEED,LADITUDE,LI,LC) FLOAT;

     GET LIST(LADITUDE,N,M,Z,HEATNEED,THOUSE);
     LI=(N-1)*Z;
     LC=M*Z;

BEGIN:
     DCL (TG(N+1),KS(N+1),T(N),A(N),Q(N),AS(N),WS(N+1),TA) FLOAT;

     GET LIST (T);          /* READ IN INITIAL WATER TEMPERATURES      */

     TG=15;                 /* SET GROUND TEMPERATURE                  */
     KS=0.4                 /* THERMAL CONDUCTIVITY OF SIDES.  FIRST NUM- */
     KS=KS/25;              /* BER IS IN BTU-IN/(HR-SQFT-DEGF). 2ND IS CM */
     KS=KS*1055/39.37/3600/.0929*9/5;          /*       THICKNESS   */
     WS=2.54/100;           /* CONVERTS TO M                           */
     A=65;                  /* SURFACE AREA                            */

              /* PHYSICAL PROPERTIES OF SALT  */
     DCL (CON(N),KAPPA(N),KBETA,AHC(N),ADEN(N)) FLOAT;
     DCL (HCAA(26),HCBB(26),DENAA(26),DENBB(26),DENCC(26)) FLOAT;
     DCL (HCA(N),HCB(N),DENA(N),DENB(N),DENC(N)) FLOAT;

     GET LIST (CON);                /* INITIAL CONCENTRATIONS          */
     KBETA=0.00248;
     GET LIST (HCAA);
     GET LIST (HCBB);
     GET LIST (DENAA);
     GET LIST (DENBB);
     GET LIST (DENCC);
     HCAA=HCAA/10000;
     HCBB=HCBB/1000000;
     DENAA=DENAA/10000;
     DENBB=DENBB/1000000;
     DENCC=DENCC/1000000000;
```

```
     DO I=1 TO N;
          DENA(I)=XINRP(CON(I),DENAA);
          DENB(I)=XINRP(CON(I),DENBB);
          DENC(I)=XINRP(CON(I),DENCC);
          HCA(I) =XINRP(CON(I),HCAA);
          HCB(I) =XINRP(CON(I),HCBB);
          ADEN(I)=DEN(CON(I),T(I),DENA(I),DENB(I),DENC(I));  /*DENSITY */
          AHC(I)=HC(CON(I),T(I),HCA(I),HCB(I),ADEN(I));   /*H CAPACITY */
     END;
     KAPPA=0.587*(1+0.00281*(T-20))*(1-KBETA*CON);     /* T CONDUCTIVITY*/

                    /* INITIALIZE ENERGY CONTENT */
/* ETUSED IS TOTAL CUMULATIVE ENERGY USED FROM TOP OF POND TO HEAT HOUSE.
   EUSEDT IS SAME FOR HOURLY PERIOD.  EXUSED IS CUMULATIVE HEAT EXTRACTED
    FROM BOTTOM OF THE POND. EUSED IS TOTAL CUMULATIVEHEAT USED TO HEAT
   HOUSE.  ETOPT IS TOTAL CUMULATIVE HEAT OUT THE TOP OF THE POND      */

     DCL (ETOP,ETUSED,EUSED,ADQEX,ADQC,ADQS,EUSEDT,EXUSED) FLOAT;
     DCL (ETOPT,DEGDAY,DEGHR,ESIDE,EOUTB) FLOAT;

     ETUSED=0;  EUSED=0;  EXUSED=0;  ETOPT=0;  DEGHR=0;  ESIDE=0;
     EOUTB=0;

     Q=AHC*Z*A*T;                                  /* HEAT CONTENT          */
     AS=2*Z*(A*3.14159)**0.5;                      /* AREA OF SIDES         */
     AS(N)=A(N)+2*M*Z*(A(N)*3.14159)**0.5;
     Q(N)=M*Z*AHC(N)*A(N)*T(N);

                   /* INSOLATION INPUT */

     DCL (EINPUT,EINPOND,QR(365,16),TIME,TIMNT,EFLUX) FLOAT;
     DCL (DAY(365)) FIXED BIN;
     DCL 1 QRAD(365), 2 DATE1 FIXED,  2 DATE2 FIXED,
                      2 RAD1(8) FLOAT,  2 RAD2(8) FLOAT;

     GET LIST (QRAD);                 /* INSOLATION DATA BEGINS AT 4 AM   */
     DAY=(QRAD.DATE1-1)/10;
     DO L=1 TO 365;                   /* CHANGE RAW DATA TO CORRECT FOR   */
          DO K1=1 TO 8;               /* CALIBRATION ERROR                */
               QR(L,K1)=QRAD(L).RAD1(K1)/.91;
               QR(L,K1+8)=QRAD(L).RAD2(K1)/.91;
          END;
     END;
                   /* CHANGE LANGLEYS/HR TO W/M**2                        */
     TIME=3600;
     EFLUX=0;   EINPUT=0;   EINPOND=0;
     QR=QR*4.186*10000/TIME;
```

```
DO L=1 TO 365;                    /* YEARLY TOTAL SURFACE INSOLATION  */
     DO K1=1 TO 16;
          EFLUX=EFLUX+QR(L,K1)*TIME;
     END;
END;
PUT EDIT ('YEARLY ENERGY FLUX AT EARTH SURFACE=',EFLUX,'J/M**2')
     (SKIP(2),X(10),A,E(12,3),A);
EFLUX=EFLUX/4.186/10000/365;
PUT EDIT ('AVERAGE DAILY FLUX AT EARTH SURFACE=',EFLUX,'LANGLEYS
     /DAY')(SKIP(1),X(10),A,E(12,3),A);


               /* INPUT WATER ABSORPTION DATA */
DCL (ALPHA,BETA,DQR(N),DQ(N)) FLOAT;
DCL 1 ABSORB(40),
                  2 LAMBDA, 2 ETA, 2 MU FLOAT;
GET LIST(ABSORB);

               /*  CALCULATE FRESNEL REFLECTION  */
DCL(LX,EX,ZSID,ZCOD,ZCOI,ZSII,ZSIR,ZCOR,TAU,GAMMA) FLOAT;
DCL (H2ON,C,B,XMU,G1,G2) FLOAT;

EX=0.40928;          /* ANGLE OF SUN AT SOLSTICE IN RADIANS        */
LX=LADITUDE*3.14159/180;          /* LADITUDE IN RADIANS           */
H2ON=1.33                         /* INDEX OF REFRACTION OF WATER*/

DO L=1 TO 365;                  /* BEGIN DAYS CALCULATION          */
     TA=9.5+16.5*SIN(2*3.14159*(L-108)/365);      /* DAYS TEMP    */
     G2=(L-172)*2*3.14159/365;
     ZSID=SIN(EX)*COS(G2);
     ZCOD=SQRT(1-ZSID*ZSID);
     DO K1=1 TO 16;                        /* START DAYTIME HOURS   */
          G1=(K1-8.5)*2*3.14159/24;
          ZCOI=COS(LX)*ZCOD*COS(G1)+SIN(LX)*ZSID;
          IF ZCOI > 0 THEN DO;
               ZSII=SQRT(1-ZCOI*ZCOI);
               ZSIR=ZSII/H2ON;
               ZCOR=SQRT(1-ZSIR*ZSIR);
               GAMMA=1/ZCOR;
               C=1/(ZCOR+H2ON*ZCOI);
               B=1/(ZCOI+H2ON*ZCOR);
               TAU=2*H2ON*(C*C+B*B)*ZCOI*ZCOR;
          END;
          ELSE DO;
               TAU=0;
               MU=0;
          END;
```

```
          /*  FIX UP MU HERE  */
BETA=0;
DO I=1 TO N-1;
     ALPHA=0;
     DO K=1 TO 40;
          XMU=ABSORB(K).MU*GAMMA;
          IF (I*Z*XMU) < 50 THEN    /* PREVENTS UNDERFLOW*/
          ALPHA=ALPHA+TAU*ABSORB(K).ETA*EXP(-I*Z*XMU);
     END;
     DQ(I)=.87334*TAU-ALPHA-BETA;
     BETA=BETA+DQ(I);
END;
DQ(N)=.87334*TAU-BETA;

     /* CALCULATE HEAT EXCHANGE  */

IF(THOUSE-TA) > 0 THEN
     DEGHR=DEGHR+THOUSE-TA;
ETOP=KAPPA(1)*A(1)*TIME/Z*2*(TA-T(1);
EINPUT=EINPUT+QR(L,K1)*A(1)*TIME;
EINPOND=EINPOND+.87334*TAU*QR(L,K1)*A(1)*TIME;
DO I=1 TO N;
     DQR(I)=DQ(I)*QR(L,K1)*A(I)*TIME;
                    /* DQR(I) IS RADIANT ENERGY ABSORBED
                       IN EACH SUBLAYER                  */
                    /* ADQC IS HEAT EXCHANGED BETWEEN
                       ADJACENT SUBLAYERS                */
     ADQC=DQC(I,J,M,N,KAPPA,A(I),TIME,T,Z,TG(N+1),
          KS(N+1),WS(N+1),TA);
                    /* HEAT LOSS OUT SIDES IS ADQS       */
     ADQS=DQS(KS(I),AS(I),TIME,TG(I),T(I),WS(I));
                    /* ADQEX IS HEAT EXTRACTED FOR LOAD */
     ADQEX=DQEX(I,N,HEATNEED,THOUSE,TA,TIME,
          ETOP,EUSEDT,QR(L,K1));
                    /* CALCULATES HEAT CONTENT           */
     Q(I)=Q(I)+DQR(I)+ADQC+ADQS+ADQEX;
     ESIDE=ESIDE+ADQS;
END;
          /* CALCULATE NEW TEMPERATURES AND PHYSICAL
             PARAMETERS FOR EACH SUBLAYER                */
T=Q/(AHC*Z*A);
T(N)=Q(N)?(M*Z*AHC(N)*A(N));
KAPPA=0.587*(1+0.00281*(T-20))*(1-KBETA*CON);
DO I=1 TO N;
     ADEN(I)=DEN(C)N(I),T(I),DENA(I),DENB(I),DENC(I));
     AHC(I)=HC(CON(I),T(I),HCA(I),HCB(I),ADEN(I));
END;
```

```
          ETUSED=ETUSED+EUSEDT;
          EXUSED=EXESUED+ADQEX;
          EUSED=EUSED+ADQEX+EUSEDT;
          ETOPT=ETOPT+ETOP;

                    /*  WRITE OUT MORNING TEMPERATURES              */
          IF K1=2 THEN
          PUT EDIT(DAY(L),' 5AM',T)(SKIP(1),X(2),F(6),A,
               (N)(X(1),F(9,3)));
                    /*  WRITE OUT EVENING TEMPERATURES              */
          IF K1=11 THEN
          PUT EDIT(DAY(L),' 4PM',T)(SKIP(1),X(2),F(6),A,
               (N)(X(1),F(9,3)));
     END;
                    /*  CALCULATE FOR NIGHT HOURS                   */
     DO K1=17 TO 24;
          IF (THOUSE-TA) > 0 THEN
               DEGHR=DEGHR+THOUSE-TA;
          ETOP=KAPPA(1)*A(1)*TIME/Z*2*(TA-T(1));
          DO I=1 TO N;
               ADQC=DQC(I.J.M,N,KAPPA,A(I),TIME,T,Z,TG(N+1),
                    KS(N+1),WS(N+1),TA);
               ADQS=DQS(KS(I),AS(I),TIME,TG(I),T(I),WS(I));
               ADQEX=DQEX(I,N,HEATNEED,THOUSE,TA,TIME,ETOP,EUSEDT,0);
               ESIDE=ESIDE+ADQS;
               Q(I)=Q(I)+ADQC+ADQS+ADQEX;
          END;
          T=Q/(AHC*Z*A);
          T(N)=Q(N)/(M*Z*AHC(N)*A(N));
          KAPPA=0.587*(1.0.00281*(T-20))*(1-KBETA*CON);
          DO I= 1 TO N;
               ADEN(I)=DEN(C)N(I),T(I),DENA(I),DENB(I),DENC(I));
               AHC(I)=HC(CON(I),T(I),HCA(I),HCB(I),ADEN(I));
          END;
          ETUSED=ETUSED+EUSEDT;
          EXUSED=EXUSED+ADQEX;
          EUSED=EUSED+ADQEX+EUSEDT;
          ETOPT=ETOPT+ETOP;
          EOUTB=EOUTB+ADQC;
     END;
END;
```

```
                    /*  OUTPUT YEARLY ENERGY BUDGET                    */

PUT EDIT ('TOTAL ENERGY AVAILABLE AT SURFACE'.EINPUT,
     'TOTAL ENERGY GOING INTO POND',EINPOND)
     (SKIP(2),A,X(4),E(10,3),SKIP(1),A,X(9),E(10,3));
PUT EDIT ("HEAT OUT TOP',ETOPT,'HEAT OUT TOP USED TO HEAT HOUSE',
     ETUSED,'TOTAL HEAT USED TO HEAT HOUSE',EUSED,
     'HEATING DEGREE HOURS', DEGHR)
     (SKIP(1),A,X(25),E(10,3),SKIP(1),A,X(6),E(10,3),SKIP(1),A,X(2),
     E(10,3),SKIP(1),A,X(8),E(10,3),SKIP(1),A,X(12),F(15,3));
DEGDAY=DEGHR/24;
PUT EDIT ('HEATING DEGREE DAYS',DEGDAY)
     (SKIP(1),A,X(13),F(15,3));
PUT EDIT ('ENERGY OUT SIDE',ESIDE)
     (SKIP(1),A,X(17),E(15,3));
PUT EDIT ('ENERGY OUT BOTTOM',EOUTB)
     (SKIP(1),A,X(15),E(15,3));
PUT EDIT ('HOUSE LOAD',HEATNEED,'W/DEG','POND AREA',A(1),
     'M**2','INSULATING LAYER',LI,'M','CONVECTING LAYER',LC,'M')
     (SKIP(1),A,F(10,3),A,SKIP(1),A,F(10,3),A,SKIP(1),A,F(10,3),A,
     SKIP(1),A,F(10,3),A,SKIP(1));
```

```
DQC: PROC(I,J,M,N,KAPPA,A,TIME,T,Z,TG,KS,WS,TA) RETURNS (FLOAT);
                          /* CALCULATES VERTICAL HEAT EXCHANGE BETWEEN  */
                          /* ADJACENT SUBLAYERS                         */
     DCL(I,J,M,N) FIXED BIN;
     DCL(KAPPA(*),A,TIME,T(*),Z,TG,KS,WS,W,X,Y,TA) FLOAT;

     X=2*A*TIME/Z;
     IF I=1 THEN
          W=X*((TA-T(I))*KAPPA(I)+(T(I+1)-T(I))/(1/KAPPA(I)+1/KAPPA(I+1)));
     ELSE IF I=N-1 THEN
          W=X*(KAPPA(I)*(T(I+1)-T(I))+(T(I-1)-T(I))
            /(1/KAPPA(I)+1/KAPPA(I-1)));
     ELSE IF I=N THEN
          W=X*KAPPA(I-1)*(T(I-1)-T(I));
     ELSE  W=X*((T(I-1)-T(I))/(1/KAPPA(I-1)+1/KAPPA(I))
             +(T(I+1)-T(I))?(1/KAPPA(I)+1/KAPPA(I+1)));
     RETURN (W);
END DQC;

DQS: PROC(KS,AS,TIME,TG,T,WS) RETURNS (FLOAT);
                          /* CALCULATES HEAT LOSS THROUGH SIDES         */
     DCL(KS,AS,TIME,TG,T,WS) FLOAT;
     DCL (W) FLOAT;

     W=KS*AS*TIME*(TG-T)/WS;
     RETURN (W);
END DQS;

DQEX: PROC(I,N,HTND,TH,T,TIME,ETOP,USEDT,SUN) RETURNS (FLOAT);
                          /* HEAT LOSS BY EXTRACTION, I.E. LOAD         */
     DCL (I,N) FIXED BIN;
     DCL (X,W,HTND,TH,T,TIME,ETOP,USEDT,SUN) FLOAT;

     IF I¬=N THEN       W=0:
          ELSE DO;
               X=HTND*(T-TH)*TIME;
               IF X > 0 THEN DO;
                    W=0;      USEDT=0;
               END;
               ELSE IF 0.001 < SUN THEN DO;
                    W=0;      USEDT=0;
               END;
               ELSE DO;
                    W=X;      USEDT=0;
               END;
          END;
     RETURN (W);
END DQEX;
```

```
HC: PROC( Q,T,A,B,D) RETURNS (FLOAT);
                          /* CALCULATES HEAT CAPACITY IN J/M**3 OF NACL */
                          /* SOLUTIONS                                  */
     DCL (Q,T,A,B,H,D) FLOAT;

     H=(0.6516+((0.3475)*(0.96285)**Q)+A*(T-20)-B*(T-20)**2;
     H=H*D*(4.186E6);
     RETURN (H);
END HC;

DEN: PROC (Q,T,A,B,C) RETURNS (FLOAT);
                          /* CALCULATES DENSITY IN GM/ML OF NACL        */
                          /* SOLUTIONS                                  */
     DCL (Q,T,A,B,C,DT,X,D25,D0) FLOAT;

     X=1+A*T+B*T*T-C*T**3;
     D25=0.99707+0.0070033*Q+(1.4059E-5)*Q*Q+(3.309E-7)*Q**3;
     D0=D25*(1+A*25+B*25*25-C*25**3);
     DT=D0/X;
     RETURN (DT);
END DEN;

XINRP: PROC (Q,A) RETURNS (FLOAT);
                          /* INTERPOLATES BETWEEN TWO KNOWN VALUES      */
     DCL (I) FIXED BIN;
     DCL (Q,A(*),W) FLOAT;

     I=Q;
     W=A(I+1)+(Q-I)*(A(I+2)-A(I+1));
     RETURN (W);
END XINRP;

END;                      /* ENDS BEGIN BLOCK                           */
END APOND;
```